



Durham E-Theses

Some topics in the calculation of QCD hard scattering processes

Makshough, Kassem M.

How to cite:

Makshough, Kassem M. (1990) *Some topics in the calculation of QCD hard scattering processes*, Durham theses, Durham University. Available at Durham E-Theses Online: <http://etheses.dur.ac.uk/5977/>

Use policy

The full-text may be used and/or reproduced, and given to third parties in any format or medium, without prior permission or charge, for personal research or study, educational, or not-for-profit purposes provided that:

- a full bibliographic reference is made to the original source
- a [link](#) is made to the metadata record in Durham E-Theses
- the full-text is not changed in any way

The full-text must not be sold in any format or medium without the formal permission of the copyright holders.

Please consult the [full Durham E-Theses policy](#) for further details.

The copyright of this thesis rests with the author.
No quotation from it should be published without
his prior written consent and information derived
from it should be acknowledged.

Some Topics in the Calculation of QCD Hard Scattering Processes

Kassem M. Makshoush,
King Saud University, Riyadh, Saudi Arabia

A thesis submitted to the University of Durham
for the Degree of Doctor of Philosophy
in the Department of Physics

May 4, 1990



25 JUN 1991

Abstract

We have studied the single effective subprocess approximation for two-jet events at large transverse momentum. This strongly suggested a factorized form for the cross-section for producing two jet events in pp and $p\bar{p}$ interactions in terms of an effective structure function and a single basic subprocesses. Also the single and two-jet fractions which are based on the effective structure function have been studied and it is shown that the contribution of these fractions in pp and $p\bar{p}$ interactions are independent of the jet angular distribution.

We then tried to explain the surprising similarity between the angular distributions of different $2 \rightarrow 3$ QCD parton-parton subprocesses in the transverse plane. This feature turns out to be associated with an exact relationship between Altarelli-Parisi splitting kernels. Our results are published in Phys. Lett. B212 (1988), 95.

The second part of our work is to handle the calculation of the matrix element squared for six-gluon scattering to the leading order in the number of colours and a compact expression was obtained in terms of kinematical variables. This resulted in Durham preprint DTP 88/40 (1989). We developed a powerful technique which strongly suggested a factorized form for the non-leading terms. Together with the leading expression, this gave the exact matrix element squared for the six-gluon scattering for the first time represented analytically in terms of kinematical invariants in a compact form.

Finally we examined how the non-leading terms are growing in importance when one increases the number of gluons in multi-gluon scattering.

Dedication

To my parents who have brought great love and affection into my life.

Acknowledgements

I would like to sincerely thank my supervisor Dr. C.J. Maxwell, of the Department of Physics, University of Durham for his advice, guidance and encouragement during the period of this present work.

Also thanks to Dr. Mike Pennington for giving me basic information on QCD during his lectures.

Thanks are due to King Saud University, Riyadh Saudi Arabia for supporting me during the period of this present work.

Contents

Abstract	i
Dedication	i
Acknowledgements	ii
1 Introduction	1
1.1 Quantum Electrodynamics	1
1.2 Quark Model	3
1.3 Why Colour?	4
1.4 The Parton model	6
1.5 Quantum Chromodynamics	7
1.6 Colour Factors	10
1.7 Feynman rules for QCD	13
1.8 The QED Coupling Constant	14
1.9 The Effective Quark-Gluon Coupling	15
1.10 Altarelli-Parisi splitting kernels	18
2 Large-P_T Hadronic Collisions	39
2.1 Two Jet Angular Distribution	40
2.2 The Structure Function in pp and $p\bar{p}$ Interactions	41
2.3 Data on The Two Jet Angular Distribution	43
2.4 Single Jet and 2-Jet Fractions	44
3 Three-Jet Production	62
3.1 $2 \rightarrow 3$ Large- P_T Hadronic Jets	62
3.2 Data on the $2 \rightarrow 3$ Angular Distribution	63
3.3 Measurement of QCD Coupling Constant	64
3.4 Common Angular Dependence of 3-jet Production	65

4	The Dokshitzer Relation	70
4.1	APPENDIX A	80
4.2	APPENDIX B	82
5	Spinor Methods	85
5.1	Introduction	85
5.2	Duality Properties	85
5.3	Spinor Definition and Properties	86
5.4	The Polarization Vector	88
5.5	Parke-Taylor Formula for n-gluon scattering	90
5.6	Six gluon scattering	93
5.7	Formalism	94
5.8	A compact expression for six-gluon scattering	94
5.9	The Non-leading terms for six-gluon scattering	98
6	Seven-gluon Scattering	107
6.1	Introduction	107
6.2	Results for Seven-Gluon Scattering	107
6.3	Comparison of Leading and Next-to-Leading Terms for the Parke-Taylor Sub-Amplitude	110
7	Summary	112

Chapter 1

Introduction

1.1 Quantum Electrodynamics

In the early 1930's, a theory emerged describing the electromagnetic interaction of electrons and photons. It is quantized and relativistically invariant. The most recent developments in particle physics, however, have revealed the relevance of a special class of such theories called "gauge theories". Quantum Electrodynamics is the simplest example of a gauge theory. Also the electromagnetic interaction of quarks and leptons are successfully described by the Quantum Electrodynamics. In this section we hope to obtain the structure of Quantum Electrodynamics which is based on the Dirac equation and the principle of local gauge invariance.

For a free electron, the Dirac equation can be written in the following form:

$$(i\gamma^\mu \partial_\mu - m)\Psi = 0. \quad (1.1)$$

which corresponds to the Lagrangian

$$L = i\bar{\Psi}\gamma_\mu \partial^\mu \Psi - m\bar{\Psi}\Psi. \quad (1.2)$$

The four components of $\bar{\Psi}$ and Ψ are regarded as the independent field variables. One can consider a phase transformation given by

$$\Psi(x) \rightarrow e^{i\alpha}\Psi(x). \quad (1.3)$$

where α in equation (1.3) is a real constant. Taking the derivative of equation (1.3) one finds,

$$\partial_\mu \Psi(x) \rightarrow e^{i\alpha} \partial_\mu \Psi(x). \quad (1.4)$$

the Lagrangian which was given in equation (1.2) is invariant under this phase transformation. To check that substitute equation (1.4) into equation (1.2) and use equation (1.3) and note that

$$\bar{\Psi}(x) \rightarrow e^{-i\alpha} \bar{\Psi}(x) \quad (1.5)$$

The transformation given in equation (1.3) generalises to the following form,

$$\Psi(x) \rightarrow e^{i\alpha(x)} \Psi(x). \quad (1.6)$$

Now $\alpha(x)$ is not constant but depends on the space and time in a completely arbitrary way. This is known as a local phase transformation. In fact this does not work. The Lagrangian in equation (1.2) is not invariant under the local phase transformation. From equation (1.6) we obtain

$$\bar{\Psi}(x) \rightarrow \bar{\Psi}(x) e^{-i\alpha(x)}. \quad (1.7)$$

So the last term of L in equation (1.2) is invariant. By taking the derivative of equation (1.6), then we have

$$\partial_\mu \Psi(x) \rightarrow e^{i\alpha(x)} \partial_\mu \Psi(x) + i e^{i\alpha(x)} \Psi(x) \partial_\mu \alpha(x). \quad (1.8)$$

The invariance of L is broken by the $\partial_\mu \alpha(x)$ term. If we demand invariance of the Lagrangian under local gauge transformation, we must seek a modified derivative, D_μ , that transforms covariantly under phase transformations, that is like Ψ itself,

$$D_\mu \Psi \rightarrow e^{i\alpha(x)} D_\mu \Psi. \quad (1.9)$$

We introduce a vector field A_μ with transformation properties such as to cancel the term which was unwanted in equation (1.8). This can be achieved by the construction

$$D_\mu \equiv \partial_\mu - ieA_\mu. \quad (1.10)$$

where A_μ transforms as the following

$$A_\mu \rightarrow A_\mu + \frac{1}{e} \partial_\mu \alpha(x). \quad (1.11)$$

where e is the charge of the particle. Now D_μ satisfies the transformation which was given in equation (1.9). The invariance of the Lagrangian L in equation (1.2) then follows if we replace ∂_μ by D_μ ,

$$L = i\bar{\Psi}\gamma^\mu D_\mu \Psi - m\bar{\Psi}\Psi. \quad (1.12)$$

By using equation (1.10) one can rewrite L in the following form,

$$L = \bar{\Psi}(i\gamma^\mu \partial_\mu - m)\Psi + e\bar{\Psi}\gamma^\mu \Psi A_\mu. \quad (1.13)$$

The vector field which appears in equation (1.13), A_μ , is called the gauge field and this couples to the Dirac particle in exactly the same way as the photon field. Compare the “minimal substitution” replacement of Electrodynamics,

$$p^\mu \rightarrow p^\mu + eA^\mu. \quad (1.14)$$

with the equation in (1.10). The interaction term in equation (1.13) can be written in the form $j^\mu A_\mu$, where j is the current density. If one regards this new field as the photon field must add to the Lagrangian a term corresponding to its kinetic energy. This kinetic term to be added must be invariant under the transformation which was given in (1.11), it can only involve the gauge invariant field strength tensor which is given by,

$$F_{\mu\nu} \equiv \partial_\mu A_\nu - \partial_\nu A_\mu. \quad (1.15)$$

we are thus led to the Lagrangian of QED, which is written in the following form:

$$L = \bar{\Psi}(i\gamma^\mu \partial_\mu - m)\Psi + e\bar{\Psi}\gamma^\mu \Psi A_\mu - \frac{1}{4}F_{\mu\nu}F^{\mu\nu}. \quad (1.16)$$

Note that the addition of a mass term $\frac{1}{2}m^2 A^\mu A_\mu$ is not allowed by gauge invariance. The gauge particle, the photon must be massless.

The conclusion is that by imposing the natural requirement of local phase invariance on the free fermion Lagrangian we are led to the interacting field theory of QED.

1.2 Quark Model

In cosmic rays and in particle accelerator experiments many elementary particles have been seen, and those particles can be grouped into families according to their spin, isospin, strangeness, parity, and other quantum numbers.

Gell-Mann and Néeman[2] expanded the isospin invariance of the strong force to a higher symmetry representation. Their starting point is the charge-independent property of the strong nuclear force. This means that particles such as proton and neutron are indistinguishable in a world where the strong force is the only interaction.

The strong interaction can be described in an elegant mathematical way by using an idea based on isospin. The charge independence can be expressed as the invariance of the strong interaction under rotations in isospin space. When isospin is added to strangeness as a property of strong interactions, it becomes clear that the strongly interacting particles are controlled by the symmetry group $SU(3)$. The representation of $SU(3)$ can be chosen from the other possibilities.

In fact this picture can be described by the quark model, together with the $SU(3)$ classification of hadrons, which was proposed by Gell-Mann and (independently) Zweig [2]. The postulate of Gell-Mann and Zweig is that, there are three

types of fermion known as quarks, with different flavours, up, down and strange, u, d, s respectively. The u and d quarks form an $s = 0$ isospin doublet $I_3 = \frac{1}{2}, -\frac{1}{2}$ for u and d respectively. The s quark carries an additional additive quantum number, "strangeness", and has $s = -1$. The isospin of the s quark is singlet $I_3 = 0$. In table (1.1) we show the quark quantum numbers, where the 'hypercharge' Y is given by

$$Y = B + S. \quad (1.17)$$

In the quark model picture, the mesons with baryon number $B = 0$ are considered to be a bound state of quark and antiquark ($q\bar{q}$). For the three flavours of quark, q, u, d , or s , there are nine possible combinations of ($q\bar{q}$). The nine states are split up into $SU(3)$ octet and $SU(3)$ singlet under the operation of the fundamental representation of the symmetry group $SU(3)$. The eight states transform among themselves but do not mix with the singlet state. This is shown in figure (1.1). The baryons, with $B = 1$, are bound states of three quarks (qqq). Each quark has baryon number $B = \frac{1}{3}$ and charge $\frac{2}{3}$ for the u quarks and $(-\frac{1}{3})$ for d and s quarks.

In fact there are 27 possible combinations of (qqq). The nine combinations of two quarks arrange themselves in two $SU(3)$ multiplets

$$q \otimes q = 3 \otimes 3 = 6 \oplus \bar{3}.$$

where six states are symmetric and 3 states are anti-symmetric under the interchange of two quarks. Adding the third quark triplet, the final representation of the group for the baryon is that

$$q \otimes q \otimes q = 3 \otimes 3 \otimes 3 = 10 \oplus 8 \oplus 8 \oplus 1.$$

The quark-model provides a very successful description of the particle spectrum.

1.3 Why Colour?

The proton is a uud bound state with baryon number 1. The neutron is obtained as a udd bound state. The Δ^{++} particle is a bound state of uuu quarks. The configuration uuu correctly matches the properties of the doubly charged Δ^{++} . Its spin $J = \frac{3}{2}$, is obtained by three identical $J = \frac{1}{2}$ u quarks which are combining together in their ground state. This means that according to the quark scheme one must combine three fermions u which are identical in a completely symmetric ground state, uuu , to provide the known properties of the Δ -particle. Of course such a state is forbidden by Fermi statistics. Even neglecting the statistics problem, the quark model is clearly unsatisfactory. Whilst it is true that (qqq), ($\bar{q}\bar{q}\bar{q}$)

and $(q\bar{q})$ states reproduce the observed sequence of baryon, antibaryon and meson, the question remains what about all the other possibilities, such as qq , $\bar{q}\bar{q}$, or single quarks themselves?

Observations, confirm that one never encounters qq combination such as, uu , which would have fractional charge $\frac{4}{3}$. Both problems which are discussed above can be resolved by introducing a new property or quantum number for quarks: Colour. One can assume that quarks come in three primary colours, those three colours namely red, green and blue can be denoted by R, G and B respectively. One postulates that hadrons consist of colour singlet combinations of quarks.

One can then write the quark wave function for the Δ -particle state as the following

$$\Delta^{++} = \frac{1}{\sqrt{6}}(u_R u_G u_B - u_R u_B u_G + u_B u_R u_G - u_B u_G u_R + u_G u_B u_R - u_G u_R u_B),$$

and the colour-singlet hadron $\pi^+ = u\bar{d}$ has the colour singlet wave function

$$\pi^+ = \frac{1}{\sqrt{3}}(u_R \bar{d}_R + u_B \bar{d}_B + u_G \bar{d}_G)$$

The colour-singlet means that the wave function is invariant under permutations of colour, this colour wave function is antisymmetric. It is clear that one can overcome the statistics problem by disposing of the identical quarks. Now Δ -state are distinguishable by three quarks and their colour quantum number. One can make the overall spin \times space \times colour wave function antisymmetric.

The existence of colour indeed resolves a number of other problems which are summarised in the following points:

(1) $\pi^0 \rightarrow \gamma\gamma$

This interaction can be described by the diagram of Figure (1.2), and the π^0 -state is given by

$$|\pi^0\rangle = \frac{1}{\sqrt{2}}(|u\bar{u}\rangle - |d\bar{d}\rangle), \text{ then one predicts } \Gamma(\pi^0 \rightarrow \gamma\gamma) = .90 eV.$$

One can note that this result is smaller than experimental data by a factor of $(3)^2$. When the quarks come in three different colours, one can find a good agreement between the result predicted by theory and the experimental result.

(2) The experimental ratio of R between the cross-section for $e^+e^- \rightarrow$ hadrons and $e^+e^- \rightarrow \mu^+\mu^-$ is given in the naive parton model (without colour) by

$$R = \frac{\sigma(e^+e^- \rightarrow \text{hadrons})}{\sigma(e^+e^- \rightarrow \mu^+\mu^-)} = \sum e_i^2. \quad (1.18)$$

For three quark flavours, the R ratio is found to be smaller than experimental data by a factor of 3. When the quarks come in three different colours, one can find a good agreement between the result which was predicted by theory and the experimental result.

The existence of colour is supported by these different phenomena. The property of colour is also responsible for the confinement of quarks within hadrons.

1.4 The Parton model

In deep inelastic scattering, a shower of hadronic products are created when an electron collides with a proton. The two particles interact through the exchange of a virtual photon (high-energies), and the internal structure of the hadronic particle is probed [3]. In figure (1.3) we show the electron-proton scattering.

The cross-section for this scattering can be written in the following form: (E and E' are the energies of the incoming and scattered electron respectively).

$$\frac{d^2\sigma}{dQ^2 d\nu} = \frac{4\pi\alpha^2}{Q^4} \cdot \frac{E}{E'} [2W_1(Q^2, \nu) \sin^2 \frac{\theta}{2} + W_2(Q^2, \nu) \cos^2 \frac{\theta}{2}]. \quad (1.19)$$

Q is the 4-momentum transferred by photon to proton and is given by the following relation

$$Q^2 = -q^2 = EE' \sin^2 \frac{\theta}{2}.$$

The energy which was lost by the electron to the proton is given by

$$\nu = E - E'.$$

W_1 and W_2 , which appear in equation (1.19) are the structure functions which correspond to the two possible polarisation states of the exchanged photon. In general these two structure functions depend on two variables Q and ν . The prediction which was given by J. Bjorken is that when Q^2 is large at fixed ν , the structure functions are only depending on one variable namely x , where

$$x = Q^2/2M\nu, (1 > x > 0).$$

$$\begin{aligned} MW_1(x, Q^2) &\rightarrow F_1(x) \\ \nu W_2(x, Q^2) &\rightarrow F_2(x). \end{aligned} \quad (1.20)$$

This is called Bjorken scaling.

The simple explanation for the behaviour of Bjorken scaling was given by Feynman [3], where he assumed that the struck nucleon is made of point-like constituents called “partons”. The scaling behaviour of the cross-section was used as an indication of scaling of point like partons, which were identified with the quarks of the constituent quark model, as they appeared to have identical quantum properties. The deep inelastic experiments gave the surprising result that the sum of the quark momentum in the proton is only 50% of the total proton momentum. This result strongly suggested the existence of another object beside quarks to carry the other half of the total proton momentum. This new particle was called the gluon. This gluon has to carry the colour charge as well which means that there are different coloured gluons corresponding to the different possible combinations.

1.5 Quantum Chromodynamics

The interaction of gluons and quarks is successfully described by the gauge theory of Quantum Chromodynamics (QCD), which is now believed to be the gauge theory of the strong interaction.

The interaction in QCD of fundamental spin $\frac{1}{2}$ quarks involves the exchange of a spin 1 gauge boson, the gluon, as a colour gauge theory. The simple properties, which the QCD theory has are summarised in the following points:

- Quarks carry colour as well as electric charge.
- Colour is exchanged by eight coloured gluons.
- There is a similarity between the electromagnetic interaction and colour interaction.
- At short distances (large momentum transfer) the coupling is so small that there is a validity to the perturbative technique. While at long distance (momentum transfer is small) the coupling is so large that the perturbative QCD technique cannot be used.

In section (1.1) we discussed the structure of QED. Here similarly one may hope to obtain the structure of Quantum Chromodynamics from the principle of local gauge invariance. The main idea of QCD is to make the $SU(3)_c$ colour symmetry local rather than global. Our starting point is that the free Lagrangian of QCD can be written in the following form.

$$L_o = \bar{q}_i (i\gamma\partial_\mu - m)q_j, \quad (1.21)$$

where q_1, q_2, q_3 denote the three colour fields. For simplicity one can take one quark flavour. To impose local gauge invariance on the free QCD Lagrangian it is sufficient to assume infinitesimal phase transformation of the form,

$$q(x) \rightarrow Uq(x) = e^{i\alpha_a(x) \cdot T_a} q(x),$$

$$Uq(x) \simeq [1 + i\alpha_a(x)T_a]q(x). \quad (1.22)$$

where U is an arbitrary 3×3 unitary matrix. T_a is the usual 3×3 generator of $SU(3)$, and α_a is characterised by group parameters. The condition $U^+ = U^{-1}$ implies that

$$\alpha_a T_a = \alpha_a^* T_a^\dagger. \quad (1.23)$$

T_a is hermitian which leads to the requirement that α_a must be real. In fact the group is non-abelian since not all the generators T_a commute with each other. The commutator of any two is a combination of all the T 's and this combination is linear, then one can write

$$[T_a, T_b] = i f_{abc} T_c. \quad (1.24)$$

The factor f_{abc} , which appears in equation (1.24) is called the structure constant of $SU(3)$. The set $a, b, c = 1, \dots, n^2 - 1$, for an $SU(N)$ algebra. This factor is antisymmetric under interchange of any pair of indices. To prove that, define

$$T_a = \lambda_a/2,$$

and comparing with equation (1.24) one can write

$$[\lambda_i/2, \lambda_j/2] = i \sum_k f_{ijk} \lambda_k/2 \delta_{ab} \quad (1.25)$$

These just generalise the Pauli-matrices and are normalised by $\text{Tr}(\lambda_a \lambda_b) = 2\delta_b$. Together with equation (1.25) one can then write

$$\text{Tr}(\lambda_c, [\lambda_a, \lambda_b]) = 4i f_{abc}.$$

Now it is easy to show that f_{abc} is totally antisymmetric.

Antisymmetry in a, b follows from

$$4i f_{abc} = \text{Tr}(\lambda_b, [\lambda_a, \lambda_c]) = -\text{Tr}(\lambda_c, [\lambda_a, \lambda_b]) = -4i f_{abc}.$$

By taking the derivative of equation (1.22), which is written in the following form,

$$\partial_\mu q(x) = [1 + i\alpha_a(x)T_a] \partial_\mu q(x) + iT_a q(x) \partial_\mu \alpha_a(x). \quad (1.26)$$

we see that the second term in equation (1.26) destroys the invariance of the Lagrangian similarly to the QED case. One can note that if $\alpha_a(x)$ is independent of the space and time, this term is zero which implies that the Lagrangian is invariant under global phase transformations. If we want the Lagrangian to be invariant under local transformations, we should look for a modified Lagrangian. To get this, we introduce the gauge field G_μ^a , where each G_μ^a transforms as:

$$G_\mu^a \rightarrow G_\mu^a - \frac{1}{g} \partial_\mu \alpha_a(x). \quad (1.27)$$

with covariant derivative

$$D_\mu = \partial_\mu + igT_a G_\mu^a \quad (1.28)$$

By substituting $\partial_\mu \rightarrow D_\mu$ in equation (1.21) and using equation (1.28) one can write the QCD Lagrangian in the following form

$$L = \bar{q}(i\gamma^\mu \partial_\mu - m)q - g(\bar{q}\gamma^\mu T_a q)G_\mu^a. \quad (1.29)$$

For the non-abelian gauge transformation, this is not enough to obtain an invariant Lagrangian. The problem is that

$$(\bar{q}\gamma^\mu T_a q) \rightarrow (\bar{q}\gamma^\mu T_a q) - f_{abc}\alpha_b(x)(\bar{q}\gamma^\mu T_c q). \quad (1.30)$$

To achieve gauge invariance of L , it is necessary that the gauge field G_μ transforms according to

$$G_\mu^a \rightarrow G_\mu^a - \frac{1}{g} \partial_\mu \alpha_a(x) - f_{abc}\alpha_b(x)G_\mu^c. \quad (1.31)$$

and finally one may add to L the gauge invariant kinetic energy terms for each of the G_μ^a fields. Then the final QCD Lagrangian is given by:

$$L = \bar{q}(i\gamma^\mu \partial_\mu - m)q - g(\bar{q}\gamma^\mu T_a q)G_\mu^a - \frac{1}{4}G_{\mu\nu}^a G_a^{\mu\nu}. \quad (1.32)$$

where $G_{\mu\nu}^a$ appearing in equation (1.32) is the QCD field strength tensor and has the following form,

$$G_{\mu\nu}^a = \partial_\mu G_\nu^a - \partial_\nu G_\mu^a - gG_\mu^b G_\nu^c f_{abc} \quad (1.33)$$

The QCD Lagrangian is describing the interaction of coloured quarks q_i^a and gluons G_μ , with coupling specified by g , and one can see that this Lagrangian is invariant under the local colour phase transformation on quark fields. Another important note to be made is that a mass term taking the form $\frac{1}{2}m^2 G_\mu G_\nu$ is not valid in the Lagrangian, hence local gauge symmetry requires the gluon to be massless like the photon in QED. The Lagrangian L in equation (1.32) can be written in the following representation,

$$1/\sqrt{2}(R\bar{R} - G\bar{G}),$$

$$1/\sqrt{3}(R\bar{R} + G\bar{G} + B\bar{B}) \text{ (colour singlet).}$$

In QED, the strength of the electromagnetic coupling between two quarks is given by $e_1 e_2 \alpha$, where e_i is the electric charge in units of e and α is the fine structure constant. Similarly in QCD the strength of the strong coupling for single-gluon exchange between two coloured quarks is $C_1 C_2 \alpha_s$. Here C_1 and C_2 are the coefficients of colour which are associated with the vertices. It has become conventional to use the notation C_F for the Casimir of the gauge group defined by [1].

$$C_F = \frac{1}{2} |C_1 C_2|. \quad (1.35)$$

Now we can show how the colour factors are calculated.

Consider the interaction between two quarks having the same colour, say, B .

There are three possible diagrams representable as in Figure 1.4.

Out of eight gluons, only one containing the combination $B\bar{B}$ can be exchanged. Then the product of $C_1 C_2$ is

$$\left[\frac{-2}{\sqrt{6}}\right]\left[\frac{-2}{\sqrt{6}}\right] = \frac{2}{3}.$$

In figures (1.4b) and (1.4c) we show the interaction between coloured R quarks which can be mediated by two different gluons. One gluon with combination of colour $\frac{1}{\sqrt{6}}(R\bar{R} + G\bar{G} - 2B\bar{B})$ and the other gluon with combination of colour $\frac{1}{\sqrt{2}}(R\bar{R} - G\bar{G})$. Then the product of $C_1 C_2$ for the interaction between coloured R quarks (the last two diagrams) is given by

$$C_1 C_2 = \left[\frac{1}{\sqrt{6}} \times \frac{1}{\sqrt{6}}\right] + \left[\frac{1}{\sqrt{2}} \cdot \frac{1}{\sqrt{2}}\right] = \frac{2}{3}$$

This result is the same as the product of $C_1 C_2$ for the interaction between coloured B in diagram (1.4a), as indeed it has to be from colour symmetry.

In the second case we assume that the interaction is between two quarks with different colour say R and B . This interaction can be described by the following diagrams of Figure (1.5).

The interactions between $R - B$ quarks can be mediated by two different gluons. One gluon has a combination of colour $\frac{1}{\sqrt{6}}(R\bar{R} + G\bar{G} - 2B\bar{B})$ and the other gluon has $R\bar{B}$ combination. For the diagram in Figure (1.5a) the $C_1 C_2$ product is given by

$$C_1 C_2 = \left[\frac{1}{\sqrt{6}} \times \frac{-2}{\sqrt{6}} \right] = -\frac{1}{3}.$$

For the diagram in Figure (1.5b) the product of $C_1 C_2$ is

$$C_1 C_2 = (1)(1) = 1.$$

In this interaction one can ask, do we add or subtract these two indistinguishable contributions?

In fact the answer depends on the symmetry of the colour wave function under interchange of the quarks. For a symmetric state we add these two contributions together and so the total product of $C_1 C_2$ for the above two diagrams is

$$C_1 C_2 = 1 - \frac{1}{3} = \frac{2}{3}.$$

For the antisymmetric state we should subtract, then the total product of $C_1 C_2$ for these two contribution is

$$C_1 C_2 = -\frac{4}{3}.$$

In fact this prediction is shown in the first case in which we assume the R-R interaction. Then one can write

$$C_1 C_2 = P - \frac{1}{3}.$$

where $P = \pm 1$ and this depends on the colour symmetric or antisymmetric state for the two quarks.

In the third case we consider the interaction between $B - \bar{B}$ and insert the minus sign at an antiquark vertex, as in QED, where the antiparticle has opposite charge to the particle. In this interaction three diagrams should be taken into account, given in Figure (1.6).

For the diagram (1.6a) the product of $C_1 C_2$ is

$$C_1 C_2 = \left[\frac{-2}{\sqrt{6}} \cdot \frac{2}{\sqrt{6}} \right] = \frac{-2}{3}.$$

The product of $C_1 C_2$ for the diagram in (1.6b) is

$$C_1 C_2 = [(1)(-1)] = -1.$$

For the diagram which was represented in figure (1.6c) the product of $C_1 C_2$ is

$$C_1 C_2 = [(1)(-1)] = -1.$$

Then the product of the total $C_1 C_2$ for the three contributions is

$$C_1 C_2 = -\frac{8}{3}.$$

Thus the colour factor C_F is $\frac{4}{3}$.

The other factors are represented in table (1.2).

1.7 Feynman rules for QCD

In section (1.5) we have discussed the structure of QCD. This structure is demonstrated in the invariant Lagrangian which was given in equation (1.37). In fact to each Lagrangian for QED or QCD, there corresponds a set of Feynman rules, and so, we identify these rules according to the following points:

- There are a set of propagators and vertex factors, associated with the various terms in the Lagrangian.
- The terms which are quadratic in the fields are responsible for the determination of the propagators, terms such as

$$\bar{q}(i\gamma_\mu \partial^\mu - m)q, G^2, \dots$$

- The other terms in the QCD or (QED) Lagrangian are associated with interaction vertices. Hence the Feynman factor for the vertex is given by the coefficient of the corresponding term in iL containing the interaction.

It is important to use the Feynman rules when one needs to calculate different processes. In table (1.3) we have listed some of the Feynman rules which are constructed from the Lagrangian of QCD [4]. The diagram labelled by "1" in table (1.3) is describing the propagator of quarks. This corresponds to the first term of equation (1.34), while the diagram "2" indicates the gluon propagator and this is corresponding to the second term of the QCD Lagrangian which was demonstrated in equation (1.34). The diagram in (3) in table (1.3) is describing the quark-gluon vertex and corresponds to the third term in equation (1.34) in the previous section, while the diagrams (4) and (5) are describing the three and four gluon vertices and these correspond to the last two terms in equation (1.34).

It is easy to show that the triple gluon vertex is given by

$$(iL)_{3g} = -\frac{g}{2} f_{abc} (g_{\mu\nu} P_{1\lambda} - g_{\lambda\mu} P_{1\nu}) G_a^\mu G_b^\nu G_c^\lambda. \quad (1.36)$$

by substituting equation (1.33) into equation (1.32) and isolating the terms containing the three gluon fields. By labelling the indices in different terms and using the following relation,

$$i\partial_\mu G_a^\mu = P_{1\mu} G_a^\mu.$$

summing over all possible orderings of the gluon one can obtain the relation which was given in equation (1.36).

1.8 The QED Coupling Constant

The relationship between the renormalised and the bare charge is given by [1] the following ($Q^2 = -q^2$).

$$e^2(Q^2) = e_0^2 \left[\frac{1}{1 + I(q)} \right]. \quad (1.37)$$

where $I(q)$ is defined by the following two loops, evaluated at two different momentum scales.

$$I(q) = \left[\begin{array}{c} \text{Diagram 1} \\ \text{at } Q^2 \end{array} - \begin{array}{c} \text{Diagram 2} \\ \text{at } \mu^2 \end{array} \right]$$

$$\sim \frac{\alpha}{3\pi} \ln \frac{M^2}{Q^2} - \frac{\alpha}{3\pi} \ln \frac{M^2}{\mu^2} = \frac{\alpha}{3\pi} \ln \frac{\mu^2}{Q^2}.$$

The equation, which is given in (1.37), is displaying the fact that the charge an experimentalist measures depends on the energy scale Q^2 of the experiment.

The charge which depends on Q^2 is referred to as the effective coupling constant, hence one can write

$$\alpha(Q^2) = e^2(Q^2)/4\pi.$$

At large $Q^2 = -q^2$ the equation in (1.37) has the following form

$$\alpha(Q^2) = \frac{\alpha_0}{1 - \frac{\alpha_0}{3\pi} \ln \frac{Q^2}{M^2}}. \quad (1.38)$$

To eliminate the explicit dependence of $\alpha(Q^2)$ on the cut-off M in equation (1.38), choose μ as a reference momentum. By using the renormalisation procedure one can find that

$$\alpha(Q^2) = \frac{\alpha(\mu^2)}{1 - \frac{\alpha(\mu^2)}{3\pi} \ln \frac{Q^2}{\mu^2}} \quad (1.39)$$

1.9 The Effective Quark-Gluon Coupling

Let us consider the contributions to the quark-gluon coupling shown in Figure (1.7). Define $\bar{g} = \bar{g}(Q)$, $\alpha_s = g^2/4\pi$, $\alpha_s(Q^2) = \bar{g}^2/4\pi$.

For the contributions of Figure (1.7) one can write [6]

$$\bar{g} = g - \frac{\beta_0}{32\pi^2} g^3 (\ln \frac{Q^2}{M^2} + \bar{c}) + \frac{3}{2} \left(\frac{\beta_0}{32\pi^2} \right) g^5 (\ln^2 \frac{Q^2}{M^2} + \dots), \quad (1.40)$$

with β_0 and \bar{c} calculable. Note that β_0 is independent of the gauge parameter ξ and also independent of the diagrams which are proportional to the colour factor $C_2(F)$. Then the definition of β_0 is that

$$\beta_0 = \frac{11}{3} C_2(A) - \frac{4}{3} N_f T_2(F). \quad (1.41)$$

The first term of equation (1.41) comes from the eighth gluon self-coupling diagram in Figure (1.7), and the second term with minus sign comes from the sixth vacuum polarisation diagram with a quark loop (as in QED). In QCD with $N_C = 3$ and the standard fermion representation one has $C_2(A) = 3$ and $T_2(F) = \frac{1}{2}$, then the equation in (1.41) can be written in the following form

$$\beta_0 = 11 - \frac{2}{3} N_f. \quad (1.42)$$

One can note that $\beta_0 > 0$ for $N_f < 16$.

By using the above definition one can write the equation which was given in (1.40) in the following form,

$$\alpha_s(Q^2) = \alpha_s - \frac{\beta_0}{4\pi} \alpha_s^2 \ln \frac{Q^2}{M^2} + \frac{\beta_0^2}{16\pi^2} \alpha_s^3 \ln^2 \frac{Q^2}{M^2} + \dots + \text{non-leading logs.} \quad (1.43)$$

Let us assume that $\alpha_s \ll 1$, $\alpha_s \ln \frac{Q^2}{M^2} \ll 1$. The expansion in (1.43) is then well-defined but clearly depends on M. Suppose that we know $\alpha_s(\mu^2)$, then

$$\alpha_s(\mu^2) = \alpha_s - \frac{\beta_0}{4\pi} \alpha_s^2 \ln \frac{\mu^2}{M^2} + \frac{\beta_0^2}{16\pi^2} \alpha_s^3 \ln^2 \frac{\mu^2}{M^2} + \dots, \quad (1.44)$$

and one can use this expansion to eliminate α_s and M, and obtain the following expansion,

$$\alpha_s(Q^2) = \alpha_s(\mu^2) - \frac{\beta_0}{4\pi} \alpha_s^2(\mu^2) \ln \frac{Q^2}{\mu^2} + \frac{\beta_0^2}{16\pi^2} \alpha_s^3(\mu^2) \ln^2 \frac{Q^2}{\mu^2} + \dots \quad (1.45)$$

The re-expansion of the perturbative series for $\alpha_s(Q^2)$ from the bare coupling α_s to an expansion in $\alpha_s(\mu^2)$ is called renormalisation. In fact $\alpha_s(\mu^2)$ and $\alpha_s(Q^2)$ do not explicitly depend on M. Let us assume this expansion makes sense, i.e.

$$\alpha_s(\mu^2) \ll 1, \quad \alpha_s(\mu^2) \ln \frac{Q^2}{\mu^2} \ll 1,$$

otherwise it is useless. Let us imagine that we know α_s at $\mu = 2$ GeV and we calculate $\alpha_s(10$ GeV), let us further imagine we have α_s at $\mu = 3$ GeV and then calculate $\alpha_s(10$ GeV). For the answers to agree $\alpha_s(Q^2)$ must be independent of μ^2 and $\alpha_s(\mu^2)$. This means all the terms in the series must be related and can be summed by solving a differential equation. Let us instead guess the answer and show it is independent of μ^2 .

The expansion in (1.45) can be written in the following approximate form,

$$\alpha_s(Q^2) \simeq \frac{\alpha_s(\mu^2)}{1 + \frac{\beta_0}{4\pi} \alpha_s(\mu^2) \ln \frac{Q^2}{\mu^2}}. \quad (1.46)$$

This is for $N_f < 16$. By comparing the equation (1.46) with equation (1.39) in the previous section, one can note that for $N_f > 16$ then β_0 in equation (1.42) is negative and hence the sign of the coefficient of $\ln \frac{Q^2}{\mu^2}$ is the same as in QED. This means that the different sign for β_0 in QED and QCD depends on the existence of the gluon, self coupling. In QED the colour factor $C_2(A) = 0$ and $T_2(F) = 1$, then in QED, β_0 is given by

$$\beta_0 = -\frac{4}{3} N_f.$$

To see that equation (1.46) is independent of μ^2 , rewrite the equation as the following

$$\frac{1}{\alpha_s(Q^2)} - \frac{\beta_0}{4\pi} \ln Q^2 = \frac{1}{\alpha_s(\mu^2)} - \frac{\beta_0}{4\pi} \ln \mu^2. \quad (1.47)$$

In equation (1.47) the right hand side is independent of Q^2 and the left-hand side is independent of μ^2 . To separate equation (1.51) one notes that each side of the above equation must be equal to a constant. This means that

$$\frac{1}{\alpha_s(Q^2)} - \frac{\beta_0}{4\pi} \ln Q^2 = \text{constant}.$$

This constant is given by $-(\beta_0/4\pi)\ln\Lambda^2$, hence

$$\alpha_s(Q^2) = \frac{4\pi}{\beta_0 \ln \frac{Q^2}{\Lambda^2}}. \quad (1.48)$$

The leading terms of equation (1.45) are summed by solving the following differential equation

$$4\pi \frac{\partial \alpha_s(Q^2)}{\partial \ln Q^2} = -\beta_0 \alpha_s^2(Q^2),$$

and the solution is that

$$\alpha_s(Q^2) = \frac{4\pi}{\beta_0 \ln \frac{Q^2}{\Lambda^2}}.$$

One can sum the next-to-leading terms by solving the following differential equation

$$4\pi \frac{\partial \alpha_s(Q^2)}{\partial \ln Q^2} = -\beta_0 \alpha_s^2(Q^2) - \frac{\beta_1}{4\pi} \alpha_s^3(Q^2), \quad (1.49)$$

and the solution is that

$$\alpha_s(Q^2) = \frac{4\pi}{\beta_0 \ln \frac{Q^2}{\Lambda^2}} - 4\pi \frac{\beta_1}{\beta_0^2} \frac{\ln \ln \frac{Q^2}{\Lambda^2}}{\ln^2 \frac{Q^2}{\Lambda^2}}. \quad (1.50)$$

This means that if we know every term in the perturbative expansion of $\frac{\partial \alpha}{\partial \ln Q^2}$, i.e. the β -function, then we can sum all logs to any order.

Equation (1.48) has the important consequence that for $\beta_0 > 0$ ($N_f < 16$) $\alpha_s(Q^2) \rightarrow 0$ as $Q^2 \rightarrow \infty$. This means that quarks and gluons appear like almost free particles when probed by high momentum. This is known as “asymptotic freedom”. The other important consequence of the equation (1.48) is that when Q^2 goes to Λ^2 , it is seen that $\alpha_s(Q^2) \rightarrow \infty$ and so the perturbative series breaks down at small Q^2 . These limits are reversed in QED for which $\beta_0 < 0$.

It is clear that the property of asymptotic freedom ensures that the running coupling constant in QCD becomes small in the kinematical regime characterized by large momentum transfer between fundamental constituents. This means that one is able to calculate an approximation to these large momentum transfer processes by using the perturbation expansion. It is sensible to organize the calculation of large transverse momentum hadron production in the framework of the parton or hard scattering model, e^+e^- annihilation into quarks and gluons can also be calculated in the QCD hard scattering formalism at large momentum transfer. At large distances (low energies) the perturbative theory of strong interactions does not apply in describing the behaviour of quarks and gluons.

Here the confinement is strong and so the perturbation theory is no longer applicable and non-perturbative effects must be introduced in describing the processes of quarks and gluons converting into hadrons (called hadronization). The models for the long time scale physics of hadronization and fragmentation cannot be calculated as yet in perturbative QCD.

1.10 Altarelli-Parisi splitting kernels

There are two aspects of the Altarelli-Parisi splitting functions.

- (1) The behaviour of scattering amplitudes in the collinear limit. We shall discuss this in more detail in Chapter 4.
- (2) Evolution of the structure functions of nucleons. The structure functions of electroproduction are given by [1],

$$(-g_{\mu\nu} + q_\mu q_\nu / q^2)W_1(x, Q^2) + (p_\mu - \frac{M\nu}{q^2}q_\mu)(p_\nu - \frac{M\nu}{q^2}q_\nu) \frac{W_2(x, Q^2)}{M^2}. \quad (1.51)$$

where p and q are the four momenta of the nucleon of mass M , and the virtual photon respectively. The parton model shows that the scaling quantities are

$$MW_1 = F_1 \quad (1.52)$$

$$\nu W_2 = F_2. \quad (1.53)$$

and the master formula of the parton model is given by

$$2xF_1(x) = F_2(x) \text{ at large } Q^2.$$

In the expression (1.51)

$$M\nu = (p \cdot q) \quad (1.54)$$

$$Q^2 = -q^2 \quad (1.55)$$

$$Q^2 = 2M\nu x \quad (1.56)$$

In fact the structure functions can be expressed in terms of the quark parton densities and is given by the following form [5]

$$2F_1 = F_2/x = \sum_i e_i^2(q^i(x) + \bar{q}^i(x)) \quad (1.57)$$

where $q^i(x)$ in equation (1.57) is the number density of quarks inside the proton target with fraction x of the proton longitudinal momentum.

Experimentally the difference between the structure function for ep and en scattering is non-singlet. Let us assume one flavour in which case the non-singlet is just defined as a difference, i.e.

$$q^{NS}(x, Q^2) = q(x, Q^2) - \bar{q}(x, Q^2). \quad (1.58)$$

The structure function corresponding to the non-singlet contribution is given by

$$F_2^{NS}(x_1 Q^2) = x q^{NS}(x, Q^2). \quad (1.59)$$

Let y be the fraction of the proton momentum carried by the quark, where $0 \leq y \leq 1$. On scattering with the photon it is observed carrying a fraction x of the proton momentum, so that scattering has changed its momentum fraction by a factor z . This is shown in figure (1.8). Then the probability that the quark emits a gluon with momentum fraction $(1-z)$ is given by $P_{qq}(z)$. The non-singlet contribution is given by the following form

$$q^{NS}(x) = \int_x^1 \frac{dy}{y} q^{NS}(y) P_{qq}(x/y). \quad (1.60)$$

The quark is carrying a momentum fraction before and after being hit by the photon. In the parton model these fractions which are carried by the quark are equal, this means $y = x$, $z = 1$ and $P_{qq}(z) = \delta(1-z)$. In perturbative QCD a gluon is radiated by the quark and so reduces its longitudinal momentum fraction. This means that $y \geq x$, so the probability in equation (1.60) is no longer a delta function, the probability for the radiation of gluons is momentum-dependent. As Q^2 increases the probability that a quark emits a gluon and so reduced its momentum fraction increases. Indeed, on increasing Q^2 to $Q^2 + dQ^2$ the probability of quark emitting a gluon is given by

$$P_{qq}(z, Q^2 + dQ^2) = \delta(1-z) + \frac{\alpha_s(Q^2)}{2\pi} P_{qq}(z) d \ln Q^2 \quad (1.61)$$

This is shown in figure (1.9).

The equations (1.60) and (1.61) determine the evolution of non-singlet structure functions to the lowest order in α_s to be

$$\frac{\partial q^{NS}(x, Q^2)}{\partial \ln Q^2} = \frac{\alpha_s(Q^2)}{2\pi} \int_x^1 \frac{dy}{y} q^{NS}(y, Q^2) P_{qq}(x/y). \quad (1.62)$$

Corresponding to the non-singlet momentum distribution we define its moment M_n^{NS} given by

$$M_n^{NS}(Q^2) = \int_0^1 dx x^{n-1} q^{NS}(x, Q^2). \quad (1.63)$$

By taking the derivative of equation (1.63) and using equation (1.62) one can write

$$\frac{\partial M_n^{NS}(Q^2)}{\partial \ln Q^2} = \frac{\alpha_s(Q^2)}{2\pi} \int_0^1 dx x^{n-1} \int_x^1 \frac{dy}{y} q^{NS}(y, Q^2) P_{qq}(x/y),$$

or

$$\frac{\partial M_n^{NS}(Q^2)}{\partial \ln Q^2} = \frac{\alpha_s(Q^2)}{2\pi} \int_0^1 dy Q^{NS}(y, Q^2) \int_0^1 \frac{dx}{y} \left(\frac{x}{y}\right)^{n-1} P_{qq}(x/y). \quad (1.64)$$

By setting $z = \frac{x}{y}$ one can write equation (1.64) in the following form

$$\frac{\partial M_n^{NS}(Q^2)}{\partial \ln Q^2} = -\frac{\alpha_s(Q^2)}{2\pi} M_n^{NS}(Q^2) \gamma_n^o(NS), \quad (1.65)$$

where γ_n^o is called the anomalous dimension and is given by

$$\gamma_n^o(NS) = -\int_0^1 dz z^{n-1} P_{qq}(z). \quad (1.66)$$

$P_{qq}(z)$ is the Altarelli-Parisi splitting kernel and is a function of z , and given by [5]

$$P_{qq}(z) = \left(\frac{N_c^2 - 1}{2N_c}\right) \frac{z^2 + 1}{1 - z} \text{ for } z < 1. \quad (1.67)$$

For SU(3) the equation (1.67) can be written in form

$$P_{qq}(z) = \frac{4}{3} \frac{z^2 + 1}{1 - z}. \quad (1.68)$$

When the quark radiates a very soft gluon ($z \rightarrow 1$) the result diverges. As is well known in e^+e^- annihilation into quarks and gluons, for instance, we can cancel these divergences by adding the virtual graph to the real graph in the same order contribution, and hence the final answer is finite. When we add the virtual graph contribution in the same order as the real graph this means that the equation in (1.67) can be written in the following form

$$P_{qq}(z) = \left(\frac{N_c^2 - 1}{2N_c}\right) \left[\frac{1 + z^2}{(1 - z)_+} + \frac{3}{2} \delta(1 - z) \right]. \quad (1.69)$$

This makes the following condition

$$\int_0^1 P_{qq}(z) dz = 0, \quad (1.70)$$

and hence the excess number of quarks over antiquarks must be constant. This means that

$$\int_0^1 q^{NS}(x, Q^2) dx = \text{constant}. \quad (1.71)$$

To prove the condition which was given in (1.70), we shall define the following regularization. We define an operation $[f(z)]_+$, where $f(z)$ is singular at $z = 1$, then with $u(z)$ a smooth weight function

$$\int_0^1 dz u(z) [f(z)]_+ = \int_0^1 dz [u(z) - u(1)] f(z). \quad (1.72)$$

By using this regularization to write equation (1.69) as

$$\begin{aligned} \int_0^1 P_{qq}(z) dz &= \left(\frac{N_c^2 - 1}{2N_c} \right) \int_0^1 [-(1+z) + 3/2\delta(1-z)] dz \\ &= \left(\frac{N_c^2 - 1}{2N_c} \right) [-3/2 + 3/2] = 0. \end{aligned}$$

By using $\alpha_s^2(Q^2) = -\frac{4\pi}{\beta_0} \frac{\partial \alpha_s(Q^2)}{\partial \ln Q^2}$ one can rewrite the equation which was given in (1.65) in the following form

$$\frac{\partial M_n^{NS}(Q^2)}{M_n^{NS}(Q^2)} = d_n^{NS} \frac{\partial \alpha_s(Q^2)}{\alpha_s(Q^2)}. \quad (1.73)$$

with

$$d_n^{NS} = 2\gamma_n^{NS}/\beta_0.$$

The solution of equation (1.73) is that

$$\ln M_n(Q^2) = C_n + d_n^{NS} \ln \alpha_s(Q^2). \quad (1.74)$$

where C_n is constant. The parameter d_n^{NS} is known for general n ,

$$d_n^{NS} = \frac{2}{\beta_0} \left(\frac{N_c^2 - 1}{2N_c} \right) \left[1 - \frac{2}{n(n+1)} + 4 \sum_{j=2}^n 1/j \right]. \quad (1.75)$$

To compare the QCD prediction with the experimental result write equation (1.74) for n th and m th moments and eliminate α_s to get

$$\ln M_m(Q^2) = \text{const.} + \frac{d_m^{NS}}{d_n^{NS}} \ln M_n(Q^2). \quad (1.76)$$

A plot of $\ln M_n$ versus $\ln M_m$ should be a straight line with slope equal to the ratio of the anomalous dimensions. For $m = 6$ and $n = 4$ one finds,

$$\begin{aligned} \frac{d_6^{NS}}{d_4^{NS}} &= 1.29 \text{ for vector gluon} \\ &= 1.06 \text{ for scalar gluon.} \end{aligned}$$

As seen from figure (1.10) where the data is taken from electron, muon and neutrino scattering one has good agreement with the vector gluon QCD predictions.

In the singlet density there is a combination of antiquark and quark densities and of the gluon density inside the proton. When the momentum is increased from Q^2 to $Q^2 + dQ^2$ the properties of these splittings are described in figure (1.11)

QCD with massless quarks is flavour-independent

$$\begin{aligned} P_{q_i g_j} &= P_{qq} \delta_{ij} \\ P_{q_i g} &= P_{gg}. \end{aligned}$$

and with massless quarks

$$P_{gq_i} = P_{gg}.$$

for all quark and antiquark types, $i = 1, 2, \dots, 2N_f$. One can write the Altarelli-Parisi master equation [5] in the following form

$$\frac{\partial}{\partial \ln Q^2} \begin{bmatrix} \sum(x, Q^2) \\ g(x, Q^2) \end{bmatrix} = \frac{\alpha_s(Q^2)}{2\pi} \int_x^1 \frac{dy}{y} \begin{pmatrix} P_{qq}(x/y) & 2N_f P_{qg} \\ P_{gq} & P_{gg} \end{pmatrix} \begin{bmatrix} \sum(x, Q^2) \\ g(x, Q^2) \end{bmatrix} \quad (1.77)$$

where

$$\sum(x, Q^2) = \sum_{i=1}^{2N_f} q_i(x, Q^2).$$

and $g(x, Q^2)$ is the density of gluons.

The Altarelli-Parisi splitting functions are given by [5]

$$P_{gq}(z) = P_{qq}(1-z) = C_2(F) \frac{1+(1-z)^2}{z} \quad (1.78)$$

$$P_{gg}(z) = P_{gg}(1-z) = T_2(F)[z^2 + (1-z)^2] \quad (1.79)$$

$$P_{gg}(z) = P_{gg}(1-z) = 2C_2(A)\left[\frac{z}{(1-z)_+} + \frac{(1-z)}{z} + z(1-z)\right] + \frac{1}{2}\beta_0\delta(1-z). \quad (1.80)$$

By defining

$$\gamma_n^o(ba) = -\int_0^1 dz z^{n-1} P_{ba}(z).$$

from the above relations one can calculate $\gamma_n^o(ba)$ given by [5,6]

$$\gamma_n^o(gq) = -C_2(F) \left[\frac{n^2 + n + 2}{n(n-1)(n+1)} \right] \quad (1.81)$$

$$\gamma_n^o(qg) = -2N_f T_2(F) \left[\frac{n^2 + n + 2}{n(n+1)(n+2)} \right] \quad (1.82)$$

$$\gamma_n^o(gg) = C_2(A) \left[\frac{(n-2)(n+1)}{n(n-1)} + \frac{(n-2)(n+5)}{6(n+1)(n+2)} + \sum_{j=3}^n \frac{2}{n} \right] + \frac{2}{3}N_f T_2(F). \quad (1.83)$$

As before define a singlet moment corresponding to the singlet distribution, and so one can write, for $n = 2$

$$\frac{\partial}{\partial \ln Q^2} \begin{bmatrix} M_2^\Sigma \\ M_2^g \end{bmatrix} = \frac{-\alpha_s(Q^2)}{2\pi} \begin{pmatrix} \frac{16}{9} & -N_f/3 \\ -\frac{16}{9} & N_f/3 \end{pmatrix} \begin{bmatrix} M_2^\Sigma \\ M_2^g \end{bmatrix}. \quad (1.84)$$

and the eigenvalues are

$$\gamma_2^- = 0, \gamma_2^+ = \frac{16}{9} + \frac{N_f}{3}.$$

The solutions for these coupled equations are given by

$$M_2^\Sigma = \left(M_2^\Sigma(Q_0^2) - \frac{3N_f}{16+3N_f} \right) \left[\frac{\alpha_s(Q^2)}{\alpha_s(Q_0^2)} \right]^{d_2^+} + \frac{3N_f}{16+3N_f} \quad (1.85)$$

$$M_2^g = - \left(M_2^\Sigma(Q_0^2) - \frac{3N_f}{16+3N_f} \right) \left[\frac{\alpha_s(Q^2)}{\alpha_s(Q_0^2)} \right]^{d_2^+} + \frac{16}{16+3N_f}. \quad (1.86)$$

with

$$d_2^+ = \left[\frac{32 + 6N_f}{99 - 6N_f} \right].$$

In the equations (1.8) and (1.86) at all Q

$$M_2^\Sigma + M_2^g = 1.$$

and this is ensured by the form of the anomalous dimensions which are given in equations (1.81) - (1.83), which give

$$\begin{aligned} \gamma_2^o(qq) &= -\gamma_2^o(gq) \\ \gamma_2^o(gg) &= -\gamma_2^o(qg). \end{aligned}$$

For large Q^2 , $\alpha_s(Q^2)$ becomes small, then

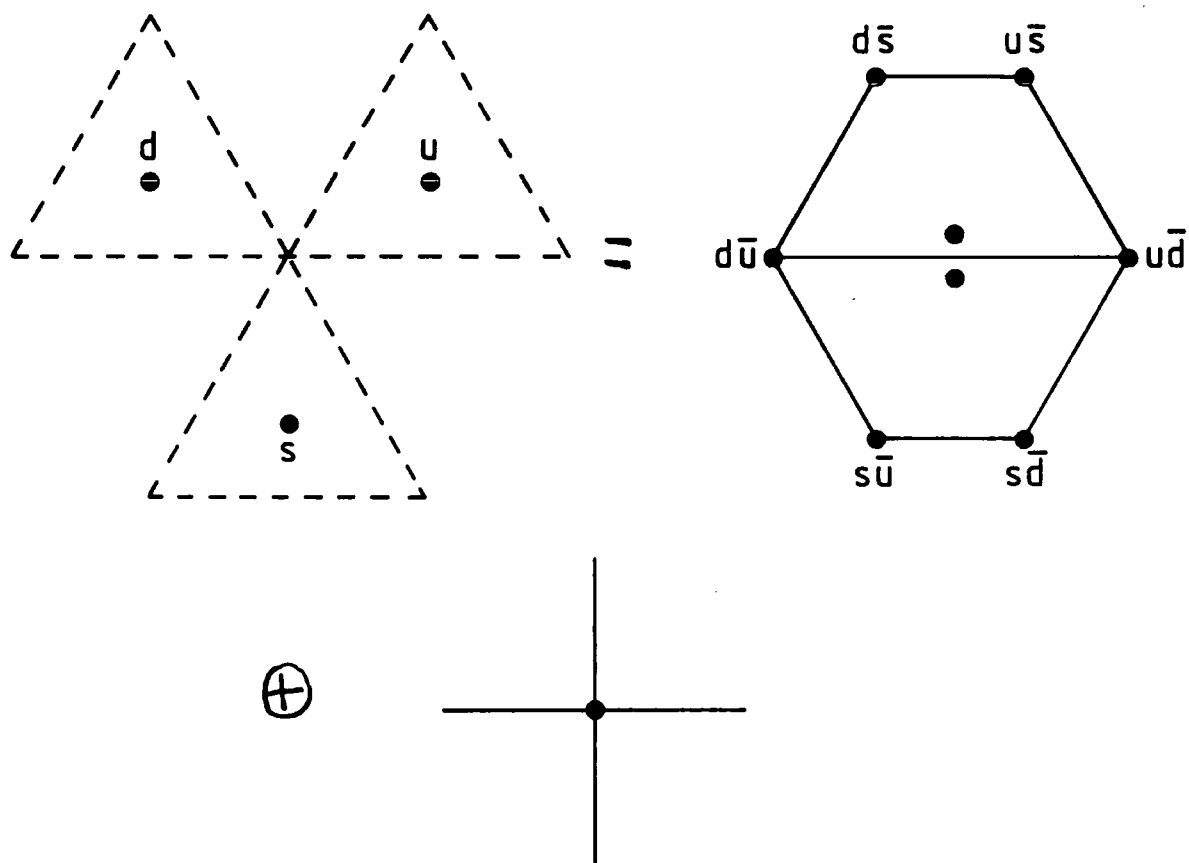
$$\begin{aligned} M_2^\Sigma &\rightarrow 3N_f/(16 + 3N_f) \\ M_2^g &\rightarrow 16/(16 + 3N_f), \end{aligned}$$

which are independent of Q^2 .

Experimentally

$$M_2^\Sigma(Q^2) = \int_0^1 dx F_2(x, Q^2).$$

agrees with the QCD prediction.



$$3 \otimes 3 = 8 \oplus 1$$

Figure 1.1: The quark content of the meson nonet

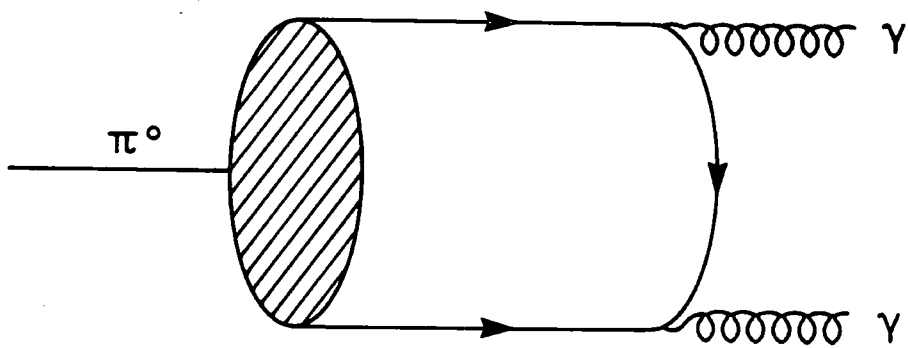


Figure 1.2: The annihilation of π^0 into two photons

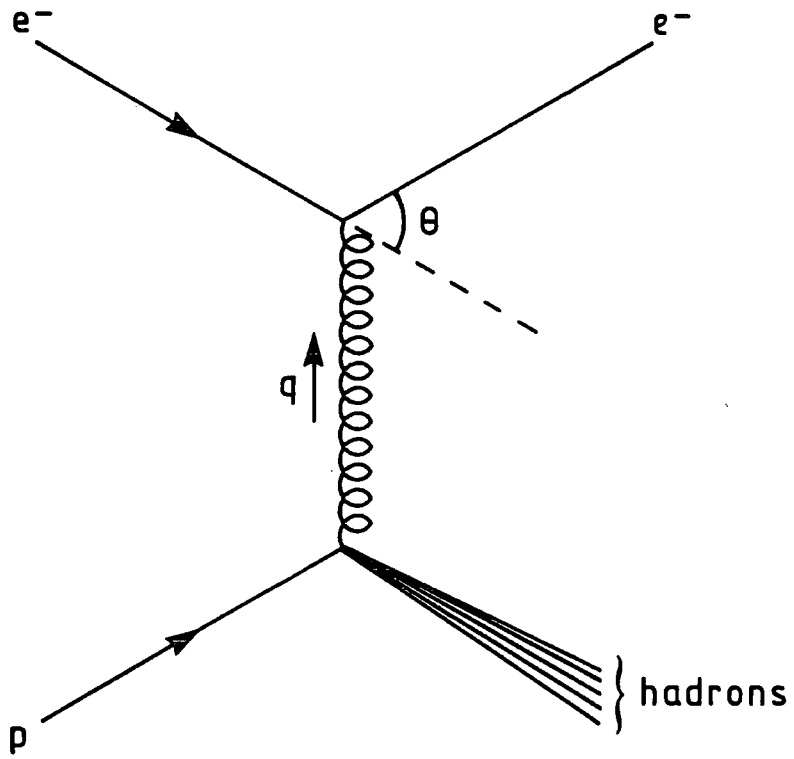


Figure 1.3: Deep inelastic scattering kinematics

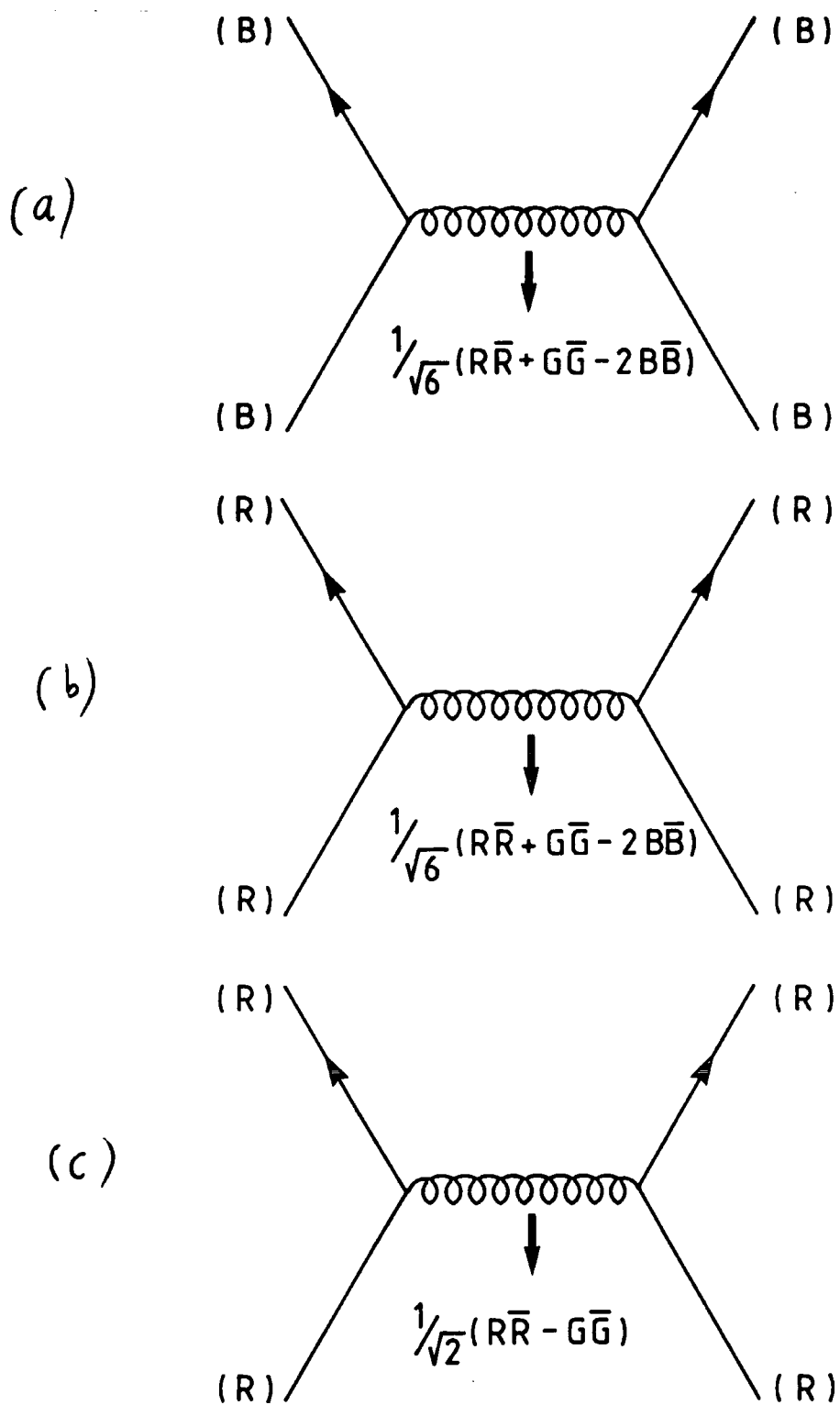


Figure 1.4: Diagrams for scattering of identical colour quark

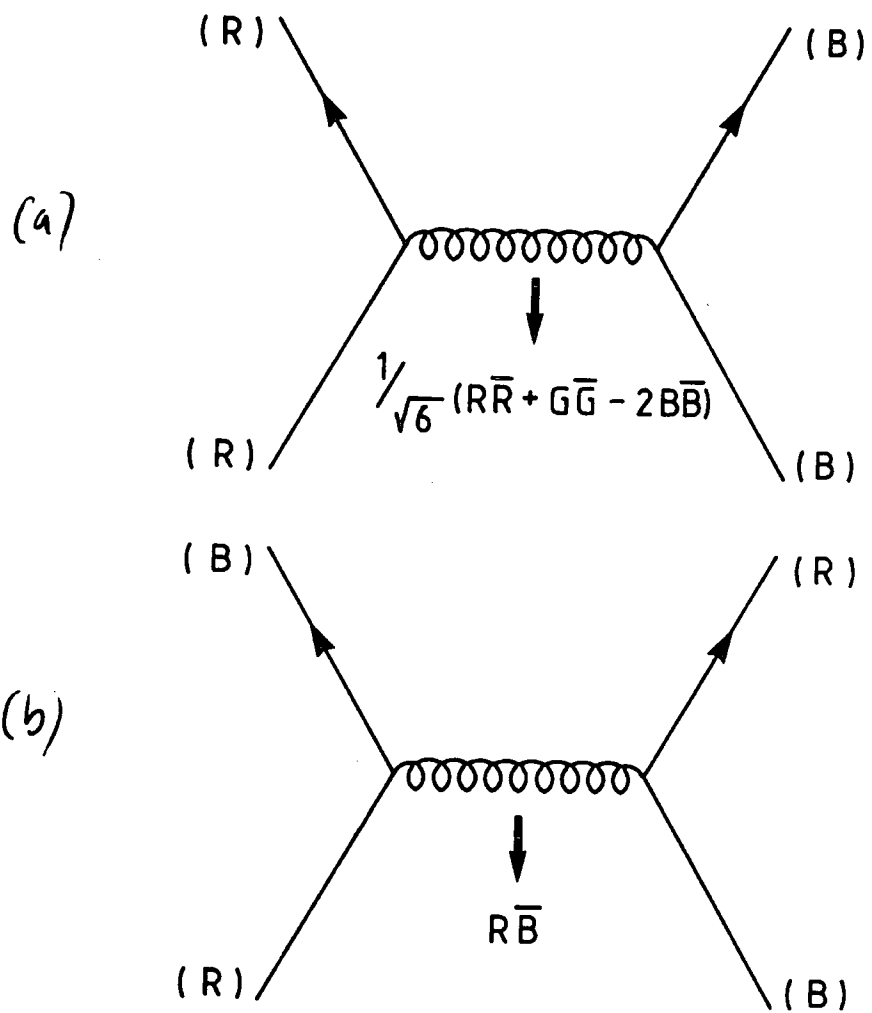


Figure 1.5: Diagrams for scattering of different colour quarks

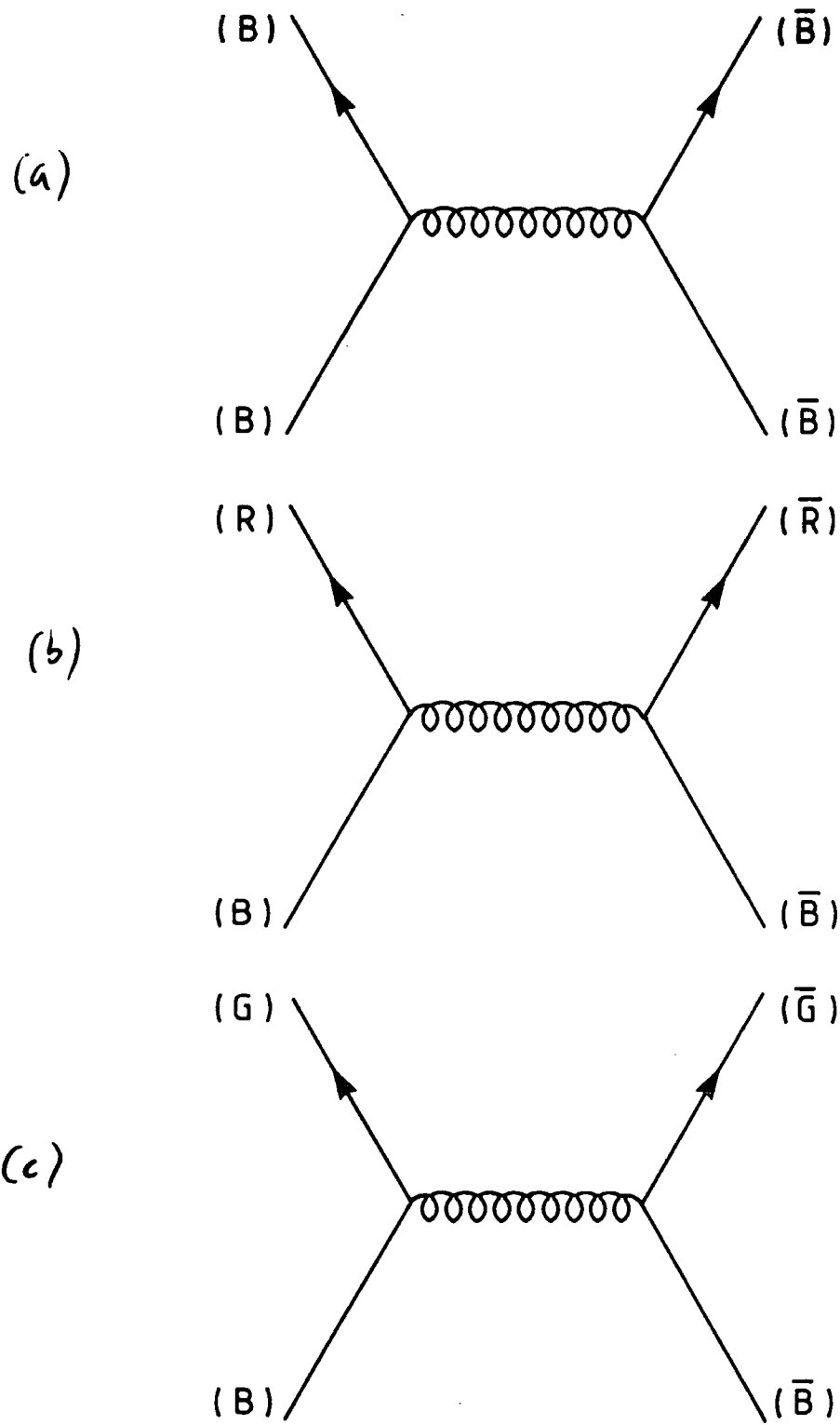


Figure 1.6: Diagrams for $B\bar{B}$

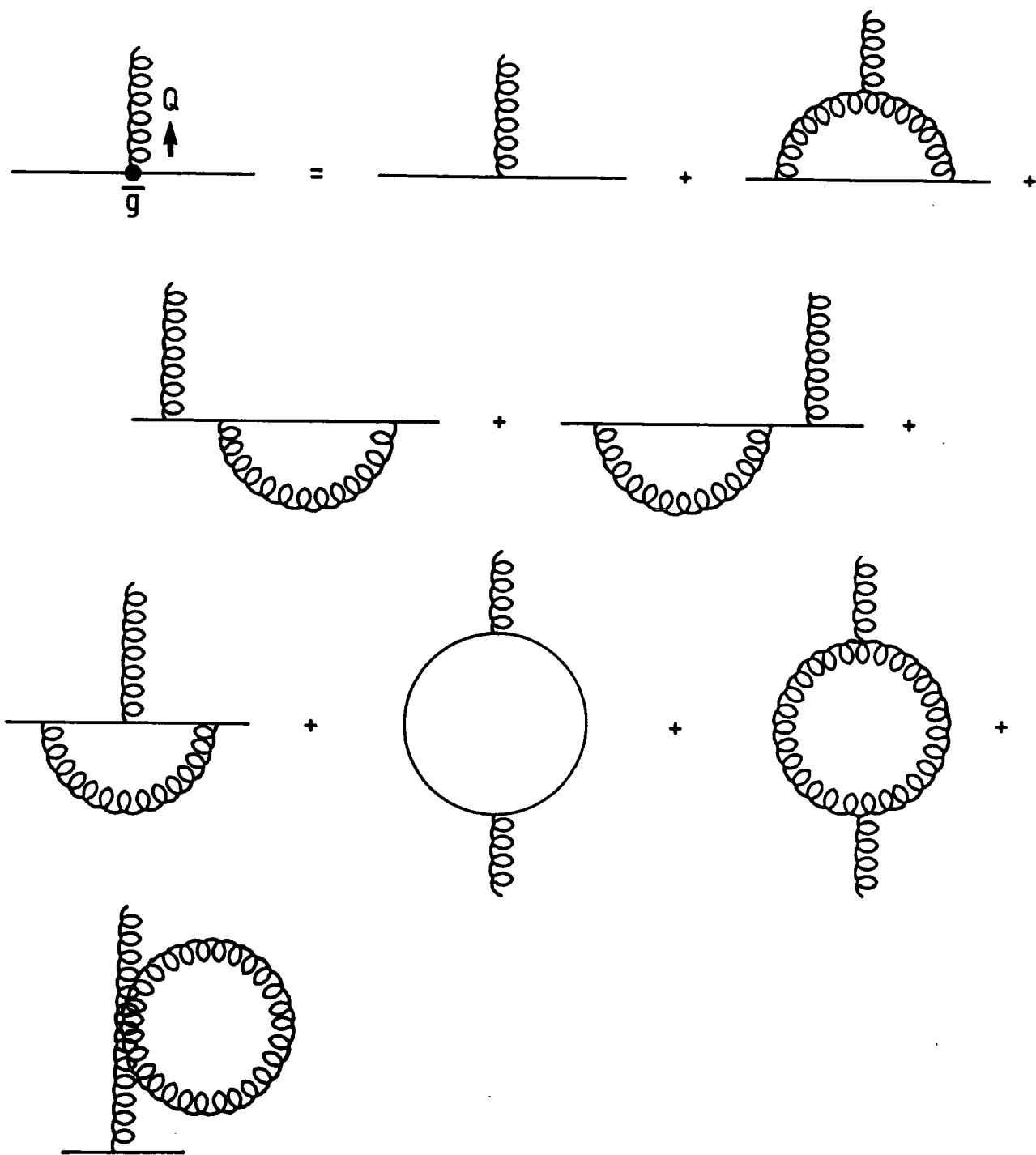


Figure 1.7: QCD corrections to the quark-gluon vertex

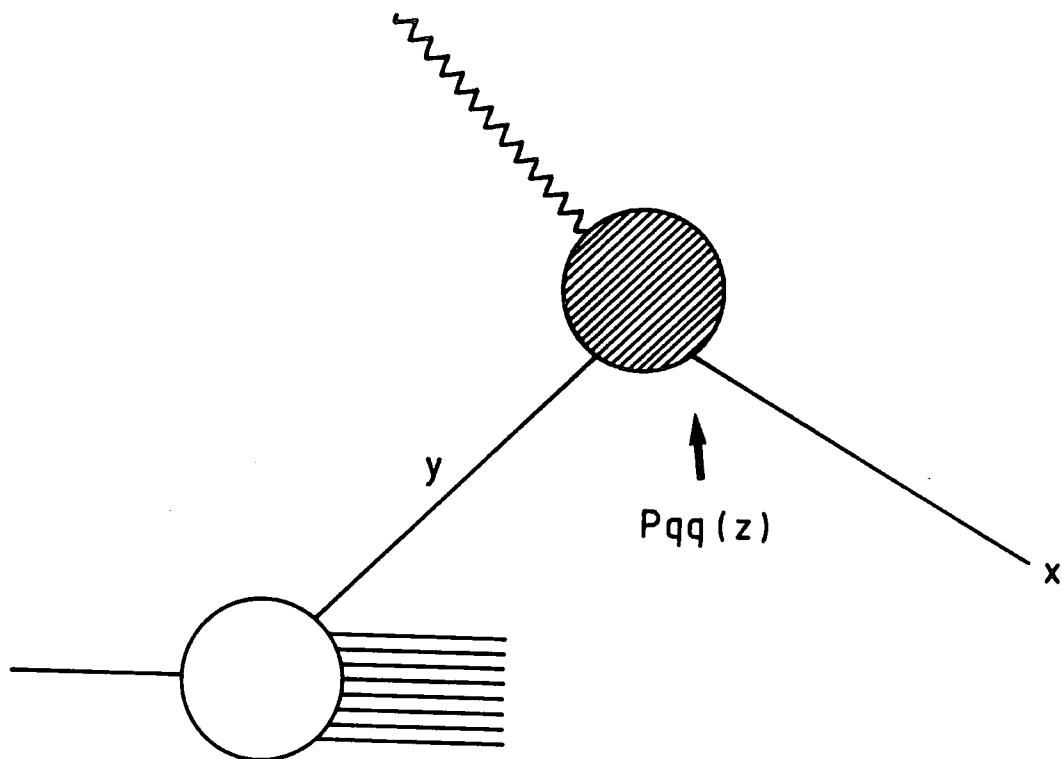


Figure 1.8: Change in momentum fraction of scattered quark by gluon radiation

$$\begin{array}{c}
 \begin{array}{c} q \quad q \\ \hline \bullet \end{array} = \begin{array}{c} q \\ \hline \end{array} + \begin{array}{c} q \\ \hline \text{g} \end{array} z \\
 \delta(1-z) \qquad \frac{\alpha_s}{2\pi} P_{qq}(z) \frac{dQ^2}{Q^2}
 \end{array}$$

Figure 1.9: Shows the probability that a quark emits a gluon in terms of Altarelli-Parisi splitting functions

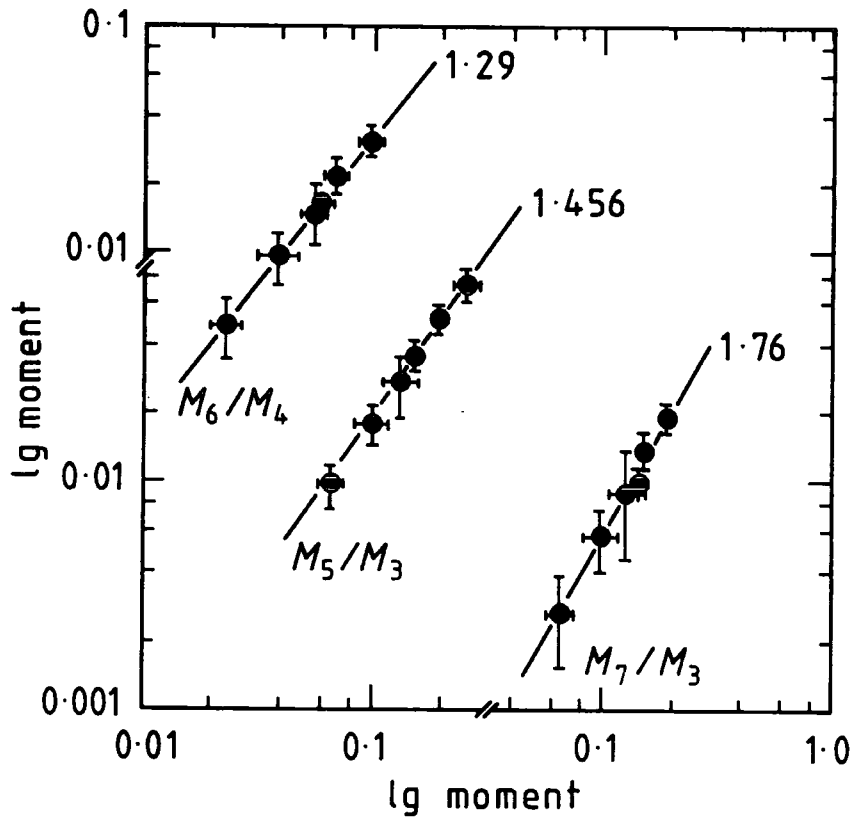


Figure 1.10: Shows a plot of $\ln M_n$ versus $\ln M_m$ for the non-singlet moments

$$\begin{array}{c}
 q \\
 \bullet \\
 \text{---} \\
 = \\
 \begin{array}{c}
 q_i \\
 \text{---} \\
 + \\
 \begin{array}{c}
 q_i \\
 \text{---} \\
 \text{---} \text{g} \\
 z \\
 + \\
 \begin{array}{c}
 q_i \\
 \text{---} \\
 \text{---} \\
 z \\
 \text{---} \\
 q_i
 \end{array}
 \end{array}
 \end{array}
 \end{array}$$

$$\begin{array}{c}
 \delta(1-z) \\
 \frac{\alpha_s}{2\pi} P_{qq} \frac{dQ^2}{Q^2} \\
 \frac{\alpha_s}{2\pi} P_{qg} \frac{dQ^2}{Q^2}
 \end{array}$$

$$\begin{array}{c}
 g \\
 \bullet \\
 \text{---} \\
 = \\
 \begin{array}{c}
 g \\
 \text{---} \\
 \text{---} \\
 q \\
 + \\
 \begin{array}{c}
 g \\
 \text{---} \\
 \text{---} \\
 z \\
 \text{---} \\
 g
 \end{array}
 \end{array}
 \end{array}$$

$$\begin{array}{c}
 \frac{\alpha_s}{2\pi} P_{gq} \frac{dQ^2}{Q^2} \\
 \frac{\alpha_s}{2\pi} P_{gg} \frac{dQ^2}{Q^2}
 \end{array}$$

Figure 1.11: Shows the P_{gg} , P_{qq} , P_{qg} splitting probabilities

Quark	spin	B	Q	I_3	S	Y
u	$\frac{1}{2}$	$\frac{1}{3}$	$\frac{2}{3}$	$\frac{1}{2}$	0	$\frac{1}{3}$
d	$\frac{1}{2}$	$\frac{1}{3}$	$-\frac{1}{3}$	$-\frac{1}{2}$	0	$\frac{1}{3}$
s	$\frac{1}{2}$	$\frac{1}{3}$	$-\frac{1}{3}$	0	-1	$-\frac{2}{3}$

Table 1.1: The quark quantum numbers

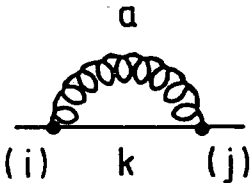
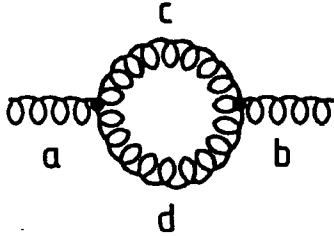
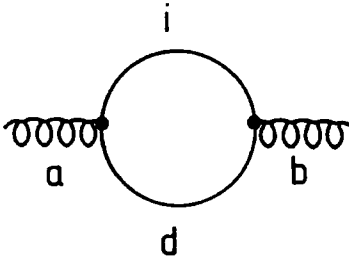
Diagram	Colour factor
	$\sum_{k=1}^N \sum_{a=1}^{N^2-1} T_{lk}^a T_{kj}^a = C_F \delta_{ij} = \frac{N^2-1}{2N_c} \delta_{ij}$
	$\sum_{c,d=1}^{N^2-1} f_{acd} f_{bcd} = C_A \delta_{ab} = N_c \delta_{ab}$
	$\sum_{i,j=1}^N T_{ij}^a T_{ji}^b = \text{tr}(T_a T_b) = \frac{1}{2} \delta^{ab}$

Table 1.2 Shows the colour factor for different diagrams

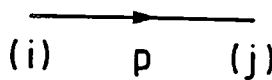
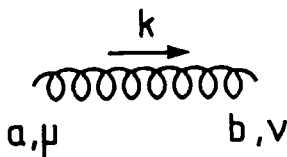
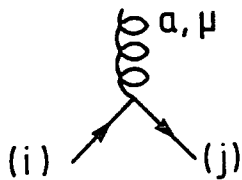
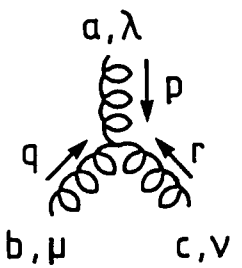
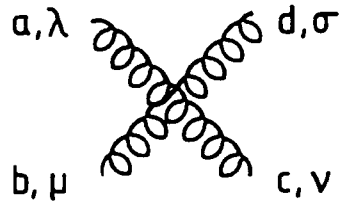
	Diagram	Feynman factor
(1)		$\delta^{ij} \left(\frac{i}{\not{p} - m} \right) = i \delta^{ij} \left(\frac{\not{p} + m}{p^2 - m^2} \right)$
(2)		$-i \frac{\delta^{ab}}{k^2} \left(g_{\mu\nu} - \frac{k_\mu k_\nu}{k^2} + \xi \frac{k_\mu k_\nu}{k^2} \right)$
(3)		$-ig\gamma^\mu T_{ij}^a$
(4)		$-gf^{abc}[(p - q)_\nu g_{\mu\lambda} + (q - r)_\lambda g_{\mu\nu} + (r - p)_\mu g_{\nu\lambda}]$
(5)		$\begin{aligned} & -ig^2 f^{abc} f^{cde} (g_{\lambda\nu} g_{\mu\sigma} - g_{\lambda\sigma} g_{\mu\nu}) \\ & -ig^2 f^{ace} f^{bde} (g_{\mu\lambda} g_{\nu\sigma}) - g_{\lambda\sigma} g_{\mu\nu} \\ & -ig^2 f^{ade} f^{cbe} (g_{\lambda\nu} g_{\mu\sigma} - g_{\lambda\mu} g_{\nu\sigma}) \end{aligned}$

Table 1.3 Shows the Feynman Rules of QCD

REFERENCES

- [1] F. Halzen and A.D. Martin, *Quarks and Leptons*, John Wiley and Sons, New York, 1984.
- [2] M. Gell-Mann and Y. Néeman, *The Eightfold Way*, Benjamin, New York, 1964.
J.J.J. Kokkedee, *The Quark Model*, Benjamin, Reading, Massachusetts, 1969.
- [3] J.D. Bjorken, *Phys. Rev.*, 179, (1969), 1547. J.D. Bjorken and E.A. Paschos, *Phys. Rev.* 185 (1969), 1975. G.G. Callan and D.J. Gross, *Phys. Rev.*, 11 (1969), 156. F.E. Close, *The Quark Parton model*, *Rep. Prog. Phys.* 42 (1976), 1285. R.P. Feynman, *Photon-hadron interactions*, Benjamin, New York, 1972.
- [4] H.D. Politzer, *Phys. Rep.* 14C, 131 (1974).
- [5] G. Altarelli and G. Parisi, *Nucl. Phys.* B126, (1977), 298.
- [6] M.R. Pennington, *Rep. Prog. Phys.* 46 (1982).

Chapter 2

Large- P_T Hadronic Collisions

In Figure (2.1) we represent the hard scattering ansatz. The theoretical cross-section for production of two jets at large transverse momentum is completely factorized into a convolution of structure functions $f_{a|h}$ which are describing the probability to find parton constituent (a) with momentum fraction x in hadron h , and hard scatterings $\hat{\sigma}_{ab \rightarrow cd}$ to be computed in perturbative QCD (at high energies) for all $2 \rightarrow 2$ parton-parton scattering subprocesses $ab \rightarrow cd$. Then the total cross-section for two jet production can be written in the form,

$$\sigma_{2-jet} = \sum_{a,b} \int \int dx_a dx_b f_{a|h} f_{b|h} \hat{\sigma}_{ab \rightarrow cd}. \quad (2.1)$$

The equation in (2.1) is normally applied to hard scattering at large angles to produce jets of high transverse momentum. Because of the Rutherford form of the subprocesses

$$\sigma(\theta) \sim \sin^{-4} \frac{\theta}{2},$$

hence the total jet cross-section is dominated by scattering at small angles and grows rapidly as energy increases at fixed P_T . The sum which appears in equation (2.1) runs over all the nine subprocesses which are given in table (2.1).

The cross-section for the various parton-parton subprocesses have been calculated to leading order in α_s by Cambridge et al. [1].

For a particular process we can define the Mandelstam invariants \hat{s} , \hat{t} and \hat{u} as the following:

$$\begin{aligned} \hat{s} &= (P_1 + P_2)^2 \\ \hat{t} &= -\hat{s}/2(1 - \cos\theta^*) = (P_1 - P_3)^2 \\ \hat{u} &= -\hat{s}/2(1 + \cos\theta^*) = (P_1 - P_4)^2 \end{aligned} \quad (2.2)$$

where P_1 and P_2 are the incoming parton momenta, and P_3 and P_4 are the outgoing parton momenta, \hat{s} is the centre-of-mass subprocess energy squared and θ^* is the

c.m.s. scattering angle. The various subprocess cross-sections can be written in terms of \hat{s} , \hat{t} and \hat{u} . In Table (2.1) we have listed the nine $2 \rightarrow 2$ subprocesses which are written in terms of \hat{s} , \hat{t} and \hat{u} and we have assumed three colours ($N_c = 3$). Since we cannot experimentally distinguish which final parton variety gives rise to a given jet, we have symmetrised the cross-section in \hat{t} and \hat{u} .

2.1 Two Jet Angular Distribution

Combridge and Maxwell suggested using a single variable (χ) defined by the following relation [2]

$$\chi = \frac{1 + \cos \theta^*}{1 - \cos \theta^*} = \frac{\hat{u}}{\hat{t}}. \quad (2.3)$$

Then the nine subprocesses which are listed in table (2.1) can be written in terms of χ and this is shown in table (2.2). We have written the expressions for a general $SU(N_c)$ gauge group.

It is clear that the subprocesses in which the final and initial particles are the same are all proportional to χ^2 , these subprocesses are $q_1 q_2 \rightarrow q_1 q_2, q_1 \bar{q}_2 \rightarrow q_1 \bar{q}_2, q_1 q_1 \rightarrow q_1 q_1, q_1 \bar{q}_1 \rightarrow q_1 \bar{q}_1, qg \rightarrow qg$ and $gg \rightarrow gg$. The subprocesses such as, $q_1 \bar{q}_1 \rightarrow q_2 \bar{q}_2, q\bar{q} \rightarrow gg$ and $gg \rightarrow q\bar{q}$, having the initial and final particles different, are all proportional to χ . This means that for large χ , the six subprocesses which are mentioned above dominate and have a common angular distribution, but the three subprocesses which are proportional to χ are becoming small for large χ .

A useful property of the variable χ is that, in the absence of scaling violations in structure functions and the scale dependences of the coupling constant α_s ,

$$\frac{d\hat{\sigma}}{d\chi} \sim \frac{\chi^2 + \chi^{-2} + \chi + \chi^{-1} + 1}{(1 + \chi)^2} \sim \text{constant}$$

for large χ .

It is interesting to note that the angular distributions of the dominant subprocesses are very similar. The ratios of $qg \rightarrow qg$ and $qq \rightarrow qq$ subprocesses normalised to the dominant one $gg \rightarrow gg$, are rather constant with numerical values around $(\frac{4}{9})$ and $(\frac{4}{9})^2$ respectively. This can be understood in terms of the colour structure of Feynman diagrams.

The relative strengths of the coupling at the three-gluon vertex compared to the quark-quark-gluon vertex are given by the colour factors C_A and C_F respectively. For $SU(3)$ we have $C_A = 3$ and $C_F = \frac{4}{3}$ implying that

$$\frac{C_F}{C_A} = \frac{4}{9}.$$

The origin of the ratio can now be explained as in the graphs in figure (2.2).

Indeed the colour structure of QCD means that

$$qq \rightarrow qq : qg \rightarrow qg : gg \rightarrow gg \simeq 1 : \frac{C_A}{C_F} : \left[\frac{C_A}{C_F} \right]^2 \quad (2.4)$$

In Figure 2.3 we show the $|\cos\theta^*|$ dependence of $qg \rightarrow qg$ and $qq \rightarrow qq$ subprocesses, which are normalised to the dominant one $gg \rightarrow gg$.

2.2 The Structure Function in pp and $p\bar{p}$ Interactions

The cross-section for $p\bar{p}$ interactions can be written in the following form (neglecting sea quarks).

$$\begin{aligned} \sigma(p\bar{p}) = & g(x_1)g(x_2) [\hat{\sigma}_{gg \rightarrow gg} + N_f \hat{\sigma}_{gg \rightarrow q\bar{q}}] + \\ & [u(x_1)d(x_2) + u(x_2)d(x_1)] \hat{\sigma}_{q_1\bar{q}_2 \rightarrow q_1\bar{q}_2} + \\ & [g(x_1)(u(x_2) + d(x_2)) + g(x_2)(u(x_1) + d(x_1))] \hat{\sigma}_{qg \rightarrow qg} \\ & + [u(x_1)u(x_2) + d(x_1)d(x_2)] \\ & [\hat{\sigma}_{q_1\bar{q}_1 \rightarrow q_1\bar{q}_1} + \hat{\sigma}_{q\bar{q} \rightarrow gg} + (N_f - 1)\hat{\sigma}_{q_1\bar{q}_1 \rightarrow q_2\bar{q}_2}] \end{aligned} \quad (2.5)$$

for proton-proton interaction, the cross-section can be written in the following form,

$$\begin{aligned} \sigma(pp) = & g(x_1)g(x_2) [\hat{\sigma}_{gg \rightarrow gg} + N_f \hat{\sigma}_{gg \rightarrow q\bar{q}}] + \\ & [u(x_1)d(x_2) + u(x_2)d(x_1)] \hat{\sigma}_{q_1q_2 \rightarrow q_1q_2} + \\ & [g(x_1)(u(x_2) + d(x_2)) + g(x_2)(u(x_1) + d(x_1))] \hat{\sigma}_{qg \rightarrow qg} + \\ & [u(x_1)u(x_2) + d(x_1)d(x_2)] \hat{\sigma}_{q_1q_1 \rightarrow q_1q_1}. \end{aligned} \quad (2.6)$$

We shall use the result which is obtained in section (2.1), that the cross-section for $gg \rightarrow gg$, $qg \rightarrow qg$ and $qq \rightarrow qq$ are in the ratio $1 : \frac{4}{9} : \left(\frac{4}{9}\right)^2$ and this enables us to rewrite equations (2.5) and (2.6) in the following form,

$$\sigma \sim F(x_1, Q^2) F(x_2, Q^2) \hat{\sigma}_{gg \rightarrow gg} \quad (2.7)$$

with

$$F(x, Q^2) = g(x, Q^2) + \frac{4}{9} [u(x, Q^2) + d(x, Q^2)] \quad (2.8)$$

where we use the subprocess $gg \rightarrow gg$ as the basic subprocess in equation (2.1). This means that the angular dependence effectively factors out leaving a convolution of effective parton distributions. This is called the single effective subprocess

(SES) approximation. The meaning of equation (2.7) is clear, that the cross-section can be understood as the convolution of two single effective structure functions and one basic subprocess, and the ratio 1 : 4/9 : 16/81 means that the product of the structure functions $F(x_1).F(x_2)$ is a perfect square and this results in the factorisation of the structure functions. It is clear that, the structure functions not only depend on x but are also functions of Q^2 . As Q^2 increases the resolving power increases and the number of gluons increases and so the momentum fraction carried by each gluon decreases. This means that there are more low momentum partons in the proton, and the structure function softens. These Q^2 dependences take the form of slowly-varying logarithmic corrections that are expected from the QCD theory and are known as scaling violations because they break the scale invariant nature of the structure functions.

In ref. [3] it has been emphasised that the transverse cross-section for production of jets at 90° to the beam direction in the overall c.m. frame,

$$\Sigma_T = \frac{d\sigma^{2-jet}}{dp_T^2 dy_1 dy_2} \Big|_{\nu_1=\nu_2=0} \simeq \frac{20}{9x_T^2 s^2} \alpha_s^2 \left[u(x_T) + d(x_T) + \frac{9}{4}g(x_T) \right]^2,$$

where $x_1 = x_T(e^{\nu_1} + e^{\nu_2})/2$, $x_2 = x_T(e^{-\nu_1} + e^{-\nu_2})/2$, and $x_T = 2P_T/\sqrt{s}$, provides a useful way of supplementing one's knowledge of the structure functions, in that it is proportional to the squared valence quark distribution at large values of x because the gluon distribution at large x is quite small, whilst being sensitive to the gluon distribution at small values of x , because the structure function of gluons will be dominant at small x . The linear combination in equation (2.8) can be obtained from a measurement of the transverse cross-section at any values of x .

The equation which was given in (2.7) can be written in the following form,

$$\frac{\sigma}{\hat{\sigma}_{gg \rightarrow gg}} \sim F(x_1, Q^2)F(x_2, Q^2) \quad (2.9)$$

In tables (2.3) and (2.4) we have tested the accuracy of the single effective subprocess approximation. The quantities $\sigma(pp)/\hat{\sigma}_{gg \rightarrow gg}$ and $\sigma(p\bar{p})/\hat{\sigma}_{gg \rightarrow gg}$ have been calculated for various values of x_1, x_2 and $p\bar{p}$ interactions. We used all the subprocesses which are obtained in lowest order QCD and used equations (2.5) and (2.6). We used the structure functions set 1 of Duke and Owens ref. [4] which are evaluated with $Q^2 = x_1 x_2 s$ compared with $F(x_1, Q^2)F(x_2, Q^2)$ of equation (2.9) with the same input, and we assumed two values of $\chi = 1, \chi = 10$. It is in a good agreement with the actual results and it is clear that the θ^* -dependence in $\sigma(pp)$ and $\sigma(p\bar{p})$ interactions is very similar to the angular distribution for the dominant subprocess $gg \rightarrow gg$, and hence this angular factor roughly cancels in $\sigma(pp)/\hat{\sigma}_{gg \rightarrow gg}$ and $\sigma(p\bar{p})/\hat{\sigma}_{gg \rightarrow gg}$. Very similar results and comments are obtained by Cambridge and Maxwell [3] but including the non-scaling effect.

In figure (2.4) we show UA1 and UA2 [5] data on the effective structure function which was given in (2.8). It is clear that, both agree well with the corresponding combination of CDHS structure functions measured in neutrino

reactions evolved in Q^2 from 20 to 2000 GeV^2 , in the region of small x , where $F(x)$ is dominated by the gluon distribution, and the large values of x , where $F(x)$ is dominated by the valence quarks.

Tables (2.3) and (2.4) show the single effective subprocess approximation test.

2.3 Data on The Two Jet Angular Distribution

The 2-jet events are measured experimentally by the UA1 and UA2 collaborations at the CERN $p\bar{p}$ collider. It is clear that only at these very large collision energies is the identification and measurement of large transverse momentum jets relatively unambiguous. At lower energies it is still difficult to separate the jets from the other underlying hadrons in the events. In practice there is a small difference between the fragmentation of quarks and gluons, in fact this difference is very hard to detect experimentally. This indistinguishability means it is hard to test QCD beyond the single effective subprocess approximation.

Recent experiments [6] at the $p\bar{p}$ collider have verified the existence of the hard scattering processes between constituents leading to jet production at high transverse momentum. The calculations which are based on perturbative QCD reproduce the form of the observed angular distributions of jets. In figure (2.5) we show data on the angular distribution taken from the UA1 collaboration [7] compared with the QCD prediction. In jet angular distribution the θ^* -dependence comes from the matrix elements squared of the subprocesses which enter in the total cross-section in equation (2.1). This is only true if the scale Q in the coupling constant α_s , and the Q which enters into the structure functions through

$$s = \ln[\ln \frac{Q^2}{\Lambda^2} / \ln \frac{Q_0^2}{\Lambda^2}]$$

is independent of θ^* . This means that one can choose the scale $Q^2 = x_1 x_2 s$ where x_1, x_2 are incoming parton Bjorken x 's and s is fixed. This is represented by the dashed line in figure (2.5). It is clear from the data that this situation is excluded, because we have neglected the non-scaling behaviour of QCD in the calculation of the theoretical curve and we have effectively assumed that $\alpha_s = \text{constant}$, but the QCD coupling constant does actually depend on the Q^2 of the interaction through

$$\alpha_s = 4\pi / \beta_0 \ln \frac{Q^2}{\Lambda^2}$$

we do not know *a priori* what the definition of Q^2 should be, so a reasonable choice has to be made.

In the solid curve we give the QCD prediction using a scale Q defined as the following,

$$Q^2 = -\hat{t} = -\frac{1}{2}\hat{s}(1 - \cos\theta^*)$$

This means that the scale Q depends on the angle and when this is compared with data it is noted that there is excellent agreement. But in the first situation there was still a good agreement with data even through $Q^2 = \hat{s}$ is disfavoured. The data which are used here clearly have steeper dependence, and this implies that as the angle decreases, the Q scale must also decrease. our conclusion is that in the total cross-section the θ^* -dependence mostly comes from the subprocesses and the structure function gives only a weak dependence on the angle through the scale Q . Thus the angular dependence of jet cross-section provides further evidence of the scaling violation consistent with the perturbative QCD.

In figure (2.6) we show the theoretical curve for $\frac{d\sigma}{d\chi}$ compared with data. The dashed curve gives the QCD prediction, where we choose $Q^2 = \hat{s}$. We are considering events which are at fixed mass and hence fixed \hat{s} so that $\alpha_s = \text{constant}$ over the whole angular range ($\chi \geq 2$) and therefore the event rate will be constant over this range. It is clear that, at large angle ($\chi = 1-2$) the scaling curve rises well above the data and at small angle ($\chi = 7-9$) it falls substantially below. This means that the particular choice of $Q^2 = \hat{s}$ does not seem to be a particularly good choice of the scale and is clearly not a good explanation of the data. In the same figure the solid curve indicates the effect of various scale-breaking corrections. The scale-breaking corrections include the Q^2 -dependence of α_s through the factor α_s^2 and the Q^2 -dependence of the effective structure function calculated assuming

$$Q^2 = -\frac{1}{2}\hat{s}(1 - \cos\theta^*)$$

and taking the QCD scale parameter $\Lambda = .20 \text{ GeV}$. The non-scaling curve seems to be in good agreement with data.

2.4 Single Jet and 2-Jet Fractions

For various kinematical configurations of the two large transverse momentum jets one can obtain simple relations based on the SES approximation, for example the inclusive single jet fraction f_q, f_g and also the 2-jet fractions f_{qg}, f_{qq} and f_{gg} . These fractions measure simple combinations of the structure functions and remarkably there are simple relationships between the two jet and inclusive single jet fractions. These results only depend on the geometrical progression which was obtained in (2.4) and this may be also considered to directly reflect the nature of the underlying theory. To obtain the inclusive single-jet fraction let us assume that the cross-section for producing quark jets is

$$\begin{aligned} \sigma_q(pp) = & N_f g(x_1)g(x_2)\hat{\sigma}_{gg \rightarrow q\bar{q}} + \\ & [u(x_1)u(x_2) + d(x_1)d(x_2)]\hat{\sigma}_{q_1q_1 \rightarrow q_1q_1} + \\ & [u(x_1)d(x_2) + u(x_2)d(x_1)]\hat{\sigma}_{q_1q_2 \rightarrow q_1q_2} + \\ & \frac{1}{2} [g(x_1)(u(x_2) + d(x_2)) + g(x_2)(u(x_1) + d(x_1))] \hat{\sigma}_{qg \rightarrow qg}, \end{aligned}$$

and similarly for $p\bar{p}$ interactions,

$$\begin{aligned} \sigma_q(p\bar{p}) = & N_f g(x_1)g(x_2)\hat{\sigma}_{gg\rightarrow q\bar{q}} + \\ & [u(x_1)u(x_2) + d(x_1)d(x_2)] [\hat{\sigma}_{q_1\bar{q}_1\rightarrow q_1\bar{q}_1} + (N_f - 1)\hat{\sigma}_{q_1\bar{q}_1\rightarrow q_2\bar{q}_2}] \\ & + [u(x_1)d(x_2) + u(x_2)d(x_1)] \hat{\sigma}_{q_1\bar{q}_2\rightarrow q_1\bar{q}_2} + \\ & \frac{1}{2} [g(x_1)(u(x_2) + d(x_2)) + g(x_2)(u(x_1) + d(x_1))] \cdot \hat{\sigma}_{qg\rightarrow qg}. \end{aligned}$$

Then

$$\begin{aligned} f_q(p\bar{p}) &= \frac{\sigma_q(p\bar{p})}{\sigma(p\bar{p})} \\ f_q(pp) &= \frac{\sigma_q(pp)}{\sigma(pp)}. \end{aligned} \quad (2.10)$$

$\sigma(p\bar{p})$ and $\sigma(pp)$ are calculated from the equations which are given in (2.5) and (2.6).

By applying equation (2.7) one can obtain

$$\begin{aligned} f_q(\text{SES}) &= \frac{u(x_1) + d(x_1)}{2F(x_1)} + \frac{u(x_2) + d(x_2)}{2F(x_2)} \\ &= \frac{1}{2} [f_q(x_1) + f_q(x_2)], \end{aligned} \quad (2.11)$$

and similarly

$$\begin{aligned} f_g(\text{SES}) &= \frac{9g(x_1)}{8F(x_1)} + \frac{9g(x_2)}{8F(x_2)} \\ &= \frac{1}{2} [f_g(x_1) + f_g(x_2)]. \end{aligned} \quad (2.12)$$

The angular integration in the numerator cancels with the angular integration in the denominator in the ratios of f_q and f_g . Thus the inclusive fraction of quark (gluon) jets in this configuration is roughly just the fractional contribution of quark (gluon) distribution to the effective structure function. In particular the measurement of the fraction of gluon or fraction of quark can be immediately converted to an estimate of the following ratio,

$$\frac{u(x) + d(x)}{g(x)}.$$

For the 2-jet fractions one can, for instance, consider the cross-section which involves only quarks in the final state in $p\bar{p}$ and pp interactions,

$$\sigma_{qq}(p\bar{p}) = [u(x_1)d(x_2) + u(x_2)d(x_1)] \hat{\sigma}_{q_1\bar{q}_2 \rightarrow q_1\bar{q}_2} = \\ [u(x_1)u(x_2) + d(x_1)d(x_2)] \left[\hat{\sigma}_{q_1\bar{q}_1 \rightarrow q_1\bar{q}_1} + (N_f - 1) \hat{\sigma}_{q_1\bar{q}_1 \rightarrow q_2\bar{q}_2} \right],$$

and for pp interaction,

$$\sigma_{qq}(pp) = [u(x_1)d(x_2) + u(x_2)d(x_1)] \hat{\sigma}_{q_1q_2 \rightarrow q_1q_2} \\ + [u(x_1)u(x_2) + d(x_1)d(x_2)] \hat{\sigma}_{q_1q_1 \rightarrow q_1q_1}$$

We define

$$f_{qq}(p\bar{p}) = \frac{\sigma_{qq}(p\bar{p})}{\sigma(p\bar{p})} \\ f_{qq}(pp) = \frac{\sigma_{qq}(pp)}{\sigma(pp)}. \quad (2.13)$$

By applying the SES approximation one can find

$$f_{qq}(SES) = \frac{[u(x_1) + d(x_1)]}{F(x_1)} \frac{[u(x_2) + d(x_2)]}{F(x_2)} \\ = f_q(x_1) f_q(x_2). \quad (2.14)$$

In the same manner one can show

$$f_{gg}(SES) = f_g(x_1) f_g(x_2) \\ f_{qg}(SES) = f_q(x_1) f_g(x_2) + f_g(x_1) f_q(x_2). \quad (2.15)$$

The relations (2.11), (2.12), (2.14) and (2.15) are independent of the initial state structure functions. The angular integration factors which are coming from the subprocesses cancel for each f individually, there is no requirement of similar angular acceptance, in the subprocess centre-of-mass frame, for the different (laboratory) kinematical configurations included in the above relations. A complication for the relations (2.11), (2.12), (2.14) and (2.15), which link processes with different kinematics are the effects which arise from the non-scaling in the structure function. This may be different from one quantity to another. For example if the large momentum scale is defined by \hat{s} , then the above relation contains a mixture of $Q^2 = x_1x_2s, x_1^2s, x_2^2s$ for fixed s , rather than being evaluated at a common value.

If one defines the scale Q by \hat{t} or some other variable which varies with the subprocess scattering angle, a similar comment applies. Further complications may arise if the different subprocesses are related with different Q^2 's. All these difficulties disappear asymptotically.

In tables (2.5) and (2.6) we have considered f_q in pp and $p\bar{p}$ interactions, and compared the real f_q which was computed in the absence of the single effective subprocess approximation by using equations which are given in (2.10) and all subprocesses, with the $f_q(\text{SES})$ which was obtained from the single effective subprocess approximation. For pp and $p\bar{p}$ interactions the approximation is good to within $\sim 10\%$ over the whole range of $x_{1,2}$. We used the set 1 Duke and Owens structure functions of ref. [4]. Also demonstrated by these tables is the fact that the θ^* -dependence in $\sigma_q(pp)$ and $\sigma_q(p\bar{p})$ is very similar to the angular distribution for $\sigma(pp)$ and $\sigma(p\bar{p})$ and hence this angular factor roughly cancels in the ratios of $\sigma_q(pp)/\sigma(pp)$ and $\sigma_q(p\bar{p})/\sigma(p\bar{p})$ leading to an independence of f_q on χ . In tables (2.7) and (2.8) we show the comparison between the real f_g computed from all the $2 \rightarrow 2$ QCD subprocesses for pp and $p\bar{p}$ interactions and $f_g(\text{SES})$ which was computed from the single effective subprocess approximation. It is clear that the results which are obtained from the single effective subprocess approximation do not agree with the real results at large values of $x_{1,2}$. This is because the subprocess $q\bar{q} \rightarrow gg$ gives a large contribution at large values of x_1, x_2 and this effect is larger in $p\bar{p}$ than pp interactions because the $p\bar{p}$ interaction involves the subprocess $q\bar{q} \rightarrow \bar{g}g$ as a significant source of large- x gluons. This effect becomes large if one moves to the transverse plane, that is $\chi = 1$.

In table (2.9) we have compared the actual f_{qg} for pp and $p\bar{p}$ interactions computed by using all subprocesses with $f_{qg}(\text{SES})$ which was calculated in the single effective subprocess approximation, again one can see a very good agreement over the whole range of $x_{1,2}$ and we assumed $\chi = 10$.

In table (2.10) we show the comparison between the 2-jet fraction, f_{qq} , in pp and $p\bar{p}$ interactions, these fractions were calculated from the $2 \rightarrow 2$ QCD subprocesses and we used the structure function in ref. [4], and are compared with SES approximation.

In table (2.11) we have compared with 2-jet fraction f_{gg} calculated by the single effective subprocess approximation and calculated by using all the $2 \rightarrow 2$ QCD subprocesses for pp and $p\bar{p}$ interactions. There is very good agreement between $f_{gg}(\text{SES})$ and the actual f_{gg} for pp . But the real f_{gg} is not quite so favourable for $p\bar{p}$, at large values of $x_{1,2}$, for the same reason discussed before.

Unfortunately fragmentation properties of quarks and gluons jets are very similar and it would be hard to measure the f 's experimentally and check the simple SES results.

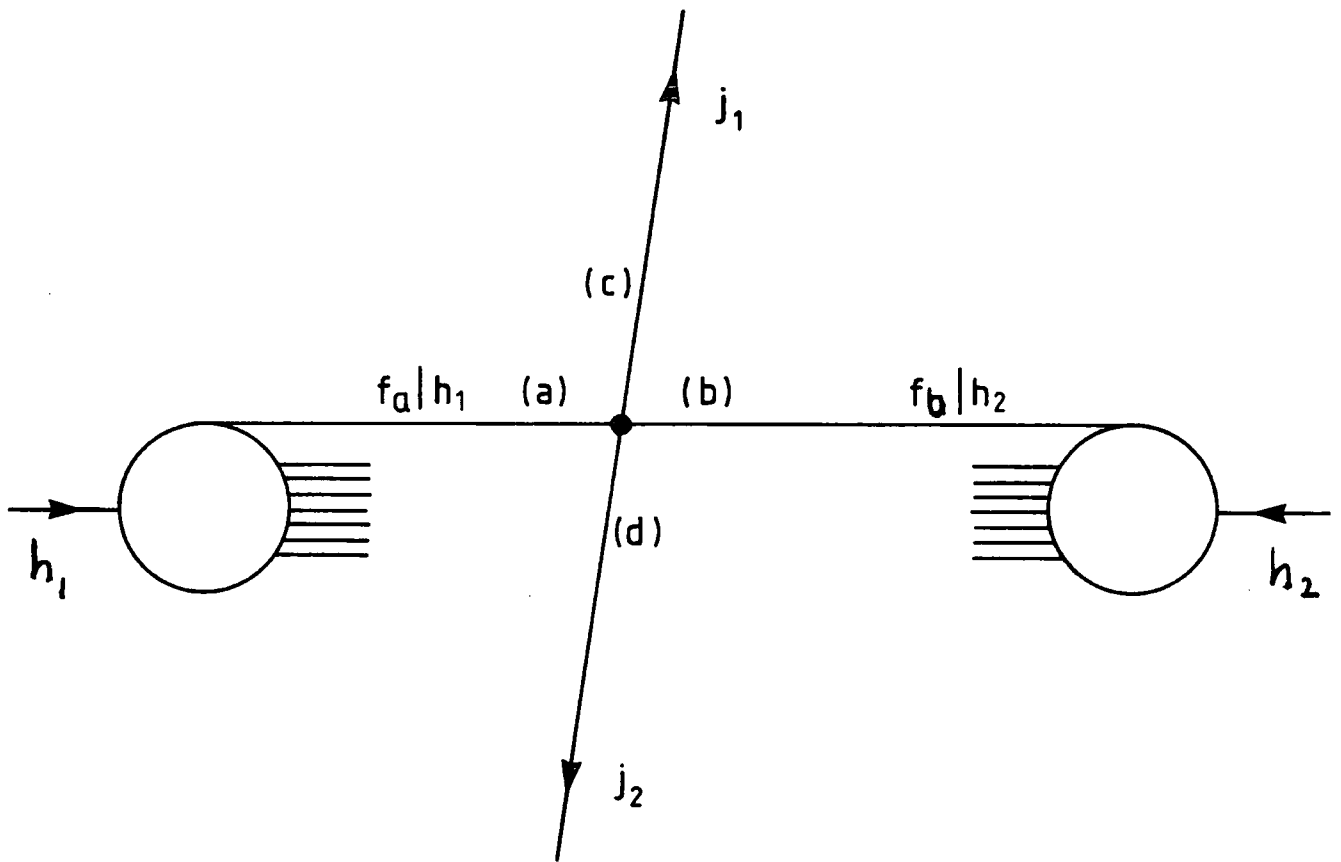


Figure 2.1 : The Hard-Scattering Ansatz

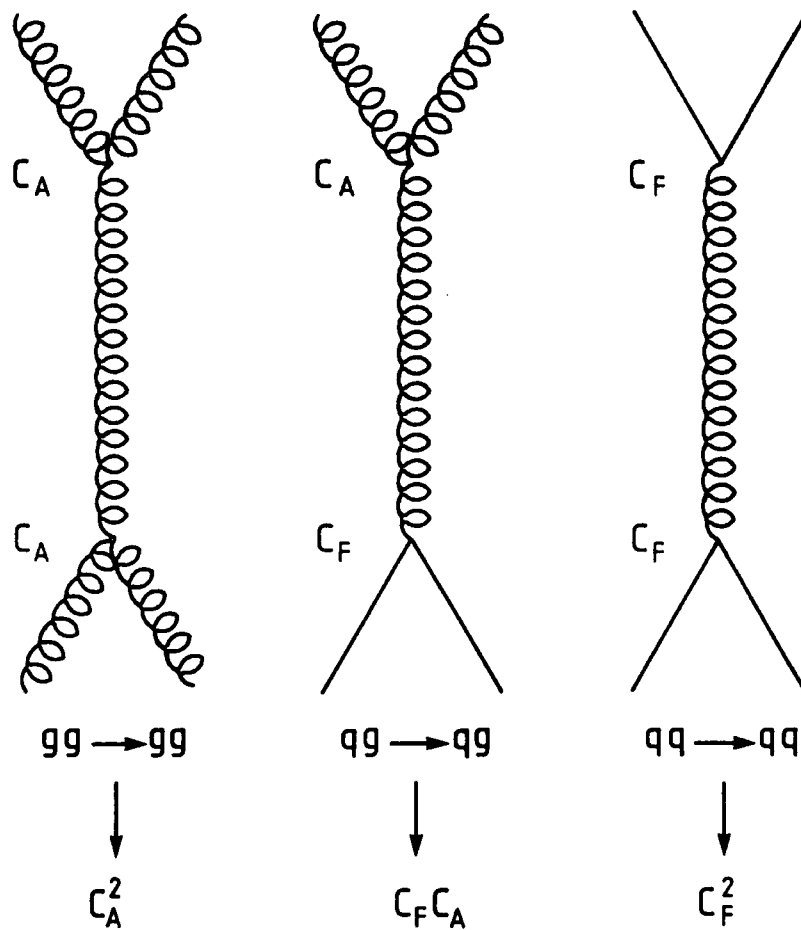


Figure 2.2 : Colour factors of the dominant subprocesses

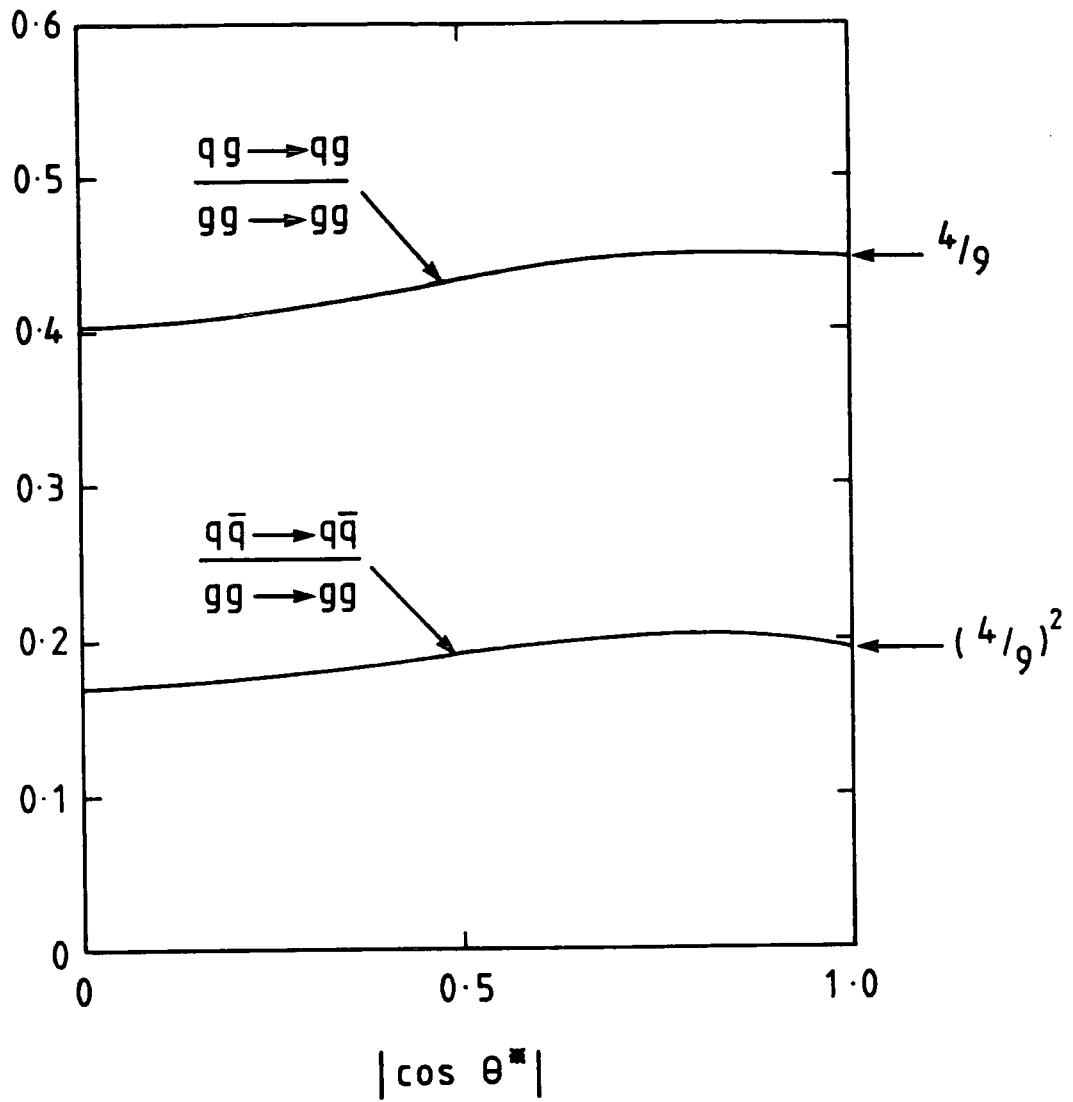


Figure 2.3 : The $|\cos \theta^*|$ dependence of $qg \rightarrow qg$ and $q\bar{q} \rightarrow q\bar{q}$ normalised to $gg \rightarrow gg$.

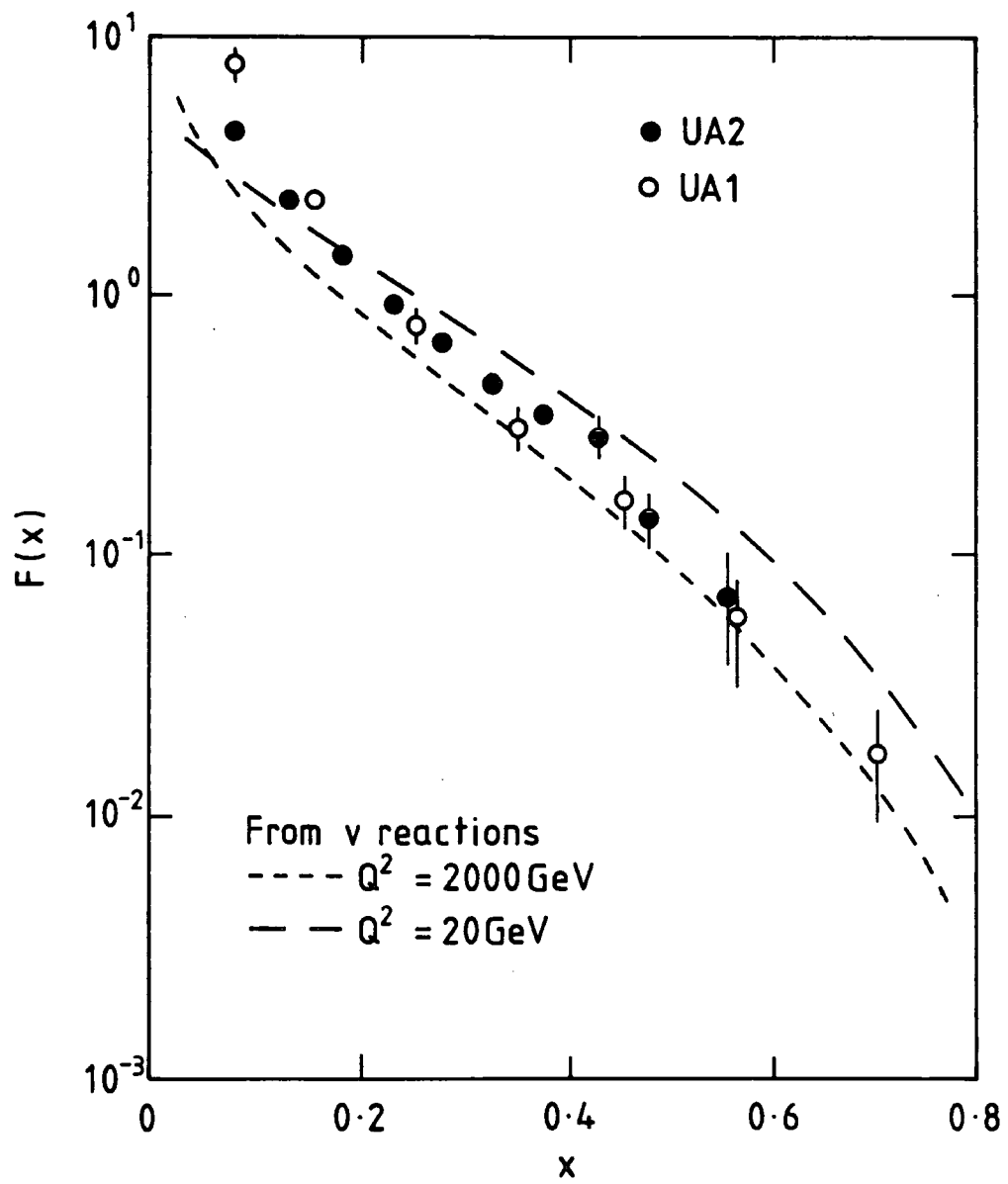


Figure 2.4 : UA1 and UA2 data on the effective structure function $F(x)$

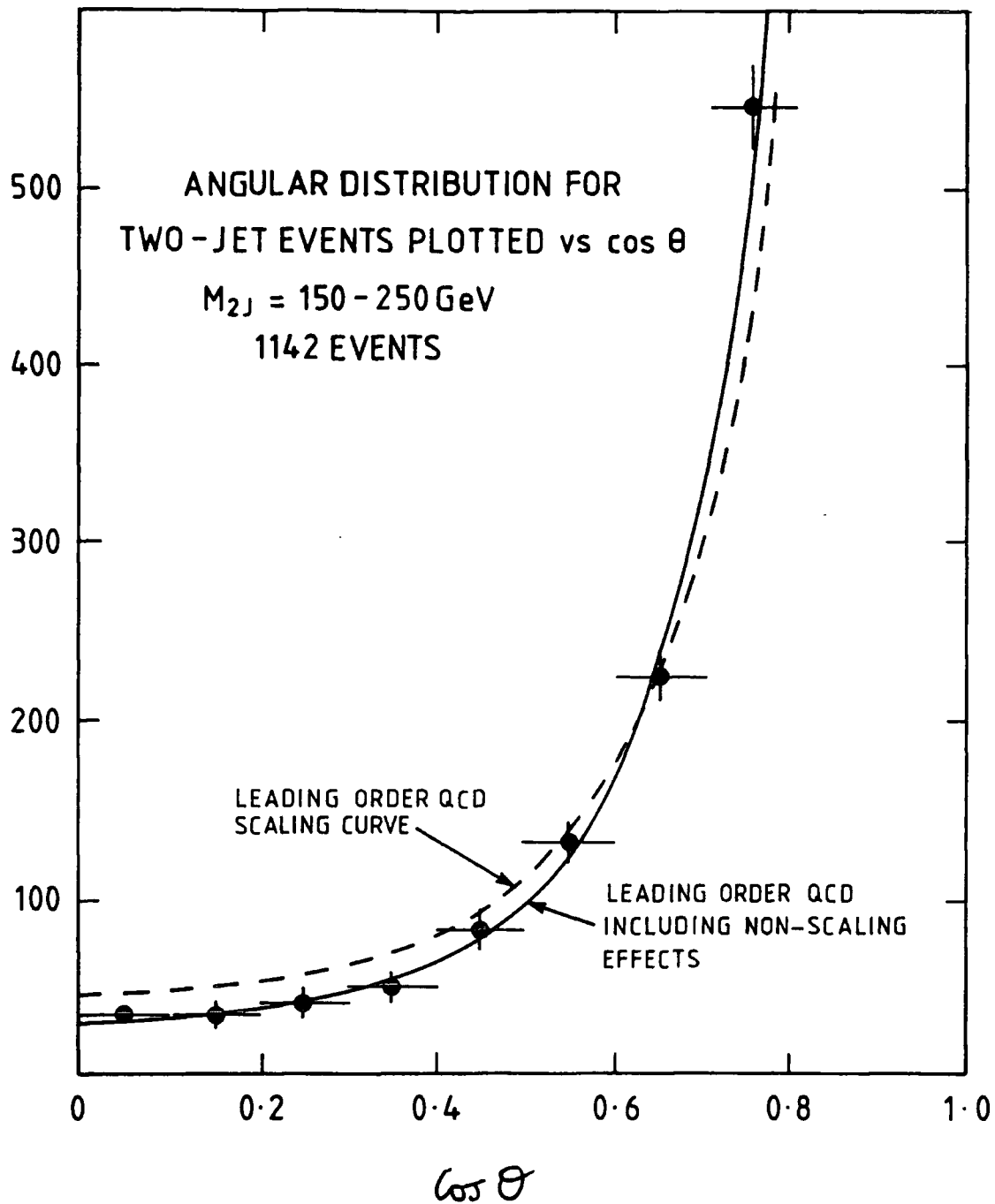


Figure 2.5 : UA1 data on angular distribution of two-jet events versus $\cos \theta$

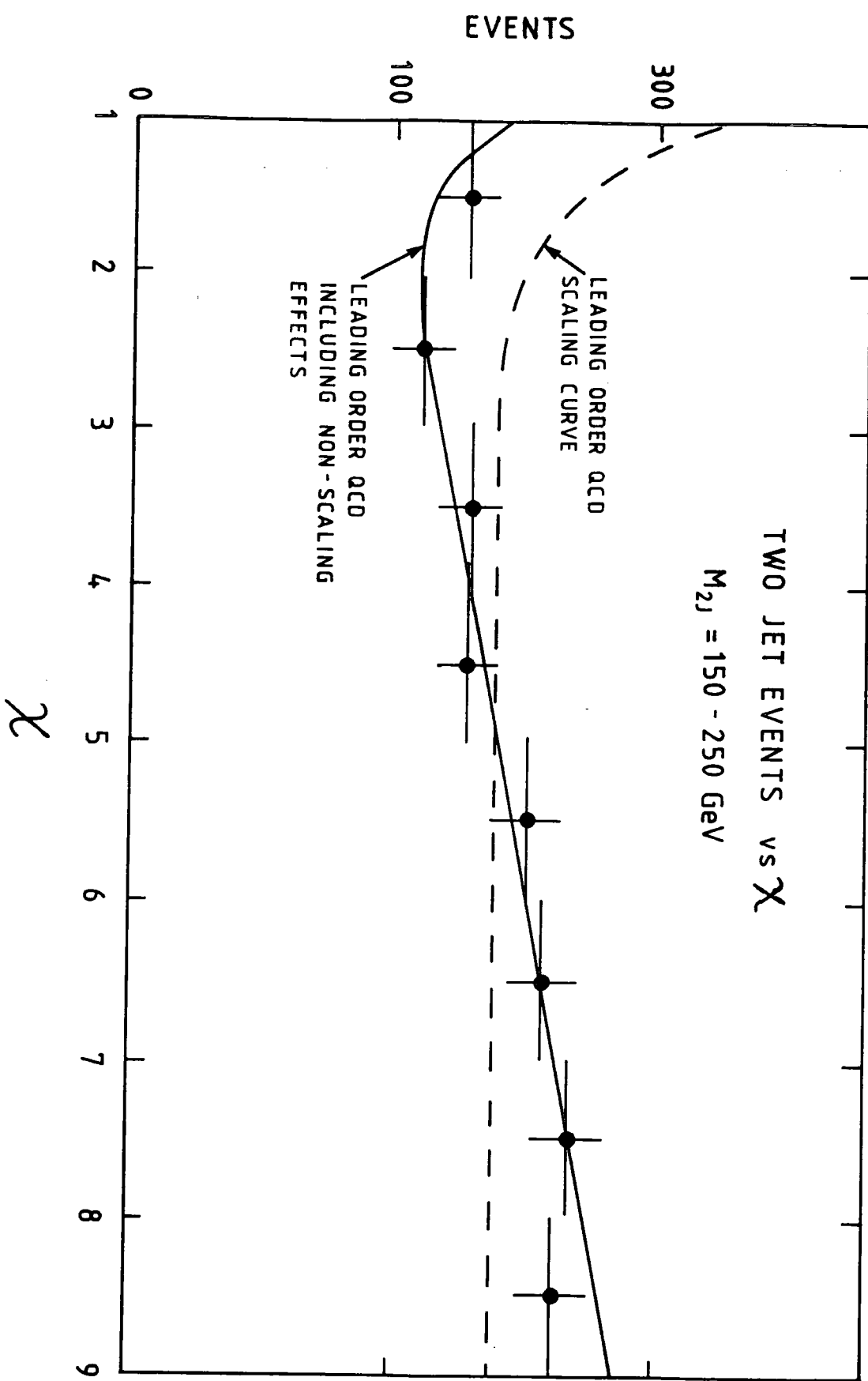


Figure 2.6 : Angular distribution of two-jet events plotted versus the variable χ

Parton Subprocess	$\Sigma = (2\hat{s}/\pi\alpha_s^2).d\hat{\sigma}/d\cos\theta$
$q_1 q_2 \rightarrow q_1 q_2$	$\frac{4}{9} \frac{\hat{s}^2 + \hat{u}^2}{\hat{t}^2}$
$q_1 \bar{q}_2 \rightarrow q_1 \bar{q}_2$	$\frac{4}{9} \frac{\hat{s}^2 + \hat{u}^2}{\hat{t}^2}$
$q_1 q_1 \rightarrow q_1 q_1$	$\frac{4}{9} \left(\frac{\hat{s}^2 + \hat{u}^2}{\hat{t}^2} + \frac{\hat{s}^2 + \hat{t}^2}{\hat{u}^2} \right) - \frac{8}{27} \frac{\hat{s}^2}{\hat{t}\hat{u}}$
$q_1 \bar{q}_1 \rightarrow q_2 \bar{q}_2$	$\frac{4}{9} \frac{\hat{t}^2 + \hat{u}^2}{\hat{s}^2}$
$q_1 \bar{q}_1 \rightarrow q_1 \bar{q}_1$	$\frac{4}{9} \left(\frac{\hat{s}^2 + \hat{u}^2}{\hat{t}^2} + \frac{\hat{t}^2 + \hat{u}^2}{\hat{s}^2} \right) - \frac{8}{27} \frac{\hat{u}^2}{\hat{s}\hat{t}}$
$q\bar{q} \rightarrow gg$	$\frac{32}{27} \frac{\hat{u}^2 + \hat{t}^2}{\hat{u}\hat{t}} - \frac{8}{3} \frac{\hat{u} + \hat{t}^2}{\hat{s}^2}$
$gg \rightarrow q\bar{q}$	$\frac{1}{6} \frac{\hat{u}^2 + \hat{t}^2}{\hat{u}\hat{t}} - \frac{3}{8} \frac{\hat{u}^2 + \hat{t}^2}{\hat{s}^2}$
$qg \rightarrow qg$	$-\frac{4}{9} \frac{\hat{u}^2 + \hat{s}^2}{\hat{u}\hat{s}} + \frac{\hat{u}^2 + \hat{s}^2}{\hat{t}^2}$
$gg \rightarrow gg$	$\frac{9}{2} \left(3 - \frac{\hat{u}\hat{t}}{\hat{s}^2} - \frac{\hat{u}\hat{s}}{\hat{t}^2} - \frac{\hat{s}\hat{t}}{\hat{u}^2} \right)$

Table 2.1: Shows the Parton Subprocesses written in terms of \hat{s} , \hat{t} and \hat{u} .

Parton Subprocess	$\Sigma = \hat{s}/\pi\alpha_s^2 \times N_g/C_F^2(1/4)d\hat{\sigma}/d\hat{t}$
$q_1 q_2 \rightarrow q_1 q_2$	$\chi^2 + \chi^{-2} + \chi^{-1} + \chi + 1$
$q_1 \bar{q}_2 \rightarrow q_1 \bar{q}_2$	$\chi^2 + \chi^{-2} + \chi^{-1} + \chi + 1$
$q_1 q_1 \rightarrow q_1 q_1$	$\chi^2 + \chi^{-2} + \chi^{-1} + \chi + 1 - N_c^{-1}(\chi + \chi^{-1} + 2)$
$q_1 \bar{q}_1 \rightarrow q_2 \bar{q}_2$	$(1 + \chi^2)(1 + \chi)^{-2}$
$q_1 \bar{q}_1 \rightarrow q_1 \bar{q}_1$	$\chi^2 + \chi^{-2} + \chi + \chi^{-1} + 1 + N_c^{-1}(\chi + \chi^{-1}) - (1 + \chi^2)(1 + \chi)^{-2}$
$q\bar{q} \rightarrow gg$	$\frac{N_g C_A}{2C_F} \left[\frac{C_F}{C_A} (\chi + \chi^{-1}) - (1 + \chi^2)(1 + \chi)^{-2} \right]$
$gg \rightarrow q\bar{q}$	$\frac{4C_F^2 C_A}{N_g} N_c \left[\frac{C_F}{C_A} (\chi + \chi^{-1}) - (1 + \chi^2)(1 + \chi)^{-2} \right]$
$qg \rightarrow qg$	$\frac{C_A}{C_F} \left[\chi^2 + \chi^{-2} + \chi + \chi^{-1} + 1 + \frac{C_F}{C_A} \left(\frac{1}{2}\chi + \frac{1}{2}\chi^{-1} + \frac{3}{2} \right) \right]$
$gg \rightarrow gg$	$\frac{C_A^2}{C_F^2} \left[\chi^2 + \chi^{-2} + \chi + \chi^{-1} + 3 - \chi(1 + \chi)^{-2} \right]$

Table 2.2: Shows the Parton subprocesses which are written in terms of the angular variable, χ . $C_F = \frac{N_c^2 - 1}{2N_c}$, $C_A = N_c$ and $N_g = N_c^2 - 1$.

x_1	.10	.10	.15	.15	.20	.25	.25	.30	.40
x_2	.10	.50	.15	.35	.20	.25	.50	.30	.40
$F(x_1)F(x_2)$	2.51	.106	.93	.199	.403	.182	.027	.085	.02
R_1	2.44	.094	.90	.178	.370	.162	.023	.073	.016
R_2	2.46	1.00	.93	.191	.390	.177	.027	.084	.02

Table 2.3: At $\chi = 1$, $R_1 = \sigma(pp)/\hat{\sigma}_{gg \rightarrow gg}$, $\sqrt{s} = 540$ GeV, $R_2 = \sigma(p\bar{p})/\hat{\sigma}_{gg \rightarrow gg}$

x_1	.10	.10	.15	.15	.20	.25	.25	.30	.40
x_2	.10	.50	.15	.35	.20	.25	.50	.30	.40
$F(x_1)F(x_2)$	2.51	.106	.93	.199	.403	.182	.027	.085	.02
R_1	2.52	.107	.96	.20	.405	.183	.027	.085	.02
R_2	2.54	.109	.97	.20	.412	.190	.029	.089	.02

Table 2.4: At $\chi = 10$, other details as Table 2.3

x_1	.10	.10	.15	.20	.20	.25	.30	.40	.45	.50
x_2	.10	.50	.35	.20	.35	.35	.30	.40	.45	.50
$f_q(\text{SES})$.18	.52	.48	.38	.53	.59	.59	.76	.82	.87
$f_q(p\bar{p})$.18	.51	.47	.38	.52	.59	.59	.70	.74	.77
$f_q(pp)$.17	.50	.45	.36	.50	.55	.55	.72	.80	.85

Table 2.5: At $\chi = 5$, $\sqrt{s} = 540$ GeV

	.10	.10	.15	.20	.20	.25	.30	.40	.45	.50
	.10	.50	.35	.20	.35	.35	.30	.40	.45	.50
$f_q(\text{SES})$.18	.52	.48	.38	.53	.59	.59	.76	.82	.87
$f_q(p\bar{p})$.18	.51	.47	.38	.52	.57	.57	.71	.76	.80
$f_q(pp)$.18	.52	.48	.38	.53	.58	.58	.75	.82	.87

Table 2.6: At $\chi = 10$, $\sqrt{s} = 540$ GeV

[These tables show a comparison between the $f_q(\text{SES})$ and the actual f_q for pp and $p\bar{p}$ interactions].

x_1	.10	.10	.15	.20	.20	.25	.30	.40	.45	.50
x_2	.10	.50	.35	.20	.35	.35	.30	.40	.45	.50
$f_g(SES)$.82	.48	.52	.62	.48	.41	.41	.24	.18	.13
$f_g(p\bar{p})$.82	.49	.53	.62	.48	.41	.41	.30	.26	.23
$f_g(pp)$.83	.50	.55	.64	.50	.45	.45	.28	.21	.15

Table 2.7: At $\chi = 5$, $\sqrt{s} = 540$ GeV

x_1	.10	.10	.15	.20	.20	.25	.30	.40	.45	.50
x_2	.10	.50	.35	.20	.35	.35	.30	.40	.45	.50
$f_g(SES)$.82	.48	.52	.62	.47	.41	.41	.24	.18	.13
$f_g(p\bar{p})$.82	.49	.53	.62	.48	.43	.43	.29	.24	.20
$f_g(pp)$.82	.48	.42	.63	.47	.42	.41	.25	.18	.13

Table 2.8: At $\chi = 10$, $\sqrt{s} = 540$ GeV.

x_1	.10	.10	.15	.20	.20	.25	.30	.40	.45	.50
x_2	.10	.50	.35	.20	.35	.35	.30	.40	.45	.50
$f_{qg}(SES)$.289	.719	.569	.473	.537	.500	.481	.369	.298	.231
$f_{qg}(pp)$.288	.721	.572	.474	.539	.502	.487	.374	.302	.253
$f_{qg}(p\bar{p})$.287	.708	.560	.466	.523	.488	.468	.349	.278	.213

Table 2.9: Shows the agreement of $f_{qg}(SES)$ and the actual f_{qg} which are computed from all the $2 \rightarrow 2$ QCD subprocesses for $p\bar{p}$ and pp interactions at $\sqrt{s} = 540$ GeV and $\chi = 10$.

x_1	.10	.10	.15	.20	.20	.25	.30	.40	.45	.50
x_2	.10	.50	.35	.20	.35	.35	.30	.40	.45	.50
$f_{qq}(SES)$.031	.076	.191	.147	.263	.240	.349	.572	.669	.751
$f_{qq}(pp)$.033	.075	.187	.144	.258	.236	.343	.566	.664	.747
$f_{qq}(p\bar{p})$.03	.075	.187	.145	.256	.234	.337	.540	.625	.694

Table 2.10: Gives the comparison between the $f_{qq}(SES)$ which are obtained from SES approximation and the real f_{qq} which was computed using all the subprocesses for pp and $p\bar{p}$ interactions at $\sqrt{s} = 540$ and $\chi = 10$.

x_1	.10	.10	.15	.20	.20	.25	.30	.40	.45	.50
x_2	.10	.50	.35	.20	.35	.35	.30	.40	.45	.50
$f_{gg}(s)$.680	.205	.240	.380	.200	.260	.170	.059	.03	.02
$f_{gg}(pp)$.682	.204	.241	.380	.203	.262	.170	.060	.03	.02
$f_{gg}(p\bar{p})$.683	.220	.253	.390	.221	.290	.160	.100	.097	.09

Table 2.11: Shows the comparison between the f_{gg} which was computed by the SES approximation and the actual f_{gg} which was calculated in non-SES approximation using the $2 \rightarrow 2$ QCD subprocesses for pp and $p\bar{p}$ interactions at $\sqrt{s} = 540$ GeV and $\chi = 10$.

REFERENCES

- [1] B.L. Combridge, J. Kripfganz and J. Ranft, Phys. Lett. B70, (1977), 234.
- [2] B.L. Combridge and C.J. Maxwell, Nucl Phys. B239, (1984), 429.
- [3] J.F. Owens, Florida preprint, FSU HEP 780609, (1978).
- [4] D.W. Duke and J.F. Owens, Phys. Rev. 1230 (1984), 49.
- [5] UA2 Collaboration, P. Bagnaia et al., Phys. Lett. B144 (283), (1984).
- [6] UA1 Collaboration, G. Arnison et al., Phys. Lett. B136 (1984), 294.
- [7] UA1 Collaboration, G. Arnison et al., Phys. Lett. B158 (1984), 495.

Chapter 3

Three-Jet Production

3.1 $2 \rightarrow 3$ Large- P_T Hadronic Jets

We have discussed in Chapter 2 some interesting features to be found at high transverse momentum for events with 2 jets in hadronic collisions. The presence of \hat{t} -channel gluon exchange in all the important QCD $2 \rightarrow 2$ hard scatterings leads to an approximately common angular dependence and hence the total cross-section for producing 2 jets can be understood by only a single subprocess and an effective structure function.

In three-jet production there are eleven $\hat{\sigma}_{ab \rightarrow cde}$ $2 \rightarrow 3$ parton-parton scattering subprocesses. All have been calculated at tree-level $O(\alpha_s^3)$ by Berends et al. [1], but no higher order corrections have been calculated or are in prospect.

The six Mandelstam variables required to describe the $2 \rightarrow 3$ QCD subprocesses can be defined as the following:

$$\begin{aligned} s &= (p_1 + p_2)^2 \\ s' &= (q_1 + q_2)^2 \\ t &= (p_1 - q_1)^2 \\ t' &= (p_2 - q_2)^2 \\ u &= (p_1 - q_2)^2 \\ u' &= (p_2 - q_1)^2 \end{aligned} \tag{3.1}$$

One can write down fairly compact expressions for them [1], for example, a subprocess like $gg \rightarrow ggg$ involves 25 Feynman diagrams and the matrix element squared is given by the following simple form

$$|M(gg \rightarrow ggg)|^2 = \frac{g^6}{2} \frac{N_c^4}{N_c^2 - 1} \sum_{i < j} (ij)^4 \frac{\Sigma(ijklm)}{\Pi(ij)}. \tag{3.2}$$

The notation $(ijklm)$ in the above expression means $(ij)(jk)(kl)(lm)(mi)$, where (ij) denotes the dot product of four-momenta $(p_i \cdot p_j)$.

For quark-quark scattering with different flavours $q_1(p_1) + q_2(p_2) \rightarrow q_1(q_1) + q_2(q_2) + g(k)$,

$$|M|^2 = \frac{1}{8} g^6 [(s^2 + s'^2 + u^2 + u'^2) [(p_1 k)(p_2 k)(q_1 k)(q_2 k)]^{-1} \times \\ \{C_1 [(u + u')(s\bar{s} + tt' - uu') + u(st + s't') + u'st' + s't]\} \\ - C_2 [(s + s')(ss' - tt' - uu') + 2tt'(u + u') + 2uu'(t + t')]\} \quad (3.3)$$

C_1 and C_2 which appear in expression (3.3) are the colour factors and are given by the following definitions

$$C_1 = (N_c^2 - 1)^2 / 4N_c^3, C_2 = (N_c^2 - 1) / 4N_c^3$$

For the process $q(p_1) + \bar{q}(p_2) \rightarrow g(k_1) + g(k_2) + g(k_3)$, the matrix element squared is simpler and given by

$$|M|^2 = g^6 \frac{(N_c^2 - 1)}{4N_c^4} \left(\sum_{i=1}^3 A_i B_i (A_i^2 + B_i^2) A_1 A_2 A_3 B_1 B_2 B_3 \right) \times \\ \left[s/2 + N_c^2 \left(s/2 - \frac{X_1}{(k_1 k_2)} - \frac{X_2}{(k_2 k_3)} - \frac{X_3}{(k_1 k_3)} \right) \right. \\ \left. + 2N_c^4 / s \left(\frac{A_3 B_3 X_1}{(k_2 k_3)(k_1 k_3)} + \frac{A_1 B_1 X_2}{(k_1 k_3)(k_1 k_2)} + \frac{A_2 B_2 X_3}{(k_1 k_2)(k_2 k_3)} \right) \right] \quad (3.4)$$

The functions X_1, X_2 and X_3 in the expression (3.4) are

$$X_1 = A_1 B_2 + A_2 B_1 \\ X_2 = A_2 B_3 + A_3 B_2 \\ X_3 = A_3 B_1 + A_1 B_3,$$

where $A_i = (p_1 k_i), B_i = (p_2 k_i), i = 1, 2, 3$.

In table (3.1) we have represented the matrix elements squared for the 2→3 QCD subprocesses of ref. [1].

3.2 Data on the 2→3 Angular Distribution

Three jet events have been experimentally isolated in UA1 and UA2 data at the CERN collider and found to have angular distributions in reasonable accord with the lowest order QCD expectation. In figure (3.1) we show the three-jet Dalitz plot x_3 versus x_4 for events with three-jets [2]. The x_i ($i = 3, 4, 5$) are the fractional

energies of the outgoing partons, ordered so that $x_3 > x_4 > x_5$ and scaled to the total subprocess CMS energy such that $x_3 + x_4 + x_5 = 2$.

It is clear that the density of events is significantly non-uniform over the range explored on the Dalitz plot. The event density increases as x_4 increases, for fixed x_3 at $\sim .85$, also for fixed x_4 at $\sim .60$ - $.80$ the event density increases significantly as x_3 increases, but less than the situation with x_3 fixed.

The solid curves which are shown in figure (3.1) normalised to data show the predicted distribution in the fractional energy x_3 and x_4 based on the single QCD bremsstrahlung formulae, and the curves shown have been summed over the contributing subprocesses. The dominant subprocesses like $qq \rightarrow qqg, qg \rightarrow qgg$ and $gg \rightarrow ggg$ are predicted to have a very similar fractional energy (x_3 and x_4) dependence over this range. The dashed curves show the corresponding phase space distribution computed assuming a constant matrix element. The conclusion is that the dominant subprocesses in the 3-jet events have very similar angular distributions. Clearly the data, which are shown here, are consistent with the predictions of QCD formulae, and inconsistent with a pure phase-space distribution.

3.3 Measurement of QCD Coupling Constant

The coupling constant α_s can be measured in a simple way by taking the ratio of 3-jet production to the 2-jet cross-section. If the invariant mass of the 3-jet production is the same as that of the 2-jet production the luminosity uncertainties, energy scale uncertainties, etc. tend to cancel in this ratio.

In practice the main problem is that the higher order perturbative corrections have not been computed for the 3-jet and 2-jet cross-sections. Then one determines not the coupling constant α_s , but rather $\alpha_s \frac{K_3}{K_2}$, where K_3 and K_2 are unknown "K-factors" associated with 3-jet and 2-jet production.

The experiments [2,3] give information on the measurement of the QCD coupling constant and show a significantly larger value for α_s than other measurements.

The UA2 collaboration quote [2]

$$\alpha_s \frac{K_3}{K_2} = .23 \pm .04 \pm .04$$

and the UA1 collaboration find [3]

$$\alpha_s \frac{K_3}{K_2} = .24 \pm .04 \pm .04$$

In the absence of the "K-factor" one would have anticipated $\alpha_s \sim .15$ at the $\langle Q^2 \rangle = 4000 \text{ GeV}^2$ relevant to this determination.

3.4 Common Angular Dependence of 3-jet Production

To highlight the common angular distributions we show in Table (3.2) the lowest-order QCD $2 \rightarrow 3$ subprocesses normalised to the dominant subprocess $gg \rightarrow ggg$. We have summed over the possible assignments of partons to jets. The x_i 's denote the fractional energy of jets in the subprocesses, $\sum_{i=1}^3 x_i = 2$. We consider transverse events with 3-jets at 90° to the beam in the subprocess centre-of-mass frame. We used the $\hat{\sigma}_{ab \rightarrow cde}$ expressions in ref. [1] with three colours and assumed $N_f = 5$ quark flavours. We consider four kinematical configurations ranging from the centre of the transverse Dalitz plot, to the edges of the Dalitz plot. Although the absolute values of the rates vary by several orders of magnitude across the transverse 3-jet Dalitz plot the relative rates are remarkably constant within 10%. Because of the sum over all the possible final states the ratios should not contain any kinematical poles.

It is noted that the subprocess $qq \rightarrow qqq$, $qg \rightarrow qgg$ and $gg \rightarrow ggg$ are dominant ones and have similar angular and fractional energy distributions [4]. Also the sub-processes which have the t-channel poles like the three subprocesses mentioned are seen to be in approximate geometrical progression [5].

$$gg \rightarrow ggg : qg \rightarrow qgg : qq \rightarrow qqq \simeq 1 : (.28) : (.28)^2$$

These features are similar to the 2-jet SES approximation. However, the constant ratios in table (3.2) occur also for the less dominant subprocesses which do not have \hat{t} -channel poles.

Subprocess	$ M_{2 \rightarrow 3} ^2$
$q_1 q_2 \rightarrow q_1 q_2 g$	$ M_1 ^2(p_1, p_2, q_1, q_2, k)$
$q_1 g \rightarrow q_1 q_2 \bar{q}_2$	$ M_1 ^2(p_1, -k, q_1, q_2, -p_2) (-3/8)$
$q_1 \bar{q}_2 \rightarrow q_1 \bar{q}_2 g$	$ M_1 ^2(p_1, -q_2, q_1, -p_2, k)$
$q_1 \bar{q}_1 \rightarrow q_2 \bar{q}_2 g$	$ M_1 ^2(p_1, -q_1, -p_2, q_2, k)$
$q_1 q_1 \rightarrow q_1 q_1 g$	$ M_2 ^1(p_1, p_2, q_1, q_2, k) (1/2)$
$q_1 g \rightarrow q_1 q_1 \bar{q}_1$	$ M_2 ^2(p_1, -k, q_1, q_2, -p_2) (-3/16)$
$q_1 \bar{q}_1 \rightarrow q_1 \bar{q} g$	$ M_2 ^2(p_1, -q_2, q_1, -p_2, k)$
$q \bar{q} \rightarrow g g g$	$ M_3 ^2(p_1, p_2, k_1, k_2, k_3) (1/6)$
$q g \rightarrow q g g$	$ M_3 ^2(p_1, -k_1, -p_2, k_2, k_3) (-3/16)$
$g g \rightarrow q \bar{q} g$	$ M_3 ^2(-k_1, -k_2, -p_1, -p_2, k_3) (9/64)$
$g g \rightarrow g g g$	$ M_4 ^2(k_1, k_2, k_2, k_4, k_5) (1/6)$

Table 3.1: Shows the eleven 2→3 QCD Subprocesses of ref [1].+ $|M_1|^2, |M_3|^2, |M_4|^2$ are given in equations (3.3), (3.4) and (3.2) respectively

Subprocesses	x_1	.9	.8	2/3
	x_2	.9	.8	2/3
	x_3	.2	.5	2/3
$q_1 q_1 \rightarrow q_1 q_1 g$.050	.050	.060	.070
$q_1 q_2 \rightarrow q_1 q_2 g$.080	.080	.090	.090
$q_1 \bar{q}_1 \rightarrow q_1 \bar{q}_1 g$.130	.130	.140	.140
$q_1 \bar{q}_2 \rightarrow q_1 \bar{q}_2 g$.120	.120	.130	.130
$gg \rightarrow q\bar{q}g$.290	.290	.280	.270
$q\bar{q} \rightarrow ggg$.030	.030	.02	.02
$gg \rightarrow q\bar{q}g$.110	.110	.130	.120
$q_1 g \rightarrow q_1 q_2 \bar{q}_2$.020	.020	.02	.020
$q_1 g \rightarrow q_1 q_1 \bar{q}_1$.00	.010	.010	.010
$q_1 \bar{q}_1 \rightarrow q_2 \bar{q}_2 g$.020	.030	.030	.030

Table 3.2: Transverse 2→3 QCD subprocess cross-sections normalised to $gg \rightarrow ggg$, for various transverse configurations.

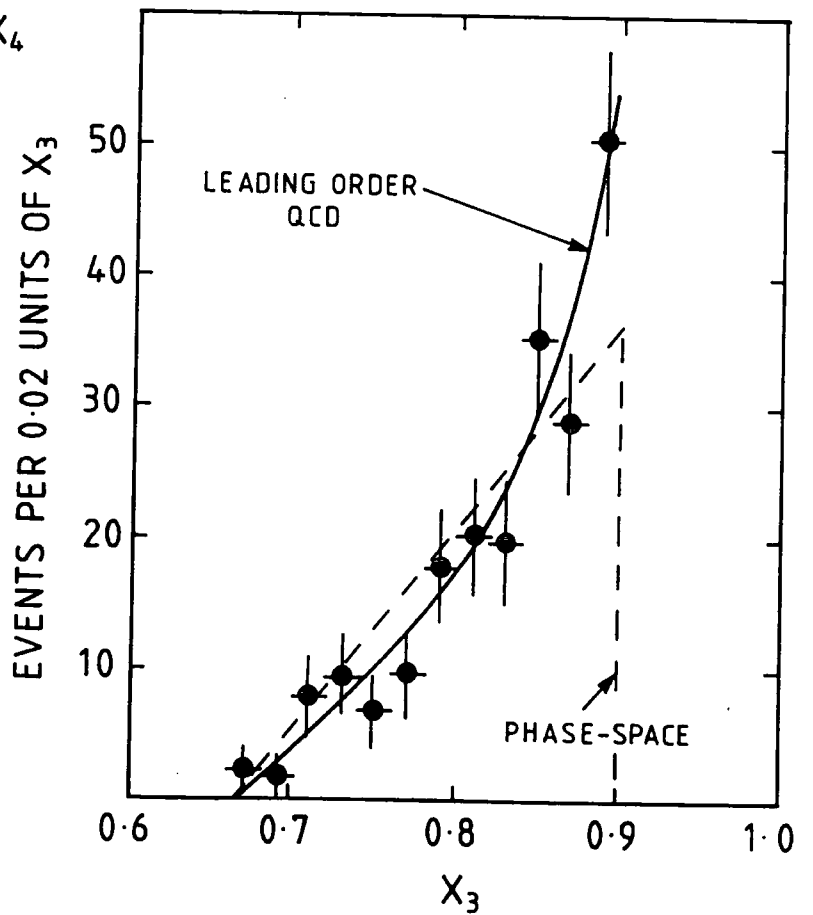
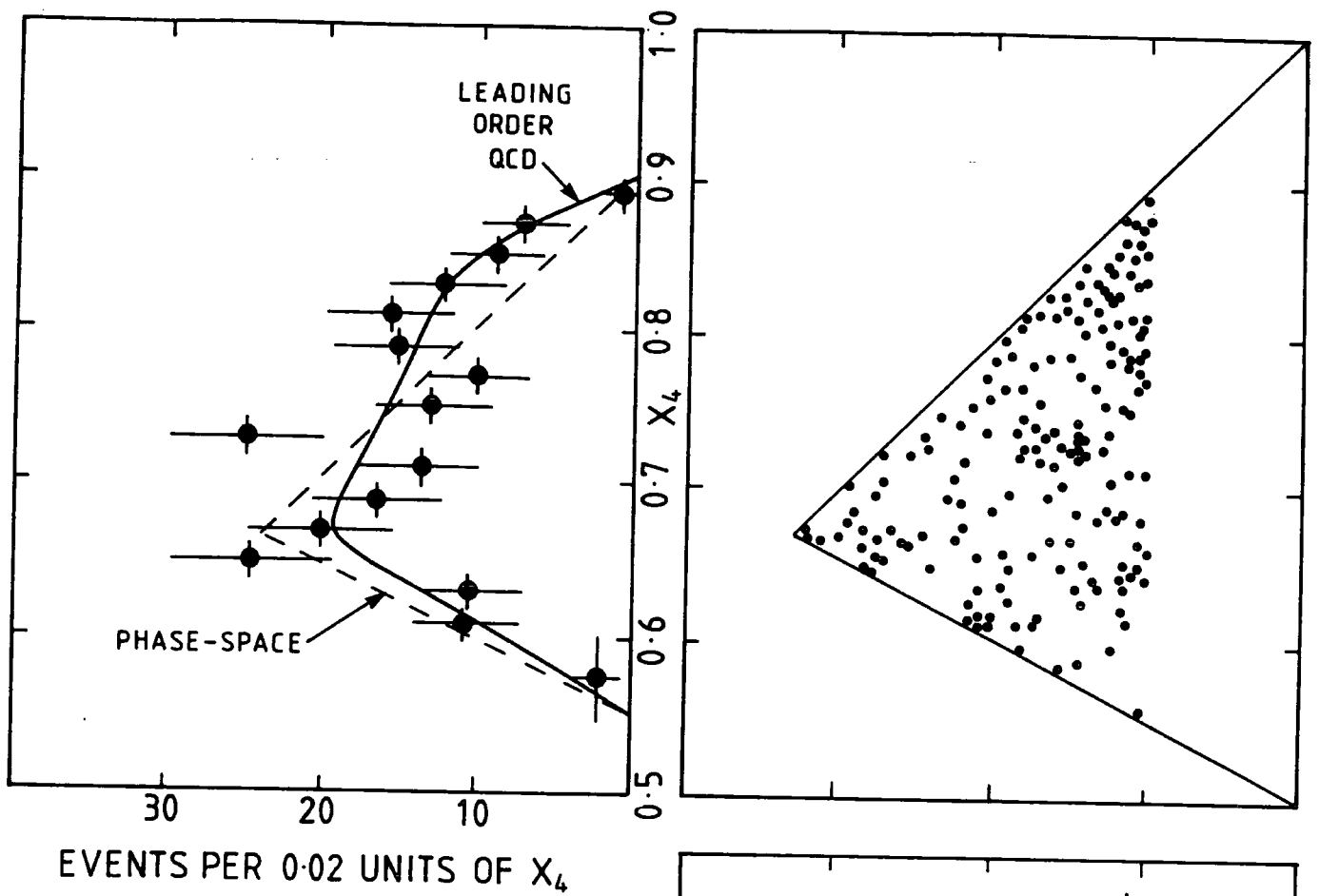


Figure 3.1 : UA1 three-jet data

REFERENCES

- [1] F.A. Berends, R. Kleiss, P. de Causmacker, R. Gastmans and T.T. Wu, Phys. Lett. **B103**, (1981) 124.
- [2] UA1 Collaboration, G. Arnison et al., Phys. Lett. **B158**, (1985), 494.
- [3] UA2 Collaboration, J.A. Appel et al., Z. Phys. **C30**, (1988), 341.
- [4] F. Halzen and P. Hoyer, Phys. Lett. **B130**, (1983), 326.
- [5] B.L. Combridge and C.J. Maxwell, Nucl. Phys. **B239**, (1984), 429.

Chapter 4

The Dokshitzer Relation

In Chapter Three we have shown that in the transverse plane all the 3-jet cross-section subprocesses, including those without t-channel poles, are proportional to each other. These features have no satisfactory explanation. In this chapter we try to understand this proportionality by studying the variation of the ratios which are listed in Chapter 3 around the boundary of the transverse Dalitz plot. In this particular region we consider collinear configurations where half the energy is taken by one jet and the remaining two jets are collinear with the fractional energies z and $(1-z)$. In this configuration one can note that the ratios of the transverse cross-section are finite. The ratios do not contain any kinematical poles. In general for a $2 \rightarrow n$ scattering amplitude in which a pair of final state particles i, j go parallel one has [1] for the full amplitude $|M_n|^2$

$$\lim_{(i,j) \rightarrow 0} (i,j) |M_n|^2 = g^2 P_{ab}(z) |M_{n-1}|^2 \quad (4.1)$$

where we shall denote (p_i, p_j) by (i, j) and g is the QCD running coupling constant ($\alpha_s = g^2/4\pi$). For two gluons of the final state going collinear we set $ab = gg$, if the quark and gluon are collinear we set $ab = qq$ or $ab = gq$, and we set $ab = q\bar{q}$ when the quark and antiquark are collinear. In this limit we consider $i \rightarrow za$ and $j \rightarrow (1-z)a$. "a" being the four momentum $i + j$ and $0 < z < 1$. The amplitude $|M_{n-1}|^2$ is computed with the reduced set of $(n-1)$ momenta obtained by replacing $i + j$ by a .

We have used equation (4.1) to write the $2 \rightarrow 3$ cross-section subprocesses in the collinear limit in terms of $2 \rightarrow 2$ subprocesses and Altarelli-Parisi kernels. In Appendix A we give the analytical expression for the ratios in the collinear limit and these subprocesses are normalised to $gg \rightarrow ggg$. We summed over all the possible final state assignments of partons to jets.

In table (4.1) we show the z -dependence of the $2 \rightarrow 3$ subprocess ratios around the boundary of the transverse Dalitz plot [5].

The functions $f(z)$ and $g(z)$ in table (4.1) are given by

$$f(z) = [P_{qq}(z) + P_{q\bar{q}}(1-z)]/P_{gg}(z),$$

$$g(z) = P_{qg}(z)/P_{gg}(z).$$

In Table 4.2 we show the behaviour of the ratios with z . We assume that $\chi = 1$, $N_c = 3$. It is clear that all the subprocesses vary very slowly over the whole range of z . The ratios of the transverse cross-section have no kinematical poles.

A curious QCD result noted by Dokshitzer [3] is that the splitting kernels are related by the following relation

$$P_{gg}(z) = \frac{9}{4} [P_{qq}(z) + P_{gq}(z)] - 6P_{qg}(z) \quad (4.2)$$

This relationship is rather mysterious, but has been conjectured to be of possible supersymmetric origin [2]. If one chooses the fermion representation in which $C_F = C_A = 2T(R)$ one can obtain the explicitly quark-gluon symmetric relation

$$P_{gg} + P_{qg} = P_{qq} + P_{gq} \quad (4.3)$$

The quantities on the right hand side of equation (4.2) are identical to the splitting kernels of QED, and the left-hand side describes the non abelian ggg vertex.

The fermion representation leading to equation (4.3) is sufficient to ensure that the Young-Mills lagrangian is supersymmetric. Equation (4.3) has been shown to hold $O(\alpha_s^2)$ if one uses a renormalization procedure which preserves supersymmetry. We rewrite the equation (4.2) in the following form

$$f(z) = \frac{4}{9} + \frac{24}{9}g(z) \quad (4.4)$$

The subprocess ratios which are represented analytically (see Appendix A) depend on two combinations of Altarelli-Parisi splitting kernels $f(z)$ and $g(z)$. In equation (4.4) one can see that since $g(z) \ll f(z)$, then $f(z) \sim \frac{4}{9}$ for all values of z , this means that all but three of the subprocess ratios are constant within $\sim 10\%$ around the boundary of the transverse Dalitz plot. The three subprocess ratios $gg \rightarrow q\bar{q}g$, $q_1g \rightarrow q_1q_2\bar{q}_2$ and $q_1g \rightarrow q_1q_1\bar{q}_1$ are dominated by the probability of a gluon splitting to a quark and antiquark, one can expect that $g(z)$ is giving a larger variation round the boundary of the transverse Dalitz plot, although for $.2 < z < .8$ they change only by 30%. From the comparison between the results which are obtained in the interior of the Dalitz plot (Table 3.2) with the results which are obtained on the boundary of the Dalitz plot (Table 4.2), one can see that both values are in good agreement. In fact the near-constancy of the subprocess ratios around the boundary of the transverse Dalitz plot, which is a direct consequence of the Dokshitzer relation (4.2), underwrites their near-constancy in the interior.

In Table (4.3) we show what happens when one moves away from the transverse plane to general three jet configurations. In this situation we are replacing the pair of jets with smallest invariant mass, i, j by a single collinear pair in the direction of momentum $i + j$ with fractional energies, $z = E_i/(E_i + E_j)$ and $(1-z)$. The resulting two-jet collinear configuration will have c.m. scattering angle θ^* and some z . It is clear that the five subprocess ratios, $q_1q_1 \rightarrow q_1q_1g$, $q_1q_2 \rightarrow q_1q_2g$,

$q_1\bar{q}_1 \rightarrow q_1\bar{q}_1g$, $q_1\bar{q}_2 \rightarrow q_1\bar{q}_2g$ and $qg \rightarrow qgg$ have a z -dependence which will involve $f(z)$ and a ratio of the $2 \rightarrow 2$ cross-sections. In $2 \rightarrow 2$ scattering the following subprocesses $q_1q_1 \rightarrow q_1q_1$, $q_1q_2 \rightarrow q_1q_2$, $q_1\bar{q}_1 \rightarrow q_1\bar{q}_1$, $q_1\bar{q}_2 \rightarrow q_1\bar{q}_2$ and $qg \rightarrow qg$ have a common angular dependence, and when we normalize the $2 \rightarrow 2$ subprocesses to the dominant one $qg \rightarrow qg$, the angular factor roughly cancels in their ratios, as we discussed in Chapter 2. The $f(z)$ is also approximately independent of z . One then obtains that these $2 \rightarrow 3$ subprocess ratios are approximately constant on the surface of (z, θ^*) collinear configurations in the full three-jet phase space. This is shown numerically in Table (4.3). In fact this result generalizes constancy around the boundary of the Dalitz plot. For the subprocess $qg \rightarrow qgg$ there is a beam-target asymmetry between $qg \rightarrow qgg$ and $gq \rightarrow qgg$ which vanishes in the transverse plane but is non-zero elsewhere [4]. This means that the subprocess ratios are only constant if one considers $(qg \rightarrow qgg + gq \rightarrow qgg)/qg \rightarrow qgg$.

For the remaining five ratios the variation with θ^* is greater because the ratios of $2 \rightarrow 2$ cross-sections involve processes which do not have \hat{t} -channel poles and hence these subprocesses have θ^* -dependence different from the θ^* -distribution in $qg \rightarrow qg$. This means that the angular factor does not cancel in the ratios of $2 \rightarrow 2$ cross-section, making these ratios depend more strongly on the angular variable (χ).

One finds that for the first five subprocesses which are represented analytically that the subprocess ratios are fairly constant over most of the three jet phase space with the proviso that we must beam-target symmetrize for $qg \rightarrow qgg$. In fact this is no longer the case when one of the final jets is rather close to the beam or target parton, since in this particular region a different collinear approximation is more appropriate. For one of the final jets close to the beam or target we suggest a formula to approximate the exact $2 \rightarrow 3$ ratios. In Appendix B we give the expression in which one of the final jets becomes parallel to the beam or target and these subprocesses are normalized to the dominant $qg \rightarrow qgg$. In Table (4.4) we show the behaviour of the subprocess ratios in this region where we consider $\chi = 5$ and $N_c = 3$. In Table (4.5) we show the same behaviour but with $\chi = 10$. Again these ratios are involving the $2 \rightarrow 2$ subprocess ratios and z -dependence. The $2 \rightarrow 2$ ratios are constant for the dominant subprocesses i.e. $qg \rightarrow qgg$, $qg \rightarrow qgg$ and $qg \rightarrow qgg$. The first five subprocesses approach their $2 \rightarrow 2$ values of $(4/9)^2$ and $(4/9)$. This means that the ratios of the subprocesses are only depending on z in this region and this is clear from Tables (4.5) and (4.4). For the remaining five subprocesses the ratios show much more variation away from the transverse plane.

We note that the first five subprocesses and $qg \rightarrow qgg$, involving \hat{t} -channel gluon exchange, dominate the three-jet rate. Since these processes have very similar angular distributions as we have just discussed, the possibility of experimentally inferring the presence of individual $2 \rightarrow 3$ subprocesses is rather limited, with the possible exception of the $qg \rightarrow qgg$ subprocess which has a distinctive, although so far experimentally elusive, beam-target asymmetry [4].

We have compared the exact $2 \rightarrow 3$ subprocess cross-sections with the approximations discussed earlier. In the last case we defined

$$z = E_i/E_i + E_j, \chi = (1 + \cos\theta^*)/1 - \cos\theta^*$$

and we applied the following cuts (in the subprocess c.m. frame): the angle between any final jet and the beam is $> 10^\circ$ and the angle between any two final jets $> 30^\circ$, ($z > .1$). For $qq \rightarrow qgg$ we find that the infra-red approximation is within 50% of the exact result for 98% of generated events, 82% of generated events are within 30% of the exact and 64% of generated events within 20%. We generated three-jet kinematical configurations using the phase space generator RAMBO [6].

For $qq \rightarrow qgg$, 100%, 92% and 80% of events were within 50%, 30%, 20% respectively, of the exact result.

A further point concerns factorization of the three-jet cross-section. In the region of phase space where the first five subprocess ratios are roughly constant the three-jet cross-section approximately factorizes.

$$\sigma_{3-jet} \sim F(x_1, Q^2)F(x_2, Q^2)\sigma_{gg \rightarrow ggg}$$

with

$$F(x, Q^2) = g(x) + \lambda[q(x) + \bar{q}(x)],$$

and $\lambda \simeq .30$. The three subprocesses which are dominant over most of phase space are $qq \rightarrow qgg$, $qg \rightarrow qgg$, $gg \rightarrow ggg$ and we noted that these subprocesses are proportional to each other. This means that

$$qq \rightarrow qgg : qg \rightarrow qgg : gg \rightarrow ggg \sim (.30)^2 : (.30) : 1$$

Approximately $f(z) \sim \frac{4}{9}$ and $\hat{\sigma}_{qg \rightarrow qgg} \sim \frac{4}{9}\hat{\sigma}_{gg \rightarrow ggg}$, and $\hat{\sigma}_{qq \rightarrow qq} \sim (\frac{4}{9})^2\hat{\sigma}_{gg \rightarrow gg}$, one expects from the collinear behaviour of the ratios

$$\begin{aligned} qq \rightarrow qgg : qg \rightarrow qgg : gg \rightarrow ggg \\ \sim \left(\frac{4}{9}\right)^3 : \frac{1}{2} \cdot \frac{4}{9} \left(1 + \frac{4}{9}\right) : 1 \end{aligned}$$

which is $(.30)^2 : (.32) : 1$, an approximate geometrical progression which appears to be a numerical accident.

For four jet production, the ratios will not be independent of z in the transverse plane. In the collinear limit one has

$$\frac{qq \rightarrow qggg}{gg \rightarrow gggg} \Big|_{z=1} = \frac{\hat{\sigma}_{qg \rightarrow qgg}}{\hat{\sigma}_{gg \rightarrow ggg}} f(z) + \frac{\hat{\sigma}_{qg \rightarrow ggg} + \hat{\sigma}_{qg \rightarrow ggg}}{\hat{\sigma}_{gg \rightarrow ggg}} \quad (4.5)$$

In equation (4.5) the orderings qgg, gqg and ggq refer to definite parton assignments for the three jets.(we have assumed above $12 \rightarrow 3456$ with 3,4 collinear.) The $2 \rightarrow 3$ subprocess ratios we previously considered were summed over all possible parton assignments and so we expect for the sum of orderings

$$\frac{\hat{\sigma}_{qg \rightarrow qgg} + \hat{\sigma}_{qg \rightarrow gqg} + \hat{\sigma}_{qg \rightarrow ggq}}{\hat{\sigma}_{gg \rightarrow ggg}} \sim 0.28, \quad (4.6)$$

The ratios for individual orderings, however, will vary between zero and $\sim .28$ depending on jet angles. This means that the subprocess ratio in equation (4.5) will depend on the three-jet angles, although it will be relatively independent of z , since it once again depends on $f(z)$. Thus one may expect a considerable variation in the subprocess ratio of equation (4.5) between $.28$ and $\frac{4}{9}(.28) \sim .12$ putting $f(z) \sim \frac{4}{9}$ and using equation (4.6). The nearly constant subprocess ratios in the transverse plane, will not persist for four or more jets, therefore.

$q_1 q_1 \rightarrow q_1 q_1 g$	$\frac{704}{6561} f(z)$
$q_1 q_2 \rightarrow q_1 q_2 g$	$\frac{320}{2187} f(z)$
$q_1 \bar{q}_1 \rightarrow q_1 \bar{q}_1 g$	$\frac{448}{6561} g(z) + \frac{1120}{6561} f(z)$
$q_1 \bar{q}_2 \rightarrow q_1 \bar{q}_2 g$	$\frac{320}{2187} f(z)$
$qg \rightarrow qgg$	$\frac{440}{2187} [1 + f(z)]$
$q\bar{q} \rightarrow ggg$	$\frac{224}{6561}$
$gg \rightarrow q\bar{q}g$	$N_f [2g(z) + \frac{7}{729} f(z)]$
$q_1 g \rightarrow q_1 q_2 \bar{q}_2$	$(N_f - 1) \frac{880}{2187} g(z)$
$q_1 g \rightarrow q_1 q_1 \bar{q}_1$	$\frac{880}{2187} g(z)$
$q_1 \bar{q}_1 \rightarrow q_2 \bar{q}_2 g$	$N_f [\frac{448}{6561} g(z) + \frac{32}{2187} f(z)]$

Table 4.1: Shows the z -dependence of QCD subprocess ratios in the transverse plane ($\chi = 1$)

<i>z/ratios</i>	.1	.2	.3	.35	.4	.45	.50
$q_1q_1 \rightarrow q_1q_1g$.05	.051	.052	.053	.053	.053	.053
$q_1q_2 \rightarrow q_1q_2g$.067	.07	.072	.072	.072	.072	.072
$q_1\bar{q}_1 \rightarrow q_1\bar{q}_1g$.079	.08	.083	.084	.084	.084	.084
$q_1\bar{q}_2 \rightarrow q_1\bar{q}_2g$.067	.07	.072	.072	.072	.072	.072
$gg \rightarrow qgg$.29	.30	.30	.30	.30	.30	.30
$q\bar{q} \rightarrow ggg$.034	.034	.034	.034	.034	.034	.034
$gg \rightarrow q\bar{q}g$.058	.076	.10	.11	.12	.12	.13
$q_1g \rightarrow q_1q_2\bar{q}_2$.00	.01	.013	.014	.015	.015	.015
$q_1g \rightarrow q_1q_1\bar{q}_1$.00	.00	.00	.00	.00	.00	.00
$q_1\bar{q}_1 \rightarrow q_2\bar{q}_2g$.015	.015	.016	.016	.017	.017	.017

Table 4.2: Shows the behaviour of the ratios with z ($\chi = 1$).

	$z=.1$	$z=.25$	$z=.50$
$q_1 q_1 \rightarrow q_1 q_1 g$.0840	.090	.090
$q_1 q_2 \rightarrow q_1 q_2 g$.0870	.090	.090
$q_1 \bar{q}_1 \rightarrow q_1 \bar{q}_2 g$.100	.100	.100
$q_1 \bar{q}_2 \rightarrow q_1 \bar{q}_2 g$.0870	.0870	.090
$qg \rightarrow qgg$.220	.230	.230
$q\bar{q} \rightarrow ggg$.024	.024	.024
$gg \rightarrow q\bar{q}g$.050	.10	.130
$q_1 g \rightarrow q_1 q_2 \bar{q}_2$.00	.001	.002
$q_1 g \rightarrow q_1 q_1 \bar{q}_1$.00	.00	.00
$q\bar{q}_1 \rightarrow q_2 q_2 q$.010	.010	.01

Table 4.3: Shows the behaviour of the subprocess ratios with z for $\chi = 5$

z	.10	.20	.30	.40	.50	.60	.70	.80	.90
$q_1 q_1 \rightarrow q_1 q_1 g$.088	.10	.12	.13	.15	.17	.19	.190	.2
$q_1 q_2 \rightarrow q_1 q_2 g$.09	.11	.12	.13	.16	.17	.19	.195	.19
$q_1 \bar{q}_1 \rightarrow q_1 \bar{q}_1 g$.10	.11	.13	.14	.16	.18	.19	.20	.2
$q_1 \bar{q}_2 \rightarrow q_1 \bar{q}_2 g$.08	.10	.12	.13	.16	.17	.19	.20	.19
$gg \rightarrow q \bar{q} g$.22	.25	.28	.32	.36	.39	.42	.44	.45
$q \bar{q} \rightarrow g g g$.02	.02	.02	.01	.01	.00	.00	.00	.00
$gg \rightarrow q \bar{q} g$.04	.06	.07	.07	.07	.07	.085	.056	.04
$q_1 g \rightarrow q_1 q_2 \bar{q}_2$.00	.00	.00	.00	.00	.00	.00	.00	.00
$q_1 g \rightarrow q_1 q_1 \bar{q}_1$.00	.00	.00	.00	.00	.00	.00	.00	.00
$q_1 \bar{q}_1 \rightarrow q_2 \bar{q}_2 g$.00	.00	.00	.00	.00	.00	.00	.00	.00

Table 4.4: Behaviour of subprocess ratios in the region where one jet is close to the beam or target direction, $\chi = 5$

z	.10	.20	.30	.40	.50	.60	.70	.80	.90
$q_1q_1 \rightarrow q_1q_1g$.10	.10	.13	.14	.16	.17	.19	.19	.20
$q_1q_2 \rightarrow q_1q_2g$.10	.11	.13	.14	.16	.17	.19	.20	.20
$q_1\bar{q}_1 \rightarrow q_1\bar{q}_1g$.10	.11	.13	.14	.16	.17	.19	.20	.20
$q_1\bar{q}_2 \rightarrow q_1\bar{q}_2g$.10	.11	.13	.14	.16	.17	.19	.20	.20
$qg \rightarrow qgg$.24	.25	.28	.32	.36	.39	.42	.44	.45
$q\bar{q} \rightarrow ggg$.00	.00	.00	.00	.00	.00	.00	.00	.00
$gg \rightarrow q\bar{q}g$.04	.05	.06	.07	.07	.07	.04	.05	.03
$q_1g \rightarrow q_1q_2\bar{q}_2$.00	.00	.00	.00	.00	.00	.00	.00	.00
$q_1g \rightarrow q_1\bar{q}_1q_1$.00	.00	.00	.00	.00	.00	.00	.00	.00
$q\bar{q}_1 \rightarrow q_2\bar{q}_2g$.00	.00	.00	.00	.00	.00	.00	.00	.00

Table 4.5: As Table (4.4) but with $\chi = 10$

4.1 APPENDIX A

Shows the 2→3 QCD subprocesses ratios, which are expressed in terms of χ and z , when a pair of the final state particles i, j goes parallel. We normalised to $gg \rightarrow ggg$ and summed over all the possible final state assignments of partons to jets.

$$F(\chi) = \chi^2 + \chi + 1 + \chi^{-1} + \chi^{-2}$$

(1) $q_1 q_1 \rightarrow q_1 q_1 g$.

$$\left(\frac{N_c^2 - 1}{2N_c^2}\right)^2 \left[\frac{F(\chi) - N_c^{-1}(\chi + \chi^{-1} + 2)}{F(\chi) + 2 - \chi(1 + \chi)^{-2}} \right] \left[\frac{P_{qq}(z) + P_{qq}(1 - z)}{P_{gg}(z)} \right]$$

(2) $q_1 q_2 \rightarrow q_1 q_2 g$.

$$\left(\frac{N_c^2 - 1}{2N_c^2}\right)^2 \left[\frac{F(\chi)}{F(\chi) + 2 - \chi(1 + \chi)^{-2}} \right] \left[\frac{P_{qq}(z) + P_{qq}(1 - z)}{P_{gg}(z)} \right]$$

(3) $q_1 \bar{q}_1 \rightarrow q_1 \bar{q}_1 g$.

$$\begin{aligned} & \left(\frac{N_c^2 - 1}{2N_c^2}\right)^2 \left[\frac{F(\chi) + N_c^{-1}(\chi + \chi^{-1} - 1) + (\chi^2 + 1)(1 + \chi)^{-2}}{f(\chi) + 2 - \chi(1 + \chi)^{-2}} \right] \left[\frac{P_{qq}(z) + P_{qq}(1 - z)}{P_{gg}(z)} \right] + \\ & \frac{1}{2N_c} \left(\frac{N_c^2 - 1}{N_c}\right)^2 \left[\frac{\frac{1}{2}N_c^{-2}(N_c^2 - 1)(\chi + \chi^{-1}) - (\chi^2 + 1)(1 + \chi)^{-2}}{F(\chi) + 2 - \chi(1 + \chi)^{-2}} \right] \frac{P_{gg}(z)}{P_{gg}(z)} \end{aligned}$$

(4) $q_1 \bar{q}_2 \rightarrow q_1 \bar{q}_2 g$.

$$\left(\frac{N_c^2 - 1}{2N_c^2}\right)^2 \left[\frac{F(\chi)}{F(\chi) + 2 - \chi(1 + \chi)^{-2}} \right] \left[\frac{P_{qq}(z) + P_{qq}(z)}{P_{gg}(z)} \right]$$

(5) $gg \rightarrow ggg$.

$$\begin{aligned} & \frac{1}{2} \left(\frac{N_c^2 - 1}{2N_c^2}\right)^2 \left[\frac{(2\chi^2 + 2\chi + 1)(1 + \chi)^{-1}\chi^{-1} + 2N_c^2(N_c^2 - 1)^{-1}(2\chi^2 + 2\chi + 1)}{F(\chi) + 2 - \chi(1 + \chi)^{-2}} \right] \times \\ & \left[\frac{P_{qq}(z) + P_{qq}(1 - z)}{P_{gg}(z)} \right] \\ & + \frac{1}{2} \left(\frac{N_c^2 - 1}{2N_c^2}\right)^2 \left[\frac{(\chi^2 + 2\chi + 2)(1 + \chi)^{-1} + 2N_c^2(N_c^2 - 1)^{-1}(2\chi^{-2} + 2\chi^{-1} + 1)}{F(\chi) + 2 - \chi(1 + \chi)^{-2}} \right] \end{aligned}$$

(6) $q\bar{q} \rightarrow ggg$.

$$\frac{(N_c^2 - 1)^3}{8N_c^5} \left[\frac{(\chi^{-1} + \chi) - 2N_c^2(N_c^2 - 1)^{-1}(1 + \chi)^{-2}}{F(\chi) + 2 - \chi(1 + \chi)^{-2}} \right]$$

(7) $gg \rightarrow q\bar{q}g$.

$$\frac{N_f}{2N_c} \left[\frac{\frac{1}{2}N_c^{-2}(N_c^2 - 1)(\chi^{-1} + \chi) - (\chi^2 + 1)(1 + \chi)^{-2}}{F(\chi) + 2 - \chi(1 + \chi)^{-2}} \right] \times$$

$$\left[\frac{P_{qq}(z) + P_{qq}(1 - z)}{P_{gg}(z)} \right] + 2N_f \frac{P_{qq}(z)}{P_{gg}(z)}$$

(8) $q_1g \rightarrow q_1q_2\bar{q}_2$.

$$(N_f - 1) \left(\frac{N_c^2 - 1}{2N_c^2} \right)^2 \left[\frac{2 + \chi^2(1 + \chi)^{-1} + 2N_c^2(N_c^2 - 1)^{-1}(2\chi^{-2} + 2\chi^{-1} + 1)}{F(\chi) + 2 - \chi(1 + \chi)^{-2}} \right] \frac{P_{qq}(z)}{P_{gg}(z)}$$

(9) $q_1g \rightarrow q_1q_1\bar{q}_1$.

$$\left(\frac{N_c^2 - 1}{2N_c^2} \right)^2 \left[\frac{2 + \chi^2(1 + \chi)^{-1} + 2N_c^2(N_c^2 - 1)^{-1}(2\chi^{-2} + 2\chi^{-1} + 1)}{F(\chi) + 2 - \chi(1 + \chi)^{-2}} \right] \frac{P_{qq}(z)}{P_{gg}(z)}(z)$$

(10) $q_1\bar{q}_1 \rightarrow q_2\bar{q}_2g$.

$$N_f \left(\frac{N_c^2 - 1}{2N_c^2} \right)^2 \left[\frac{(1 + \chi^2)(1 + \chi)^{-2}}{F(\chi) + 2 - \chi(1 + \chi)^{-2}} \right] \left[\frac{P_{qq}(z) + P_{qq}(1 - z)}{P_{gg}(z)} \right]$$

$$+ \frac{N_f}{2N_c} \left(\frac{N_c^2 - 1}{N_c} \right)^2 \left[\frac{\frac{1}{2}N_c^{-2}(N_c^2 - 1)(\chi + \chi^{-1}) - (\chi^2 + 1)(1 + \chi)^{-2}}{F(\chi) + 2 - \chi(1 + \chi)^{-2}} \right] \frac{P_{qq}(z)}{P_{gg}(z)}$$

4.2 APPENDIX B

Shows the 2→3 QCD subprocess ratios in the limit when one particle of the final state goes parallel to the beam or target. $z = E_i/E_1$ or E_i/E_2 .

1. $q_1 q_1 \rightarrow q_1 q_1 g$

$$\begin{aligned} & \left(\frac{N_c^2 - 1}{2N_c^2} \right)^2 \left[\frac{F(\chi) - N_c^{-1}(\chi + \chi^{-1} + 2)}{F(\chi) + 2 - \chi(1 + \chi)^{-2}} \right] \frac{P_{qq}(1-z)}{P_{gg}(z)} \\ + & \left(\frac{N_c^2 - 1}{2N_c^2} \right) \left[\frac{F(\chi) + \frac{1}{2}N_c^{-2}(N_c^2 - 1)(\frac{1}{2}\chi + \frac{1}{2}\chi^{-1} + \frac{3}{2})}{F(\chi) + 2 - \chi(1 + \chi)^{-2}} \right] \frac{P_{qq}(z)}{P_{gg}(z)} \end{aligned}$$

2. $q_1 q_2 \rightarrow q_1 q_2 g$

$$\begin{aligned} & \left(\frac{N_c^2 - 1}{2N_c^2} \right)^2 \left[\frac{F(\chi)}{F(\chi) + 2 - \chi(1 + \chi)^{-2}} \right] \frac{P_{qq}(1-z)}{P_{gg}(z)} \\ + & \left(\frac{N_c^2 - 1}{2N_c^2} \right) \left[\frac{F(\chi) + \frac{1}{2}N_c^{-2}(N_c^2 - 1)(\frac{1}{2}\chi + \frac{1}{2}\chi^{-1} + \frac{3}{2})}{F(\chi) + 2 - \chi(1 + \chi)^{-2}} \right] \frac{P_{qq}(z)}{P_{gg}(z)} \end{aligned}$$

3. $q_1 \bar{q}_1 \rightarrow q_1 \bar{q}_1 g$

$$\begin{aligned} & \left(\frac{N_c^2 - 1}{2N_c^2} \right)^2 \left[\frac{F(\chi) + N_c^{-1}(\chi + \chi^{-1} - 1) + (\chi^2 + 1)(1 + \chi)^{-2}}{F(\chi) + 2 - \chi(1 + \chi)^{-2}} \right] \frac{P_{qq}(1-z)}{P_{gg}(z)} \\ + & \left(\frac{N_c^2 - 1}{2N_c^2} \right) \left[\frac{F(\chi) + \frac{1}{2}N_c^{-2}(N_c^2 - 1)(\frac{1}{2}\chi + \frac{1}{2}\chi^{-1} + \frac{3}{2})}{F(\chi) + 2 - \chi(1 + \chi)^{-2}} \right] \frac{P_{qq}(z)}{P_{gg}(z)} \end{aligned}$$

4. $q_1 \bar{q}_2 \rightarrow q_1 \bar{q}_2 g$

$$\begin{aligned} & \left(\frac{N_c^2 - 1}{2N_c^2} \right) \left[\frac{F(\chi)}{F(\chi) + 2 - \chi(1 + \chi)^{-2}} \right] \frac{P_{qq}(1-z)}{P_{gg}(z)} \\ + & \left(\frac{N_c^2 - 1}{2N_c^2} \right) \left[\frac{F(\chi) + \frac{1}{2}N_c^{-2}(N_c^2 - 1)(\frac{1}{2}\chi + \frac{1}{2}\chi^{-1} + \frac{3}{2})}{F(\chi) + 2 - \chi(1 + \chi)^{-2}} \right] \frac{P_{qq}(z)}{P_{gg}(z)} \end{aligned}$$

5. $gg \rightarrow qgg$

$$\begin{aligned} & \left(\frac{N_c^2 - 1}{2N_c^2} \right) \left[\frac{F(\chi) + \frac{1}{2}N_c^{-2}(N_c^2 - 1)(\frac{1}{2}\chi + \frac{1}{2}\chi^{-1} + \frac{3}{2})}{F(\chi) + 2 - \chi(1 + \chi)^{-2}} \right] \frac{P_{qq}(1-z)}{P_{gg}(z)} \\ & + \frac{P_{qq}(z)}{P_{gg}(z)} \end{aligned}$$

6. $q\bar{q} \rightarrow ggg$

$$\frac{1}{N_c} \left(\frac{N_c^2 - 1}{2N_c^2} \right)^2 \left[\frac{\frac{1}{2}N_c^{-2}(N_c^2 - 1)(\chi + \chi^{-1}) - (\chi^2 + 1)(1 + \chi)^{-2}}{F(\chi) + 2 - \chi(1 + \chi)^{-2}} \right] \frac{P_{qg}(1 - z)}{P_{gg}(z)}$$

7. $gg \rightarrow q\bar{q}g$

$$\begin{aligned} & \frac{N_f}{N_c} \left[\frac{\frac{1}{2}N_c^{-2}(N_c^2 - 1)(\chi + \chi^{-1}) - (\chi^2 + 1)(1 + \chi)^{-2}}{F(\chi) + 2 - \chi(1 + \chi)^{-2}} \right] \\ & + 2N_f \left(\frac{N_c^2 - 1}{2N_c^2} \right) \left[\frac{F(\chi) + \frac{1}{2}N_c^{-2}(N_c^2 - 1)(\frac{1}{2}\chi + \frac{1}{2}\chi^{-1} + \frac{3}{2})}{F(\chi) + 2 - \chi(1 + \chi)^{-2}} \right] \frac{P_{qg}(z)}{P_{gg}(z)} \end{aligned}$$

8. $q_1g \rightarrow q_1q_2\bar{q}_2$

$$\begin{aligned} & (N_f - 1) \left(\frac{N_c^2 - 1}{2N_c^2} \right)^2 \left[\frac{(\chi^2 + 1)(1 + \chi)^{-2}}{F(\chi) + 2 - \chi(1 + \chi)^{-2}} \right] \frac{P_{qg}(z)}{P_{gg}(z)} \\ & + 2 \left(\frac{N_c^2 - 1}{2N_c^2} \right)^2 \left[\frac{F(\chi)}{F(\chi) + 2 - \chi(1 + \chi)^{-2}} \right] \frac{P_{qg}(z)}{P_{gg}(z)} \end{aligned}$$

9. $q_1g \rightarrow q_1q_1\bar{q}_1$

$$\left(\frac{N_c^2 - 1}{2N_c^2} \right)^2 \left[\frac{F(\chi) + N_c(\chi + \chi^{-1} - 1) + (\chi^2 + 1)(1 + \chi)^{-2}}{F(\chi) + 2 - \chi(1 + \chi)^{-2}} \right] \frac{P_{qg}(z)}{P_{gg}(z)}$$

10. $q_1\bar{q}_1 \rightarrow q_2\bar{q}_2g$

$$N_f \left(\frac{N_c^2 - 1}{2N_c^2} \right)^2 \left[\frac{(\chi^2 + 1)(1 + \chi)^{-2}}{F(\chi) + 2 - \chi(1 + \chi)^{-2}} \right] \frac{P_{qg}(1 - z)}{P_{gg}(z)}$$

REFERENCES

- [1] G. Altarelli and G. Parisi, Nucl. Phys. B126, (1977), 298.
- [2] I. Antoniadis and E.G. Floratos, Nucl. Phys. B191, (1982), 217.
- [3] Yu. L. Dokshitzer, Sov. Phys. JET P., 46, (1977), 641.
- [4] B.L. Combridge and C.J. Maxwell, Nucl. Phys. B239, (1984), 429, Phys. Lett. 151B, (1988), 299.
- [5] K. Makshoush and C.J. Maxwell, Phys. Lett. B212, (1988), 95.
- [6] R. Kleiss, W.J. Stirling and S.D. Ellis, Comput. Phys. Commun. 40, (1986), 389.

Chapter 5

Spinor Methods

5.1 Introduction

Many multijet events will be generated at present and future hadron colliders. It is important to model these theoretically so that one may use these results to test perturbative QCD and also so that one can estimate the conventional QCD background to multi-jet signatures for new physics processes.

The QCD exact matrix elements for $2 \rightarrow 2$ and $2 \rightarrow 3$ parton-parton scattering are known and can be written analytically in a compact form. For the four-jet production only numerical codes exist and require large amounts of CPU time when used in computer Monte Carlos [1]. Mangano, Parke and Xu [2] suggested a new technique and obtain a significant improvement over the calculations which were obtained previously in ref. [1] for six gluon scattering. The basis of this technique is to decompose the n-gluon amplitude into sub-amplitudes weighted by Chan-Paton like traces of colour matrices. In fact this technique shows how the calculation could be simplified. The tree-level vector particle scattering amplitude, for the colours a_1, a_2, \dots, a_n , momenta p_1, p_2, \dots, p_n and helicities, e_1, e_2, \dots, e_n , can be written in the following form;

$$M_n = \sum_{perm.s} tr(\lambda^{(a_1)} \dots \lambda^{(a_n)}) m(p_1, \epsilon_1, ; \dots; p_n, \epsilon_n) \quad (5.1)$$

where the sum which appears in equation (5.1) is over all the $(n-1)!$ non-cyclic permutations of the momenta. The $m(\)$ in equation (5.1) are called the sub-amplitudes and they are only functions of the kinematical variables of the process, i.e. momenta and helicities of the external gluons, these variables are represented in shorthand by the notation $(1,2,3,\dots,n)$.

5.2 Duality Properties

The sub-amplitudes which are thus obtained are found to satisfy some properties for any particular set of helicities. We summarize these properties in the following

points:

- $m(1,2,3,\dots,n)$ is gauge invariant.
- $m(1,2,3,\dots,n)$ is invariant under cyclic permutations of the momenta.
- $m(n,n-1,\dots,1) = (-1)^n m(1,2,3,\dots,n)$.
- The Ward Identity: $m(1,2,3,\dots,n) + m(2,1,3,\dots,n) + m(2,3,1,\dots,n) + \dots + m(2,3,\dots,1,n) = 0$.
- $m(1,2,3,\dots,n)$ factorizes on multi-gluon poles.
- $|M_n|^2 = N_c^{n-2} \frac{(N_c^2-1)}{2^n} \sum_{p^*} [|m(1,2,\dots,n)|^2 + O(N_c^{-2})]$

where N_c is the number of colours.

5.3 Spinor Definition and Properties

For massless spinors with momentum p and helicity λ , $u^{(\pm)}(p)$, $v^{(\pm)}(p)$, $\bar{u}^{(\pm)}(p)$ and $\bar{v}^{(\pm)}(p)$ satisfy the following equations.

$$\begin{aligned}
 p_\mu \gamma^\mu u(p) &= p_\mu \gamma^\mu v(p) = 0 \\
 \bar{u}(p) p_\mu \gamma^\mu &= \bar{v}(p) p_\mu \gamma^\mu = 0, \\
 p^2 &= 0 \\
 (1 \mp \gamma_5) u^{(\pm)}(p) &= (1 \pm \gamma_5) v^{(\pm)}(p) = 0 \\
 \bar{u}^{(\pm)}(p) (1 \pm \gamma_5) &= \bar{v}^{(\pm)}(p) (1 \mp \gamma_5) = 0
 \end{aligned} \tag{5.2}$$

with the normalization

$$\bar{u}^{(\pm)}(p) \gamma_\mu u^{(\pm)}(p) = \bar{v}^{(\pm)}(p) \gamma_\mu v^{(\pm)}(p) = 2p_\mu.$$

By convention one can put

$$\begin{aligned}
 u^{(\pm)}(p) &= v^{(\mp)}(p) = |p_\pm \rangle, \\
 \bar{u}^{(\pm)}(p) &= \bar{v}^{(\mp)}(p) = \langle p_\pm |.
 \end{aligned} \tag{5.3}$$

The following relations then hold for any massless momenta p and q and are easy to show:

$$\begin{aligned}
 |p_\pm \rangle \langle p_\pm| &= \frac{1}{2} (1 \pm \gamma_5) p_\mu \gamma^\mu \\
 \langle p_+ | q_+ \rangle &= \langle p_- | q_- \rangle = 0 \\
 \langle p_- | q_+ \rangle &= - \langle q_- | p_+ \rangle, \quad \langle p_- | p_+ \rangle = \langle p_+ | p_- \rangle = 0
 \end{aligned} \tag{5.4}$$

For simplicity one can put

$$\begin{aligned}
 \langle p_- | q_+ \rangle &= \langle pq \rangle, \text{ therefore} \\
 \langle q_- | p_+ \rangle &= - \langle pq \rangle \\
 \langle q_+ | p_- \rangle &= [pq] \\
 \langle p_+ | q_- \rangle &= -[pq], \text{ and} \\
 \langle pq \rangle [pq] &= 2(p \cdot q) = s_{qp}.
 \end{aligned}$$

According to ref. [4], in general, if $|A_{\pm}\rangle$ is any spinor which satisfies

$$\begin{aligned}
 (1 \mp \gamma_5) |A_{\pm}\rangle &= 0 \\
 |A_+\rangle^* &= |A_-\rangle,
 \end{aligned}$$

in which $|A_+\rangle^*$ is the charge conjugation of $|A_+\rangle$, then one has

$$\begin{aligned}
 \langle A_{\mp} | B_{\pm} \rangle &= - \langle B_{\mp} | A_{\pm} \rangle, \text{ where} \\
 \langle A_{\pm} | &= | \overline{A_{\pm}} \rangle.
 \end{aligned}$$

If $|A_{\pm}\rangle$ has the following form

$$|A_{\pm}\rangle = \begin{cases} \not{k}_1 \dots \not{k}_n |q_{\pm}\rangle & (\text{n is even}) \\ \not{k}_1 \dots \not{k}_n |q_{\mp}\rangle & (\text{n is odd}), \text{ then} \end{cases}$$

$$|A_{\pm}\rangle^* = \begin{cases} \not{k}_1 \dots \not{k}_n |q_{\mp}\rangle & (\text{n is even}) \\ -\not{k}_1 \dots \not{k}_n |q_{\pm}\rangle & (\text{n is odd}). \end{cases}$$

One can also note some special properties

$$\langle p_- | \not{k}_1 \dots \not{k}_n | q_+ \rangle = - \langle q_- | \not{k}_n \dots \not{k}_1 | p_+ \rangle,$$

where n is even.

$$\langle p_+ | \not{k}_1 \dots \not{k}_n | q_- \rangle = - \langle q_+ | \not{k}_n \dots \not{k}_1 | p_- \rangle \text{ for n is odd.}$$

A quantity like $|B_+\rangle \langle A_+|$ can be expanded into a linear sum of $1, \gamma_{\mu}, \gamma_5, \gamma_{\mu}\gamma_5$ and $\gamma_{\nu}\gamma_{\mu} (\mu \neq \nu)$.

$2 |B_+\rangle \langle A_+| = \langle A_+ | \gamma_{\mu} | B_+ \rangle \gamma^{\mu \frac{1}{2}} (1 - \gamma_5)$, if one multiplies both sides by $\langle C_- |$ from the left and $|D_- \rangle$ from the right, then one can obtain the following relation

$$\langle A_+ | \gamma_{\mu} | B_+ \rangle \langle C_- | \gamma^{\mu} | D_- \rangle = 2 \langle A_+ | D_- \rangle \langle C_- | B_+ \rangle$$

from the following property

$$|B_+\rangle\langle A_-| - |A_+\rangle\langle B_-| = \langle A_-|B_+\rangle \frac{1}{2}(1 + \gamma_5),$$

one can obtain a useful rearrangement of spinor products.

$$\langle A_-|B_+\rangle\langle C_-|D_+\rangle = \langle A_-|D_+\rangle\langle C_-|D_+\rangle + \langle A_-|C_+\rangle\langle B_-|D_+\rangle.$$

5.4 The Polarization Vector

The fundamental quantity which was used in the calculation of the six-gluon scattering is the polarization vector, which was defined by the following relation

$$\epsilon^\pm = N[\not{k}\not{q}'\not{q}(1 \pm \gamma_5) - \not{q}'\not{q}\not{k}(1 \mp \gamma_5)] \quad (5.5)$$

In fact this polarization vector was used by CALKUL collaboration [3]. One can note that there is a term dropped in the equation (5.5) and this term is $\mp 2(q \cdot q')\not{k}\gamma_5$. When this term is added to equation (5.5) the gauge invariance of the theory no longer holds. Thus gauge invariance of the theory strongly suggests that one should discard this term from equation (5.5). Also one can note that the definition of the polarization vector in equation (5.5) is not the contraction with γ^μ of a four-vector. This means that one is unable to use this polarization vector, which was given in the above equation, in direct QCD calculations.

Zhan Xu, Da-Hua Zhang and Lee Chang suggested [4] to restore the discarded term and rewrite equation (5.5) in the following form:

$$\epsilon^\pm = N[\not{k}\not{q}'\not{q}(1 \pm \gamma_5) + \not{q}\not{q}'\not{k}(1 \mp \gamma_5) - 2(q \cdot q')\not{k}] \quad (5.6)$$

Again for the gauge invariance of the theory the last term in equation (5.6) must be discarded and the equation (5.6) can be written in the following form:

$$\epsilon^\pm = N[\not{k}\not{q}'\not{q}(1 \pm \gamma_5) + \not{q}\not{q}'\not{k}(1 \mp \gamma_5)] \quad (5.7)$$

Now this expression is the contraction with γ^μ of the four-vector

$$\epsilon_\mu^\pm = \frac{1}{\sqrt{2}}(\epsilon_\mu^\parallel \pm i\epsilon_\mu^\perp) + \frac{1}{2}\sqrt{\frac{(q\bar{q})}{(qk)(q'k)}}k_\mu \quad (5.8)$$

Where k is the momentum of single gluon, and q, \bar{q} are the reference momenta and they satisfy $q^2 = 0, \bar{q}^2 = 0$ respectively and $(q \cdot k), (\bar{q} \cdot k)$ are not equal to zero. When the reference momenta are changed from q, \bar{q} to p, \bar{p} , the polarization vectors $\epsilon_q^\pm(k, q', q)$ and $\epsilon_p^\pm(k, p', p)$ are still connected by the following relation

$$\epsilon_p^\pm = e^{\pm i\phi} \epsilon_q^\pm + \beta^\pm k \quad (5.9)$$

where $e^{\pm i\phi}$ is the phase factor defined by the following relation

$$e^{\pm i\phi} = -N_q N_p \text{Tr}[\not{q}' \not{k} \not{p}' \not{k} (1 \pm \gamma_5)] \quad (5.10)$$

The trace which appears in equation (5.10) can be translated into terms of spinors. This means one can rewrite equation (5.10) in the following form

$$e^{\pm i\phi} = \sqrt{2} N_q \langle k_{\mp} | \not{q}' \not{q} | k_{\pm} \rangle \cdot \sqrt{2} N_p \langle k_{\pm} | \not{p}' \not{p} | k_{\mp} \rangle \quad (5.11)$$

Since the polarization vector ϵ^{\pm} is complex, the phase freedom can be exploited to simplify the relations. N which was appearing in equation (5.11) is a real normalization factor given by the following relation

$$N_q = [16(q \cdot q')(q \cdot k)(q' \cdot k)]^{-\frac{1}{2}},$$

which can be written in terms of spinors as

$$\begin{aligned} N_q &= \pm [\sqrt{2} \langle q'_{\pm} | q_{\mp} \rangle \langle k_{\mp} | q'_{\pm} \rangle \langle q_{\mp} | k_{\pm} \rangle]^{-1} \\ &= \pm [\sqrt{2} \langle k_{\mp} | \not{q}' \not{q} | k_{\pm} \rangle]^{-1} \end{aligned} \quad (5.12)$$

Now the normalization factor is a complex quantity, then the phase factor becomes $e^{\pm i\phi} = 1$ and hence the equation which was given in (5.9) can be written in the following form:

$$\epsilon_q^{\pm} = \epsilon_p^{\pm} + \beta^{\pm} k \quad (5.13)$$

One can show that the reference momentum q' drops out from the definition of the polarization vector, this means that the polarization vector which was defined in this way only depends on one reference momentum. To show that, one can write equation (5.7) in the following form:

$$\begin{aligned} \not{\epsilon}^{\pm}(k, q', q) &= 2N_q^{\pm} [| k_{\mp} \rangle \langle k_{\mp} | q'_{\pm} \rangle \langle q'_{\pm} | q_{\mp} \rangle \langle q_{\mp} | + \\ & \quad | q_{\pm} \rangle \langle q_{\pm} | q'_{\mp} \rangle \langle q'_{\mp} | k_{\pm} \rangle \langle k_{\pm} |] \end{aligned} \quad (5.14)$$

By using equation (5.12) we obtain

$$\not{\epsilon}^{\pm}(k, q) = \pm \sqrt{2} [| k_{\mp} \rangle \langle q_{\mp} | + | q_{\pm} \rangle \langle k_{\pm} |] / \langle q_{\mp} | k_{\pm} \rangle \quad (5.15)$$

then the helicity eigenstate of a gluon with momentum k is given by

$$\epsilon_{\mu}^{\pm} = \langle k_{\pm} | \gamma_{\mu} | q_{\pm} \rangle \sqrt{2} \langle q_{\mp} | k_{\pm} \rangle \quad (5.16)$$

In fact the polarization vector satisfies a number of identities which are extremely helpful in n-gluons scattering calculations. These properties [2] are summarized in the following points:

$$\begin{aligned} k \cdot \epsilon^\pm(k, q) &= 0 \\ \epsilon^\pm(k, q) \cdot \epsilon^\pm(k, q) &= -1 \\ \epsilon^\pm(k, q) \cdot \epsilon^\pm(k, q) &= 0 \end{aligned}$$

These properties are the standard properties of the polarization vectors.

$$\epsilon_\mu(k, q') = \epsilon_\mu(k, q) + \beta(k, q', q) \cdot k_\mu$$

Supplemented by gauge invariance i.e. $m(1,2,3,\dots,n)|_{\epsilon_i=p_i} = 0$, the meaning of this equation is clear, when the polarization vector of an external gauge boson is put equal to its momentum, then the scattering amplitude must vanish because of the gauge invariance of the theory. This implies that β is irrelevant and hence one can choose different reference momenta for each of the gluons and different reference momenta for a given gluon in different sub-amplitudes.

$$q \cdot \epsilon^\pm(k, q) = 0$$

This property can eliminate many terms. The reference momentum vector could be chosen as a light-like momentum vector in the n-gluon scattering calculations.

$$\begin{aligned} \epsilon^\pm(k_1, q) \cdot \epsilon^\pm(k_2, q) &= 0 \\ \epsilon^\pm(k_1, k_2) \cdot \epsilon_\pm(k_2, q) &= 0 \end{aligned}$$

The meaning of the last two properties is that, for a given sub-amplitude calculation, all gluons with the same helicity should have the same reference momentum.

5.5 Parke-Taylor Formula for n-gluon scattering

For five gluon scattering there is a very compact expression obtained in ref. [13] which we can write in the form

$$|M_{gg \rightarrow ggg}|^2 = \frac{g^6}{2} \sum (ij)^4 \frac{\sum (ijklm)}{\pi(ij)} \quad (5.17)$$

The notation (ijklm) in the equation (5.17) means (ij)(jk)(kl)(lm)(mi), where (ij) denotes the dot product of four-momenta ($p_i \cdot p_j$). This simple form suggests that one might be able to obtain an equally simple expression for n-gluon scattering.

To generalize the result to n-gluon scattering we consider the following conjectured form

$$|M_n|^2 = \sum (ij)^4 \cdot \frac{S}{\pi(ij)} \quad (5.18)$$

In fact the full result must contain poles such as $t_{ijk} = (i+j+k)^2$ in addition to the single pole $s = (i+j)^2$, thus equation (5.18) cannot in fact be the full result. We shall try and determine the numerator unknown "S" by imposing certain constraints which the amplitude must satisfy:

- The scattering amplitude has the correct Altarelli- Parisi behaviour when a pair of gluons go collinear.
- The amplitude has the correct mass dimension to give a cross-section.

In the case of gluons i, j going collinear then the full result for the amplitude in this limit is given by equation (4.1), in Chapter 4, and the Altarelli-Parisi splitting kernel which one can write in the form

$$P_{gg}(z) = N_c \frac{(z^4 + (1-z)^4 + 1)}{z(1-z)} \quad (5.19)$$

where N_c is the number of colours. If the conjectured expression in (5.18) is to have the correct Altarelli-Parisi behaviour as $(ij) \rightarrow 0$ then we require that

$$\sum (ij)^4 \rightarrow az^4 + b(1-z)^4 + c, \quad (a = b = c)$$

where the coefficients a, b and c are combinations of the dot products. $\pi(ij) \rightarrow z^4(1-z)^4$. To obtain a correct z -dependence as in equation (5.19) this implies that

$$S \rightarrow z^3(1-z)^3$$

For clarity let us assume that $n = 6$. Then $|M_6|^2$ has dimensions of $()^{-2}$, where we shall denote the dimensions of the dot product by $()$. If we expand $\pi(ij)$ as $(12)(13)(14)(15)(16)(23)(24)(25)(26)(34)(35)(36)(45)(46)(56)$. This means that $\pi(ij)$ has dimension $()^{15}$. Thus to give an overall dimension of $()^{-2} \sum (ij)^4$. S should have dimensions of $()^{13}$, i.e. the S should have a dimension of $()^9$. Insisting on the total symmetry of the amplitude under interchange of momenta and using the fact that S must give $z^3(1-z)^3$ as $(ij) \rightarrow 0$, we can conclude that S is a sum of strings of nine dot products such that each of the six momenta occur 3 times. Strings such as $(13)(14)(15)(24)(25)(26)(35)(36)(46)$. Also one can see that each such string is the complement with respect to the denominator of equation (5.18), $\pi(ij)$ of one of the $(ijklm)$ i.e. S is proportional to

$$\sum_{\substack{p \\ \text{prn}}} \frac{1}{(ijklm)} \pi(ij)$$

In the $2 \rightarrow 3$ case this is just (ijklm), as in equation (5.17). The equation in (5.18) be now be written in the following form,

$$|M_n^{PT}|^2 = g^{2n-4} \frac{N_c^{n-2}}{(N_c - 1)} 2^{4-n} \sum_{i < j}^4 s_{ij}^4 \sum_{"p"} \frac{1}{s_{12}s_{23}\dots s_{n1}} \quad (5.20)$$

This formula is just the formula given by Parke and Taylor [1]. In the expression (5.20) "P" denotes a sum over the $(n-1)!/2$ distinct permutations of $1,2,3,\dots,n$, and the amplitude squared is helicity and colour summed and averaged.

Parke and Taylor claim that the equation (5.20) is a particular helicity sub-amplitude to leading order in the number of colours. In fact there are spinorial recursion relations for n-gluon scattering developed by Giele and Berends [15] and they verified the Parke and Taylor claim.

The full amplitude can be expanded in helicity sub-amplitudes and is given by

$$|M_n|^2 = \sum_S |M_n^{(S)}|^2 \quad (5.21)$$

where $S = |\sum \lambda_i|$ labels the total helicity, all particles assumed outgoing. $S = n, n-2, n-4, \dots, 1(0)$. In ref. [1] it is claimed that

$$\begin{aligned} |M_n^{(n)}|^2 &= |M_n^{(n-2)}|^2 = 0 \\ |M_n^{(n-4)}|^2 &= |M_n^{PT}|^2 + O(N_c)^{-2} \end{aligned} \quad (5.22)$$

The most helicity-violating sub-amplitudes in which all the gluons have the same positive (negative) helicity or one gluon has negative (positive) and the others have positive (negative) helicity, this sub-amplitude is vanishing due to helicity conservation arguments. The first non-vanishing sub-amplitude has two gluons with negative(positive) and the others with positive (negative) helicity. For $n = 4$ and 5 , $gg \rightarrow gg$ and $gg \rightarrow ggg$, the interference terms are zero and the Parke-Taylor formula gives the known exact results for $n = 4$ and 5 and hence

$$|M_4|^2 = \frac{1}{2} |M_4^{PT}|^2, |M_5|^2 = |M_5^{PT}|^2 \quad (5.23)$$

For $n = 6$, $gg \rightarrow gggg$, $|M_6^{PT}|^2$ is typically about $(\frac{1}{2} - \frac{2}{3})$ of the total six-gluon scattering amplitude. This relative dominance of the most helicity-violating sub-amplitude may be anticipated, since this is noted first by Bassetto et al. [14], in the approximation of strongly ordered gluon momenta one has

$$|M_n|^2 \sim |M_n^{PT}|^2 + O(N_c)^{-2} \quad (5.24)$$

5.6 Six gluon scattering

By decomposing the n -gluon amplitude into sub-amplitudes weighted by Chan-Paton like traces of colour matrices, Mangano, Parke and Xu [2], and independently Berends and Giele [6] showed how the calculation could be simplified, and compact expressions obtained in terms of spinors for the unsquared sub-amplitudes.

For six-gluon scattering the possible helicity combinations are $4+,2-$ (or $4-,2+$) and $(3+,3-)$. The first of these is just that which gives rise to the Parke-Taylor formula (equation (5.20)) when squared, and the unsquared amplitude in terms of spinors is

$$m_{4+2-}(1,2,3,4,5,6) = i8g^4 \frac{\langle ij \rangle^4}{\langle 12 \rangle \langle 23 \rangle \langle 34 \rangle \langle 45 \rangle \langle 56 \rangle \langle 61 \rangle} \quad (5.25)$$

When this expression is squared and summed over orderings the $|M|^2$ terms produce equation (5.20) and the cross-terms are $O(N_c^{-2})$, as implied by the final duality property.

In the numerator of equation (5.25), i and j are the momenta of the two gluons with opposite helicity which are independent of their ordering in the sub-amplitude, and the denominator of equation (5.25) is determined by the order of the spinor products for the momenta in the sub-amplitude.

The other helicity configuration is $(+++- -)$ and the sub-amplitude for the six-gluon scattering can be written in the following form [2],

$$m(123456) = i8g^4 \left[\frac{\alpha^2}{t_{123}s_{12}s_{23}s_{45}s_{56}} + \frac{\beta^2}{t_{234}s_{23}s_{34}s_{56}s_{16}} \right. \\ \left. + \frac{\gamma^2}{t_{345}s_{34}s_{45}s_{12}s_{16}} + \frac{t_{123}\beta\gamma + t_{234}\gamma\alpha + t_{345}\alpha\beta}{s_{12}s_{23}s_{34}s_{45}s_{56}s_{16}} \right] \quad (5.26)$$

The "Ward" identity and permutation invariances of the sub-amplitudes imply three inequivalent helicity structures $(+ - + - + -)$, $(++ - + - -)$ and $(+++ - - -)$. The α, β and γ of equation (5.26) are given in table (5.1) in terms of spinors for these three helicity structures.

The notation which was used in Table (5.1) is that $\langle i | \hat{K} | j \rangle = [ik] \langle Kj \rangle$, if $K^2 = 0$ ($\hat{K} = K \cdot \gamma$). We assume $\sum_{i=1}^6 p_i = 0$.

In the denominator of equation (5.26), the t_{ijk} are defined as

$$t_{ijk} = (p_i + p_j + p_k)^2 = s_{ij} + s_{jk} + s_{ki}$$

We shall denote the three amplitudes of (5.26) as $m_1(1,2,3,4,5,6)$, $m_2(1,2,3,4,5,6)$ and $m_3(1,2,3,4,5,6)$ for $(+ - + - + -)$, $(++ - + - -)$, $(+++ - - -)$ respectively.

5.7 Formalism

In this section we shall give some relations which are helpful when one needs to calculate the matrix element squared for six-gluon scattering. We can convert all the spinors into traces by the following relations

$$[i_1 i_2] \langle i_2 i_3 \rangle \dots \langle i_{2n} i_1 \rangle = \frac{1}{2} \text{Tr}(i_1 i_2 \dots i_{2n}) + \frac{1}{2} \text{Tr}(i_1 i_2 \dots i_{2n} \gamma_5) \quad (5.27)$$

$$\langle i_1 i_2 \rangle [i_2 i_3] \dots \langle i_{2n} i_1 \rangle = \frac{1}{2} \text{Tr}(i_1 i_2 \dots i_{2n}) - \frac{1}{2} \text{Tr}(i_1 i_2 \dots i_{2n} \gamma_5) \quad (5.28)$$

One can note that the expressions which are given in (5.27) and (5.28) are complex conjugate to each other. As an immediate consequence of the above two expressions

$$\text{Tr}^2(i_1 i_2 \dots i_{2n}) - \text{Tr}^2(i_1 i_2 \dots i_{2n} \gamma_5) = 4s_{j_1 i_3} \dots s_{j_{2n} i_1} \quad (5.29)$$

and one can generalize the expression in (5.29) as

$$\begin{aligned} \text{Tr}(i_1 i_2 i_3 \dots i_{2n} \gamma_5) \cdot \text{Tr}(j_1 j_2 j_3 \dots j_{2m} \gamma_5) &= \text{Tr}(i_1 i_2 i_3 \dots i_{2n}) \cdot \text{Tr}(j_1 j_2 j_3 \dots j_{2m}) \\ &- 2 [[i_1 i_2] \langle i_2 i_3 \rangle \dots \langle i_{2n} i_1 \rangle \langle j_1 j_2 \rangle [j_2 j_3] \dots [j_{2m} j_1] + c.c] \end{aligned} \quad (5.30)$$

The relation which was given in (5.30) reduces all the traces which are involving γ_5 's.

5.8 A compact expression for six-gluon scattering

This is an important part of the calculations, because the squaring procedure determines the complexity of the cross-section. Our calculations are based on converting all the spinor products into traces which are evaluated in terms of kinematical invariants.

In this section we shall give a compact expression in terms of kinematical invariants for the squared matrix element of the process $gg \rightarrow gggg$, to leading order in the number of colours, and we shall check the accuracy of the result and confirm that the non-leading terms typically constitute less than 5% of the full result, making our compact expressions of potential use in simulating four jet events.

We shall write the six-gluon scattering matrix element squared, $|M_6|^2$, as

$$|M_6|^2 = |M_6^{PT}|^2 + |M_6^{REST}|^2 + 0(N_c^{-2}) \quad (5.31)$$

$|M_6^{PT}|^2$ is the contribution of the $(- - + + +)$, and permuted, helicity orderings which is given by the formula of Parke and Taylor

$$|M_6^{PT}|^2 = g^8 N_c^4 (N_c^2 - 1) \sum_{i < j} (ij)^4 \sum_P \frac{1}{(12)(23)(34)(45)(56)(61)} \quad (5.32)$$

(ij) denotes the dot product of four-momenta $p_i \cdot p_j$. The matrix elements squared are summed over colour and helicities, but a colour and helicity averaging factor should be added to these expressions. P denotes a sum over the non-cyclic permutations of 1,2,3,4,5,6.

For the remaining helicity orderings we shall write, following ref. [2]

$$|M_6^{REST}|^2 = 2g^8 N_c^4 (N_c^2 - 1) \sum_{P_6} \left[\frac{1}{6} H_1(1, 2, 3, 4, 5, 6) + H_2(1, 2, 3, 4, 5, 6) + \frac{1}{2} H_3(1, 2, 3, 4, 5, 6) \right] \quad (5.33)$$

In the expressions which follow we shall use the basic kinematical quantities

$$\begin{aligned} s_{ij} &= (p_i + p_j)^2 = 2(p_i p_j) \\ t_{ijk} &= (p_i + p_j + p_k)^2 = s_{ij} + s_{ik} + s_{jk} \\ T_1 &= t_{123} s_{12} s_{23} s_{45} s_{56} \\ T_2 &= t_{234} s_{23} s_{34} s_{56} s_{61} \\ T_3 &= t_{345} s_{34} s_{45} s_{61} s_{12} \\ S &= s_{12} s_{23} s_{34} s_{45} s_{56} s_{61} \\ t_{ijkl} &= s_{ij} s_{kl} - s_{jk} s_{il} \end{aligned} \quad (5.34)$$

We assume a convention with all momenta outgoing and $\sum_{i=1}^6 p_i = 0$. P_6 in equation (5.33) denotes a sum over the 720 permutations of the external momenta (1,2,3,4,5,6).

H_1 , H_2 and H_3 are the contributions of the $(+ - + - + -)$, $(++ - + - -)$ and $(+++ - - -)$ helicity combinations, respectively.

To leading order in N_c , in terms of the amplitudes of equation (5.26), $H_i(1,2,3,4,5,6) = |m_i(1,2,3,4,5,6)|^2$, $i = 1,2,3 \dots$

We shall compute the H_i by directly squaring the spinor expressions of Table (5.1) and using the trace relations of Section 5.7.

The expression for H_1 can then be written in the [16] compact form:

$$\begin{aligned}
H_1(1, 2, 3, 4, 5, 6) = & \frac{3}{4} \frac{A_1^2 s_{13}^2 s_{46}^2}{T_1^2} + \frac{3[(A_4 + A_5)^2 + 2A_5 t_{135}^2 s_{34} s_{16} + A_5^2]}{T_2 T_3} \\
& + 3A_1 s_{13} s_{46} t_{234} (A_6 + 2A_7) / ST_1 \\
& + \{3s_{34} s_{16} [(A_6 + A_7)(A_8 + A_9) + A_7 A_9 + t_{135}^2 s_{13} s_{46} A_{10}] \\
& + \frac{3}{2} t_{234} t_{345} s_{13} s_{46} A_1 (A_4 + 2A_5) - \frac{3}{4} t_{123}^2 A_2 A_3 A_5\} / S^2 \quad (5.35)
\end{aligned}$$

There are 10 quantities A_i consisting of three triplets which transform cyclically under the permutation π_+ : $(123456) \rightarrow (234561)$; (A_1, A_2, A_3) , (A_4, A_6, A_8) , (A_5, A_7, A_9) and the quantity A_{10} which is invariant under π_+ .

$$\begin{aligned}
A_1 &= 2(t_{135} t_{123} - s_{13} s_{46}) \\
A_2 &= \pi_+ A_1 \\
A_3 &= \pi_+ A_2 \\
A_4 &= -t_{135} (t_{135} t_{234} t_{345} - t_{135} s_{34} s_{16} - t_{345} s_{15} s_{24} - t_{234} s_{35} s_{26}) \\
A_5 &= -s_{15} s_{35} s_{26} s_{24} \\
A_6 &= \pi_+ A_4 \\
A_7 &= \pi_+ A_5 \\
A_8 &= \pi_+ A_6 \\
A_9 &= \pi_+ A_7 \\
A_{10} &= -\frac{1}{2} (t_{1526} t_{2345} + t_{1524} t_{2563} + t_{2315} t_{2465} \\
& + t_{2315} s_{26} s_{45} + t_{2614} s_{25} s_{35} + t_{4563} s_{12} s_{25} \\
& + t_{2465} s_{12} s_{35} + s_{12} s_{35} s_{24} s_{56}) \quad (5.36)
\end{aligned}$$

The expression for H_2 is also quite compact,

$$\begin{aligned}
H_2(1, 2, 3, 4, 5, 6) = & \frac{1}{4} s_{12}^2 s_{56}^2 B_1^2 / T_1^2 + \frac{1}{2} s_{24}^2 s_{56}^2 B_2^2 / T_2^2 \\
& + [(B_4 + B_5)^2 + 2t_{124}^2 B_5 s_{16} s_{34} + B_5^2] / T_2 T_3 \\
& + s_{12}^2 [(B_6 + B_7)^2 + B_7(3B_7 + 2B_6) + t_{124}^2 (B_{10}^2 - 4s_{35} s_{45} s_{46} s_{36})] / T_1 T_3 \\
& + B_1 s_{12}^2 s_{56}^2 t_{234} (B_6 + 2B_7) / T_1 S + B_2 s_{24} s_{56} [s_{56} t_{345} (B_8 + 2B_9) + t_{123} (B_4 + 2B_5)] / T_2 S \\
& + [s_{12} s_{23} s_{56} ((B_6 + 2B_7)(B_4 + 2B_5) - t_{124} B_4 B_{11} - 2t_{124}^2 s_{35} s_{34} s_{56} B_{13}) \\
& + s_{12} s_{34} s_{56} s_{16} (\frac{1}{2} (B_6 + 2B_7)(B_8 + 2B_9) + t_{124}^2 B_{12}) - \frac{1}{4} t_{123}^2 B_2 B_3 B_5 \\
& + \frac{1}{2} t_{234} t_{345} s_{12} s_{56} B_1 (B_4 + 2B_5) \\
& + \frac{1}{2} t_{234} B_3 B_7 (s_{12} t_{234} B_1 + 2t_{123} (B_8 + 2B_9))] / S^2 \quad (5.37)
\end{aligned}$$

The thirteen quantities B_i contain some pairs which are related by the permutation $\pi_r: (123456) \rightarrow (654321)$.

$$\begin{aligned}
B_1 &= 2(t_{123}t_{124} - s_{12}s_{56}) \\
B_2 &= 2(t_{124}t_{234} - s_{24}s_{56}) \\
B_3 &= \pi_r B_2 \\
B_4 &= -t_{124}(t_{124}t_{345}t_{234} - t_{124}s_{34}s_{16} - t_{345}s_{24}s_{56} - t_{234}s_{12}s_{35}) \\
B_5 &= -s_{12}s_{24}s_{35}s_{56} \\
B_6 &= -t_{124}(t_{123}s_{35} - t_{124}s_{45} + t_{345}s_{56}) \\
B_7 &= s_{12}s_{56}s_{35} \\
B_8 &= \pi_r B_6 \\
B_9 &= \pi_r B_7 \\
B_{10} &= s_{35}s_{46} - s_{34}s_{56} + s_{36}s_{45} \\
B_{11} &= B_{10}(4 \leftrightarrow 6) \\
B_{12} &= \frac{1}{2}(t_{2346}s_{14}s_{35} + t_{1345}s_{24}s_{36} - s_{23}s_{15}s_{46}s_{34} \\
&\quad - s_{26}s_{13}s_{34}s_{45} + t_{1634}s_{23}s_{45} + t_{1463}s_{34}s_{25} - 2s_{13}s_{46}s_{34}s_{25} \\
&\quad + t_{1643}s_{35}s_{24} + t_{2615}s_{34}^2) \\
B_{13} &= s_{12}s_{46} - s_{14}s_{46} + s_{16}s_{24}
\end{aligned} \tag{5.38}$$

The expression for H_3 is already given in a compact form in ref. [2] and is given by the following expression

$$\begin{aligned}
H_3(1, 2, 3, 4, 5, 6) &= \frac{t_{123}^3(t_{123}s_{34}s_{16} + t_{234}s_{45}s_{12} + t_{345}s_{56}s_{23})}{t_{234}t_{345}s_{12}s_{23}s_{34}s_{45}s_{56}s_{61}} \\
&\quad - \frac{4t_{123}^2}{t_{234}t_{345}s_{34}s_{16}} + \frac{(t_{123}t_{234}t_{345} - t_{234}s_{45}s_{12} - t_{345}s_{56}s_{23})^2}{t_{234}^2 t_{345}^2 s_{34}^2 s_{61}^2}
\end{aligned} \tag{5.39}$$

The results, which were obtained by Mangano et al. [2] for the six-gluon scattering, to leading order in number of colours, are left in the form of a table involving some traces still to be evaluated. This yields a FORTRAN code of some two hundred lines when reduced to kinematical invariants [7]. Our results which are represented here involve far fewer terms.

We have checked our compact expressions against the FORTRAN code supplied by the authors of ref. [2] with complete numerical agreement. One detail should be mentioned. Our results for H_1 and H_2 are not identically equal to the squared matrix element for these helicity combinations. We have exploited the summation over all permutations in equation (5.33), and the permutation invariance of various parts of the expression, to reduce the number of terms.

It is of interest to compare the compact leading N_c expression with the exact squared matrix element for the six-gluon scattering. For this purpose we have generated $2 \rightarrow 4$ events using the phase space generator RAMBO [8], and applied

cuts in the parton-parton c.m. to select hard, well-separated jets. The cuts applied were as follows: $\sqrt{\hat{s}} = 100\text{GeV}$, $p_T^i > 15\text{GeV}$, $E_T > 70\text{GeV}$, for each pair of jets $\cos(\theta_{ij}) < .643$ and $|\eta| < .80$. E_T denoting the transverse energy of the four final jets. These are the cuts used in ref. [9]. We found that the compact leading N_c expression is within 20% of the exact result for all of the generated events, 93% of generated events are within 10% of the exact result, and 47% of generated events within 5%. The ratio of leading N_c to exact cross-section is .96. The exact expression used was that of ref. [10].

By comparing the leading N_c result with the multi-gluon approximation which was based on the Parke and Taylor formula multiplied by a correction factor (for more details see ref. [11,12]) using identical cuts, 99%, 89%, 61%, of events were within 20%, 10%, 5% respectively of the exact result [12].

5.9 The Non-leading terms for six-gluon scattering

We shall write the non-leading terms for the six-gluon scattering as

$$\begin{aligned}
|M^{NON}|^2 = & 16g^8 N_c^2 (N_c^2 - 1) \sum_{i < j} (ij)^4 \sum_P H_f(1, 2, 3, 4, 5, 6) \\
& + 2g^8 N_c^2 (N_c^2 - 1) \sum_{P_6} \left[\frac{1}{6} H_{f1}(1, 2, 3, 4, 5, 6) + H_{f2}(1, 2, 3, 4, 5, 6) + \right. \\
& \left. \frac{1}{2} H_{f3}(1, 2, 3, 4, 5, 6) \right] \quad (5.40)
\end{aligned}$$

H_f is the non-leading form which contributes to the PT helicity contribution (- - + + + +), and H_{f1} , H_{f2} and H_{f3} are the non-leading terms corresponding to H_1 , H_2 and H_3 . "P" denotes a sum over the $(n-1)!/2$ non-cyclic permutations of (1,2,3,4,5,6). In terms of the amplitudes of (5.25) and (5.26)

$$\begin{aligned}
H_f(1, 2, 3, 4, 5, 6) = & [m_{4+2-}^*(1, 2, 3, 4, 5, 6) (m_{4+2-}(1, 3, 5, 2, 6, 4) \\
& + m_{4+2-}(1, 3, 6, 4, 2, 5) + m_{4+2-}(1, 4, 2, 6, 3, 5)) + c.c.] \quad (5.41)
\end{aligned}$$

$$\begin{aligned}
H_{f1}(1, 2, 3, 4, 5, 6) = & [m_1^*(1, 2, 3, 4, 5, 6) (m_3(1, 3, 5, 2, 6, 4) + \\
& m_3(5, 1, 3, 6, 4, 2) + m_3(3, 5, 1, 4, 2, 6)) + c.c.] \quad (5.42)
\end{aligned}$$

$$\begin{aligned}
H_{f2}(1, 2, 3, 4, 5, 6) = & [m_2^*(1, 2, 3, 4, 5, 6) (m_2^*(3, 5, 2, 6, 4, 1) \\
& + m_2(4, 2, 5, 1, 3, 6) + m_3(1, 4, 2, 6, 3, 5)) + c.c.] \quad (5.43)
\end{aligned}$$

$$H_{f3}(1, 2, 3, 4, 5, 6) = [m_3^*(1, 2, 3, 4, 5, 6) (m_2(1, 3, 5, 2, 6, 4) + m_2^*(6, 4, 2, 5, 1, 3) + m_1(1, 4, 2, 6, 3, 5)) + c.c.] \quad (5.44)$$

In equation (5.41) m_{4+2-} is given by equation (5.25) but excluding the $\langle ij \rangle^4$ in the numerator.

We shall use the spinor expressions of equations (5.25) and (5.26) and Table 5.1 to evaluate the H_f 's in terms of kinematical invariants.

The evaluation of the various terms in equations (5.42) - (5.44) will require technical tricks.

In evaluating a particular product of the spinors of Table 5.1, for instance $\gamma_i \gamma_j^*$ or $\beta_i \beta_j^*$ ($ij = 1, 2, 3$ denoting the helicity structures), one can use the relations of Section 5.7 to write them in terms of traces, and traces involving γ_5 . Schematically

$$(\gamma_i \gamma_j^*) = \frac{1}{2} Tr(\hat{i}_1 \hat{i}_2 \dots) + \dots - \frac{1}{2} Tr(\hat{i}_1 \hat{i}_2 \dots \gamma_5) \quad (5.45)$$

$\hat{i}_1, \hat{i}_2, \dots$, here denote external gluon momenta and $\hat{i} = p_i \cdot \gamma$.

We found it convenient to write equation (5.45) in the following form,

$$(\gamma_i \gamma_j^*) = \frac{1}{2} E_i + \frac{\frac{1}{2}(E_i u_{i_1 i_2 i_3 i_4} + E_j)}{Tr(\hat{i}_1 \hat{i}_2 \hat{i}_3 \hat{i}_4 \gamma_5)} \quad (5.46)$$

where

$$u_{ijkl} = s_{ij} s_{kl} + s_{jk} s_{il} - s_{ik} s_{jl}. \quad (5.47)$$

E_i represents the results of evaluating traces and E_j is a calculable function of momenta. In calculating $|M|^2$ one needs to multiply by other pairs, say $(\beta_i \beta_j^*)$. These can be written with a similar structure,

$$(\beta_i \beta_j^*) = \frac{\frac{1}{2} F_i + \frac{1}{2}(F_i u_{j_1 j_2 j_3 j_4} + F_j)}{Tr(\hat{j}_1 \hat{j}_2 \hat{j}_3 \hat{j}_4 \gamma_5)} \quad (5.48)$$

one then obtains

$$(\gamma_i \cdot \gamma_j^*)(\beta_i \beta_j^*) + c.c. = \frac{1}{2} E_i F_i + \frac{RW}{2X} \quad (5.49)$$

c.c. denoting the addition of the complex conjugate. The cross-terms linear in $Tr(\hat{i}_1 \hat{i}_2 \hat{i}_3 \hat{i}_4 \gamma_5)$ vanish since $\gamma_5 \rightarrow -\gamma_5$ in the c.c. terms.

In equation (5.49) $X = Tr(\hat{i}_1 \hat{i}_2 \hat{i}_3 \hat{i}_4 \gamma_5) Tr(\hat{j}_1 \hat{j}_2 \hat{j}_3 \hat{j}_4 \gamma_5)$ which can be trivially reduced using equation (5.30)

$$R = F_i u_{j_1 j_2 j_3 j_4} + F_j$$

$$W = E_i u_{i_1 i_2 i_3 i_4} + E_j$$

The products of all spinor pairs can be written in the form of equation (5.46). We shall see that the entire answer for the non-leading amplitude squared can be written as a sum over terms of the form of equation (5.49) involving only six different functions for E,F and three different functions for X and R,W.

In our calculations we shall use the basic kinematical quantities

$$t_{ijklmn} = t_{ijk} t_{jkl} t_{klm} - t_{ijk} s_{kl} s_{ln} - t_{jkl} s_{ij} s_{lm} - t_{klm} s_{jk} s_{mn}$$

$$u_{ijkl} = s_{ij} s_{kl} - s_{ik} s_{jl} + s_{jk} s_{il}$$

$$T_5 = t_{135} s_{24} s_{26} s_{35} s_{15}$$

$$T_6 = t_{236} s_{26} s_{36} s_{15} s_{14}$$

$$T_7 = s_{14} s_{24} s_{26} s_{36} s_{35} s_{15}$$

$$T_8 = t_{135} s_{13} s_{35} s_{26} s_{46}$$

$$T_9 = t_{134} s_{52} s_{26} s_{14} s_{13}$$

$$T_{10} = t_{235} s_{35} s_{52} s_{46} s_{14}$$

The expression for H_f is simple and given by

$$H_f(1, 2, 3, 4, 5, 6) = \frac{1}{4S} \left[\frac{(12u_{1254} u_{2356} u_{3461} - 6u_{2356} L_2 - 3u_{1254} L_1)}{s_{13} s_{35} s_{52} s_{46} s_{14} s_{26}} \right] \quad (5.50)$$

The functions L_1, L_2 are given by

$$L_1 = u_{2346} u_{1356} + t_{3126} t_{5436} + t_{2635} t_{3416} + t_{2135} s_{36} s_{46} + t_{1356} s_{32} s_{46} + t_{5416} s_{32} s_{36}$$

$$L_2 = t_{1245} t_{1634} + t_{1245} s_{16} s_{34} + t_{1634} s_{14} s_{52} + t_{6245} s_{d13} s_{14}$$

$$+ u_{3125} s_{14} s_{46} + t_{2356} s_{14}^2 + t_{6215} s_{14} s_{34} + t_{4235} s_{16} s_{14}$$

In our calculations for H_{f_1}, H_{f_2} and H_{f_3} we defined the following basic functions:

$$R(123456) = -B(123456) u_{1462} + C(123456)$$

$$V(123456) = E(123456) u_{1534} + F(123456)$$

$$W(123456) = G(123456) u_{1453} + A(123456)$$

with

$$\begin{aligned}
A(123456) &= -2s_{26}s_{13}s_{35}(-u_{1453}s_{34} + u_{1543}s_{14} + u_{1435}s_{45} + 2s_{15}s_{14}s_{45}) \\
B(123456) &= s_{13}(t_{153462} + t_{146235} + u_{1462}s_{15} + u_{3462}s_{35}) \\
C(123456) &= 2s_{13}s_{46}s_{26}(u_{1435}s_{12} + u_{1532}s_{14} + u_{1432}s_{35} + 2s_{12}s_{14}s_{15}) \\
G(123456) &= s_{26}(-u_{3431}s_{35} - u_{1435}s_{13} - u_{1345}s_{35} + u_{1453}s_{15}) \\
E(123456) &= t_{235146}s_{24} + t_{153426}s_{46} - t_{235164}s_{26} + u_{1534}s_{24}s_{46} \\
F(123456) &= -2s_{35}s_{15}(u_{3462}s_{14}s_{24} + u_{4261}s_{46}s_{34} - t_{3624}s_{14}s_{26} \\
&\quad - t_{1243}s_{46}s_{26} + 2s_{24}s_{46}s_{34}s_{14})
\end{aligned}$$

and we defined X, Y and Z as the following:

$$\begin{aligned}
X(123456) &= u_{3546}u_{1246} - 2t_{124536}s_{46} \\
Y(123456) &= u_{6531}u_{6534} - 2u_{1643}s_{56}s_{35} \\
Z(1234) &= u_{1234}^2 - 4s_{12}s_{23}s_{34}s_{14}
\end{aligned}$$

The expression for H_{f_1} can then be written in the compact form:

$$\begin{aligned}
H_{f_1}(123456) &= 3 \left[t_{123} \left(E(456123)G(123456) - \frac{V(456123)W(123456)}{X(352164)} \right) \right. \\
&\quad + t_{234} \left(-B(123456)G(123456) + \frac{W(123456)R(123456)}{X(352164)} \right) \\
&\quad - t_{354} \left(B(123456)E(456123) + \frac{R(123456)V(456123)}{Z(1426)} \right) \Big] / (ST_9) \\
&\quad + \frac{3}{2}t_{135} \left[t_{123} \left(E(123456)G(123456) + \frac{W(123456)V(123456)}{Z(1453)} \right) \right. \\
&\quad \left. - t_{234} \left(B(123456)G(456123) + \frac{R(123456)W(456123)}{Z(1426)} \right) \right. \\
&\quad \left. + t_{345} \left(-B(456123)E(456123) + \frac{R(456123)V(456123)}{X(352164)} \right) \right] / (S.T_{10}) \\
&\quad + \frac{3}{2}t_{135} \left[\left(E(123456)E(456123) - \frac{V(456123)V(123456)}{X(352164)} \right) / (T_2T_{10}) \right. \\
&\quad + \left(G(456123)G(123456) - \frac{W(123456)W(456123)}{X(352164)} \right) / (T_3T_{10}) \\
&\quad \left. + \left(B(456123)B(123456) - \frac{R(123456)R(456123)}{X(352164)} \right) / (T_1T_{10}) \right] \\
&\quad + 3 \left[\left(B^2(123456) + \frac{R^2(123456)}{Z(1426)} \right) / (T_1T_9) + \left(E^2(456123) \right. \right. \\
&\quad \left. \left. + \frac{V^2(456123)}{Z(1426)} \right) / (T_2T_{10}) + \left(G^2(123456) + \frac{W^2(123456)}{Z(1453)} \right) / (T_3T_9) \right] \quad (5.51)
\end{aligned}$$



The expression for H_{f_2} can then be written in the following form

$$\begin{aligned}
H_{f_2}(1, 2, 3, 4, 5, 6) = & 2 \left[\left(G^2(164325) + \frac{W^2(164325)}{Z(1234)} \right) / (T_2 T_9) \right. \\
& + \left(E^2(346251) + \frac{V^2(346251)}{Z(2653)} \right) / (T_1 T_8) + \left(G^2(451326) + \frac{W^2(451326)}{Z(1234)} \right) (T_1 T_9) \left. \right] \\
& + \left(E^2(346152) + \frac{V^2(346152)}{Z(1653)} \right) / (T_1 T_{11}) + \left(G^2(325164) + \frac{W^2(325164)}{Z(1653)} \right) / (T_2 T_8) \\
& + \left(E^2(643152) + \frac{V^2(643152)}{Z(1653)} \right) / (T_3 T_9) + \left(G^2(345162) + \frac{W^2(345162)}{Z(1653)} \right) / (T_2 T_5) \\
& + \left(E^2(254316) + \frac{V^2(254316)}{Z(1234)} \right) / (T_3 T_6) + \frac{1}{2} \left(E^2(523164) + \frac{V^2(523164)}{Z(1653)} \right) / (T_1 T_6) \\
& \quad + \frac{1}{2} \left(E^2(346251) + \frac{V^2(346251)}{Z(2653)} \right) / (T_1 T_5) \\
& + t_{124} \left[\frac{1}{2} t_{123} \left(E(254316)G(345162) + \frac{V(254316)W(345162)}{X(426351)} \right) \right. \\
& + t_{234} \left(-E(523164)G(432615) + \frac{V(523164)W(432615)}{X(423651)} \right) \left. \right] / ST_7 \\
& + \left[t_{123} t_{235} \left(G(164325)G(432615) + \frac{W(164325)W(432615)}{Y(652341)} \right) \right. \\
& + 2t_{345} t_{235} \left(-G(451326)G(325164) - \frac{W(451326)W(325164)}{X(426351)} \right) \\
& + 2t_{234} t_{235} \left(-E(643152)E(346251) + \frac{V(643152)V(346251)}{Y(143256)} \right) \\
& + 2t_{345} t_{135} \left(G(164325)E(346152) - \frac{W(164325)V(346152)}{X(426351)} \right) \\
& \quad + t_{134} t_{345} \left(E(346251)E(623451) + \frac{V(623451)V(346251)}{Y(413256)} \right) \\
& + t_{234} t_{135} \left(G(251643)G(451326) + \frac{W(251643)W(451326)}{Y(652341)} \right) \left. \right] / (ST_{10}) \\
& + t_{124} \left[\frac{1}{2} \left(E(346251)E(523164) - \frac{V(346251)V(523164)}{Y(143256)} \right) / (T_1 T_7) \right. \\
& + \left(G(345162)E(523461) - \frac{W(345162)V(523461)}{Y(123456)} \right) \left. \right] / (T_2 T_9) \\
& + \left[\frac{1}{2} t_{123} \left(E(254316)E(523461) + \frac{V(254316)V(523461)}{X(126453)} \right) \right. \\
& + t_{234} \left(-E(254316)E(523164) + \frac{V(254316)V(523164)}{X(426351)} \right) \left. \right] / (ST_6) \\
& + \left[\frac{1}{2} t_{123} \left(G(345162)G(432615) + \frac{W(345162)W(432615)}{X(423651)} \right) \right.
\end{aligned}$$

$$\begin{aligned}
& +t_{234} \left(-E(346251)G(432615) + \frac{V(346251)W(4312615)}{X(354612)} \right) \Big] / (ST_5) \\
& \quad + 2 \left[t_{123} \left(E(623451)G(251643) + \frac{W(251643)V(623451)}{X(123456)} \right) \right. \\
& \quad \quad \left. + t_{234} \left(-E(346152)G(251643) + \frac{V(346152)W(251643)}{X(423651)} \right) \right. \\
& \quad \left. + t_{345} \left(-E(346152)E(623451) - \frac{V(346152)V(623451)}{Y(123456)} \right) \right] / (ST_{11}) \\
& \quad + 2 \left[t_{123} \left(G(432615)G(325164) + \frac{W(432615)W(325164)}{X(423651)} \right) \right. \\
& \quad \quad \left. + t_{234} \left(-G(432615)E(346251) + \frac{W(432615)V(346251)}{X(354612)} \right) \right. \\
& \quad \left. + t_{345} \left(-G(325164)E(346251) - \frac{W(325164)V(346251)}{Y(143256)} \right) \right] / (ST_8) \\
& \quad + 2 \left[t_{123} \left(G(164325)E(643152) + \frac{W(164325)V(643152)}{X(426351)} \right) \right. \\
& \quad \quad \left. + t_{234} \left(-G(451326)E(643152) + \frac{W(451326)V(643152)}{X(426351)} \right) \right. \\
& \quad \left. + t_{345} \left(-G(451326)G(164325) + \frac{W(451326)W(164325)}{Z(1234)} \right) \right] / (ST_9)
\end{aligned} \tag{5.52}$$

The expression for H_{f_3} is also quite compact

$$\begin{aligned}
H_{f_3}(1, 2, 3, 4, 5, 6) &= \left[t_{135} \left(E(153426)E(426153) + \frac{V(153426)V(426153)}{X(562134)} \right) \right. \\
& \quad \left. + 2t_{134} \left(-E(153426)E(526143) + \frac{V(153426)V(526143)}{X(562134)} \right) \right] / (T_3T_{10}) \\
& \quad + \left[t_{135} \left(G(426153)G(153426) + \frac{W(426153)W(153426)}{X(562134)} \right) \right. \\
& \quad \left. + 2t_{134} \left(-G(426153)E(251634) + \frac{W(426153)V(251634)}{X(542136)} \right) \right] / (T_2T_{10}) \\
& \quad + t_{123} \left[t_{135} \left(G(426153)E(426153) + \frac{W(426153)V(426153)}{Z(1564)} \right) \right. \\
& \quad \left. + 2t_{134} \left(-E(153426)E(251634) - \frac{V(153426)V(251634)}{Y(651423)} \right) \right] / (ST_{10}) \\
& \quad + \left[t_{135} \left(G(152634)G(425361) + \frac{W(152634)W(425361)}{X(124356)} \right) \right. \\
& \quad \left. + 2t_{124} \left(G(152634)E(253416) - \frac{W(152634)V(253416)}{Y(651423)} \right) \right] / (T_3T_7)
\end{aligned}$$

$$\begin{aligned}
& +t_{123} \left[\frac{1}{2}t_{135} \left(-B(342615)G(425361) - \frac{R(342615)W(425361)}{Z(3564)} \right) \right. \\
& +t_{124} \left(E(524361)G(152634) + \frac{W(152634)V(524361)}{X(124356)} \right) \left. \right] / (ST_9) \\
& +t_{123} \left(E(526143)E(251634) + \frac{V(526143)V(251634)}{X(542136)} \right) / (ST_8) \\
& +2 \left(G(153426)E(426153) + \frac{W(153426)V(426153)}{X(562134)} \right) / (ST_9) \\
& +\frac{1}{2} \left(E(524361)E(253416) + \frac{V(524361)V(253416)}{X(126453)} \right) / (ST_5) \\
& + \left(-B(342615)G(152634) - \frac{R(342615)W(152634)}{X(124356)} \right) / (ST_6) \\
& +2 \left[\left(G^2(153426) + \frac{W^2(153426)}{Z(1234)} \right) / (T_2T_4) + \left(E^2(426153) + \frac{V^2(426153)}{Z(1564)} \right) / (T_3T_9) \right. \\
& + \left. \left(B^2(342615) + \frac{R^2(342615)}{Z(3564)} \right) / (T_2T_6) \right] + \left(E^2(524381) + \frac{V^2(524361)}{Z(3564)} \right) / (T_2T_5) \\
& + \left(E^2(251634) + \frac{V^2(251634)}{Z(1236)} \right) / (T_2T_8) + \left(E^2(526143) + \frac{V^2(526143)}{Z(1564)} \right) / (T_3T_8)
\end{aligned} \tag{5.53}$$

Together with the compact expression to leading order in the number of colours, we compared our result numerically with the exact result of ref. [10] and are in complete agreement.

	$1^+2^-3^+4^-5^+6^-$	$1^+2^+3^-4^+5^-6^-$	$1^+2^+3^+4^-5^-6^-$
α	$\langle 46 \rangle [13]$ $\langle 5 \hat{1} + \hat{3} 2 \rangle$	$-\langle 56 \rangle [12]$ $\langle 4 \hat{1} + \hat{2} 3 \rangle$	$-$ 0
β	$\langle 24 \rangle [51]$ $\langle 3 \hat{5} + \hat{1} 6 \rangle$	$\langle 56 \rangle [24]$ $\langle 1 \hat{2} + \hat{4} 3 \rangle$	$\langle 56 \rangle [23]$ $\langle 1 \hat{2} + \hat{3} 4 \rangle$
γ	$\langle 62 \rangle [35]$ $\langle 1 \hat{3} + \hat{5} 4 \rangle$	$\langle 35 \rangle [12]$ $\langle 4 \hat{1} + \hat{2} 6 \rangle$	$\langle 45 \rangle [12]$ $\langle 3 \hat{1} + \hat{2} 6 \rangle$

Table 5.1: Shows the coefficients of α, β and γ of equation (5.26) in terms of spinors

REFERENCES

- [1] S. Parke and T. Taylor, Nucl. Phys. B269 (1986), 410.
Z. Kunszt, Nucl. Phys. 271 (1986), 333.
J. Gunion and J. Kalinowski, Phys. Rev. D34, (1986), 2119.
- [2] M. Mangano, S. Parke and Zhan Xu, Nucl. Phys. B298, (1988), 653.
- [3] P. De Causmaecker, R. Gastmans, W. Troost and T.T. Wu, Nucl. Phys. B206 (1982), 53.
- [4] Zhan Xu, Da-Hua Zhang and Lee Chang, Nucl Phys. B291, (1987), 392.
- [5] F.A. Berends, R. Kleiss, P. De Causmaecker, R. Gastmans, W. Troost and T.T. Wu, Nucl. Phys. B206, (1982), 61.
- [6] F.A. Berends and W.T. Giele, Nucl. Phys. B294, (1987), 700.
- [7] S. Parke, private communication.
- [8] R. Kleiss, W.J. Stirling and S.D. Ellis, Comput. Phys. Commun. 40, (1986), 359.
- [9] Z. Kunszt and W.J. Stirling, Phys. Lett. B171, (1986), 307.
- [10] Z. Kunszt, Nucl. Phys. B271, (1986), 333.
- [11] C.J. Maxwell, Phys. Lett. B192, (1987), 190.
- [12] C.J. Maxwell, Nucl. Phys. B316, (1989), 321.
- [13] F.A. Berends, R. Kleiss, P. De Causmaecker, G. Gastmans and T.T. Wu, Phys. Lett. 103B, (1981), 124.
- [14] A. Bassetto, M. Giafaloni and P. Marchesini, Phys. Rep. C100, (1983), 201.
- [15] F.A. Berends and W.T. Giele, Leiden University preprint 88-0100, (1988).
- [16] K. Makhshoush and C.J. Maxwell, Durham preprint DTP 88/40 (1989).

Chapter 6

Seven-gluon Scattering

6.1 Introduction

We have seen in chapter 5 that spinor techniques enabled compact expressions in terms of spinors to be produced for the unsquared amplitude for six-gluon scattering and we were able to convert these to compact expressions in terms of kinematical invariants for the squared matrix element. Our results for the next-to-leading in N_c terms involved only six independent kinematical functions and the numerator of each kinematical pole had an identical algebraic structure.

The simplicity of the results is due to the ingenious decomposition into sub-amplitudes of equation (5.1). A similar spinor calculation has now been completed for seven-gluon scattering by Berends, Giele and Kuijf [1].

6.2 Results for Seven-Gluon Scattering

The permutation and other invariance properties of the sub-amplitudes given in Section 5.2 ensure that the number of inequivalent helicity structures is always just the number of cyclically inequivalent orderings of +, - helicities around a circle. We have for seven gluons the + + - - - - (and + \leftrightarrow - and permuted) orderings which are given, to leading order in N_c , by the Parke-Taylor (PT) formula equation (5.30), and the structures (+ + + - - -), (+ + - + - -), (+ + - - + -) and (+ - + - + -).

For each of these structures the next-to-leading in colour terms are given by [1].

$$\begin{aligned} H_f(1234567) &= m^*(1234567) \\ &+ 3m(1235746) + 3m(1236475) + 3m(1246357) \\ &+ 3m(1253647) + 3m(1345726) + 3m(1356724) \\ &+ m(1357246) + 3m(1352467) + 3m(1372456) \end{aligned}$$

$$\begin{aligned}
& -3m(1372654) - 3m(1376524) - m(1473625) \\
& +3m(1425367) + 3m(1572346) - 3m(1574326) \\
& - 3m(1543726)] + c.c.
\end{aligned} \tag{6.1}$$

In this chapter we shall use equation (6.1) to obtain a compact expression in terms of kinematical invariants for the next-to-leading terms of the squared Parke-Taylor helicity sub-amplitude (+ + - - - -). This is the first step in a program to obtain the full squared matrix element for seven-gluon scattering in a compact form.

For this PT sub-amplitude we then have

$$|M_{5+2-}|^2 = |M_7^{PT}|^2 + \frac{1}{8}g^{10}N_c^3(N_c^2 - 1) \sum_{i<j} s_{ij}^4 \sum_P H_f(1234567) \tag{6.2}$$

$|M_7^{PT}|^2$ is given by equation (5.20). "P" denotes a sum over the 360 non-cyclic permutations of (1,2,3,4,5,6,7). H_f is given by equation (6.1) with

$$m(1,2,3,4,5,6,7) = \frac{1}{\langle 12 \rangle \langle 23 \rangle \langle 34 \rangle \langle 45 \rangle \langle 56 \rangle \langle 67 \rangle \langle 71 \rangle} \tag{6.3}$$

For the PT sub-amplitude various of the m^*m products in (6.1) are permutations of each other and we can exploit the sum over permutations in equation (6.2) to write

$$\begin{aligned}
H_f(1234567) = \{ & m^*(1234567)[15m(1235746) \\
& +12m(1246357) + 15m(1425367) \\
& -2m(1473625)] + c.c. \}
\end{aligned} \tag{6.4}$$

The direct evaluation of the four terms in equation (6.4) is in principle straightforward, requiring only the use of the trace relations of Section 5.7. However, unless some technical tricks are used the result is extremely lengthy. Consider for instance the term $m^*(1234567) m(1473625) + c.c.$ This can be expressed as

$$\begin{aligned}
m^*(1234567)m(1473625) + c.c. = \\
\frac{Tr(\hat{1}\hat{4}\hat{5}\hat{1}\hat{2}\hat{5}\hat{6}\hat{2}\hat{3}\hat{6}\hat{7}\hat{3}\hat{4}\hat{7})}{S_{S_{14}S_{47}S_{73}S_{36}S_{62}S_{25}S_{15}}}
\end{aligned} \tag{6.5}$$

with $S = s_{12}s_{23}s_{34}s_{45}s_{56}s_{67}s_{71}$.

This involves a trace of fourteen objects which would be very laborious to expand out in kinematical invariants. The technical trick which we use is to multiply top and bottom of the expression by an extra s_{ij} . In the example we

are considering we choose $s_{45} = \langle 45 \rangle [45]$. This adds an extra pair of spinors to the numerator trace which may be re-expanded into spinors. The resulting product of sixteen spinors in the numerator now factorizes into sub-traces of four objects and these are trivially evaluated. The result is now compact but we are left with an extra 'fake' s_{45} pole in the denominator. This must of course be a factor of the numerator, but to factor s_{45} out and cancel it off would involve rewriting the numerator using momentum conservation, and the resulting expression would again be lengthy. We have already used a similar trick in Section 5.9 where the expressions for H_{f_1} , H_{f_2} , H_{f_3} have denominators of X, Y, Z . These must cancel with corresponding factors in the R, V, W numerators, but to perform this cancellation would involve making the expressions very lengthy.

Using this trick on the other terms in equation (6.4) we finally arrive at the compact result

$$\begin{aligned}
H_f(1234567) = \frac{1}{4S} & \left[\frac{15A(1234567)}{s_{13}s_{16}s_{46}s_{74}s_{57}s_{35}} \right. \\
& + \frac{12B(1234567)}{s_{24}s_{46}s_{36}s_{35}s_{57}s_{45}} + \frac{15C(1234567)}{s_{14}s_{42}s_{25}s_{53}s_{36}s_{13}} \\
& \left. - \frac{D(1234567)}{s_{14}s_{47}s_{73}s_{36}s_{62}s_{25}s_{15}s_{45}} \right] \tag{6.6}
\end{aligned}$$

with

$$\begin{aligned}
A(1234567) &= -[u_{7546}u_{7431}u_{3561} + u_{7546}X(1234567) \\
&\quad - u_{7431}X(5264317) - u_{3561}X(4271563)] \\
B(1234567) &= u_{2453}u_{4675}u_{4563} + 2u_{2453}Y(4215673) \\
&\quad + u_{4563}X(5142763) \\
C(1234567) &= u_{1453}u_{1342}u_{2563} + u_{2563}Y(1673425) \\
&\quad - u_{1342}X(3754261) + u_{1453}X(3724561) \\
D(1234567) &= -[3u_{1452}u_{4715}u_{3762}u_{4563} - u_{4563}u_{3762}Y(1364527) \\
&\quad + u_{1452}(u_{4715}X(3162457) - 2u_{4563}Z(1763254) \\
&\quad + (Z(1763254) - 3u_{4715}u_{3762})X(5742361)].
\end{aligned}$$

We define for convenience the functions X, Y, Z :

$$\begin{aligned}
X(1234567) &= u_{7431}u_{5631} - 2t_{156347}s_{13} \\
Y(1234567) &= u_{1456}u_{1457} - 2u_{1756}s_{14}s_{45} \\
Z(1234567) &= t_{1457}s_{23}s_{26} + t_{1564}s_{12}s_{32} \\
&\quad + t_{2756}s_{13}s_{24} + t_{2473}s_{15}s_{26} + t_{1275}s_{24}s_{36} \\
&\quad + t_{3567}s_{12}s_{24} + t_{1627}s_{24}s_{35} + t_{1463}s_{27}s_{52} \\
&\quad + t_{3764}s_{12}s_{52} + t_{1362}s_{47}s_{52} + t_{1734}s_{26}s_{52} \\
&\quad + u_{6745}s_{12}s_{32}
\end{aligned}$$

6.3 Comparison of Leading and Next-to-Leading Terms for the Parke-Taylor Sub-Amplitude

It is of interest to numerically compare the relative sizes of the leading and next-to-leading in colour terms for the PT sub-amplitude.

In Chapter 5, Section 5.8 we have already compared the leading N_c expression for six-gluon scattering with the exact matrix element. We shall now perform a similar exercise for the PT sub-amplitude of seven-gluon scattering. Again we shall generate events using the phase-space generator RAMBO [2] and apply (for n -gluons) the cuts: $p_T^i/\sqrt{\hat{s}} > 0.6/(n-2)$, $E_T/\sqrt{\hat{s}} > 0.7$ and for each pair of final jets $\cos \theta_{ij} < \cos(200^\circ/(n-2))$, $|\eta| < 0.8$. For $n = 6$ these reduce to the cuts considered previously.

We find for seven-gluon scattering that for 99% of generated events the leading N_c PT result is within 20% of the exact PT result, 35% of generated events are within 10% and 9% within 5%.

The leading order in N_c cross-section is 89% of the exact PT cross-section.

If we had compared the leading N_c PT to the exact PT for six-gluon scattering we would have found 100%, 92%, 47% (within 20%, 10%, 5%) and the leading order in N_c cross-section 96% of the exact PT cross-section. Thus it seems that the non-leading colour terms increase in relative importance for seven-gluon scattering as compared to six-gluon scattering.

REFERENCES

- [1] F.A. Berends, W.T. Giele and H. Kuijf, "Exact and Approximate Expressions for Multi-gluon Scattering", Leiden pre-print (1989).
- [2] R. Kleiss, W.J. Stirling and S.D. Ellis, *Comput. Phys. Commun.* 40, (1986), 359.

Chapter 7

Summary

The principal new results obtained in our work are an understanding of the striking similarity between the angular distributions of all $2 \rightarrow 3$ parton-parton scattering subprocesses (Chapter 4), and compact expressions in terms of kinematical invariants for the squared matrix element of six-gluon scattering (Chapter 5), and for one helicity sub-amplitude of seven-gluon scattering in Chapter 6.

In the six-gluon scattering each pole structure in the squared amplitude has a simple numerator with a common algebraic structure in terms of only six basic kinematical functions. Before our work no explicit expression for the full squared matrix element in terms of dot products was available, although a very lengthy computer code for the leading N_c terms did exist. Our expression for the full squared result is very compact and is not substantially longer than the spinor expressions for the unsquared amplitude. Various technical tricks were developed to enable the strings of spinors to be reduced to factorized products of traces of four and six objects, and avoid the laborious evaluation of traces of ten objects and more.

